

19960408 013

DETERMINING THE EFFECTS OF WASTE COAL ASH  
ON LANDFILL RADON LEVELS

THESIS

Richard S. Krysiak Jr., Captain, USAF

AFIT/GEE/ENP/95D-04

**DISTRIBUTION STATEMENT A**

Approved for public release

Distribution Unlimited

DEPARTMENT OF THE AIR FORCE

AIR UNIVERSITY

**AIR FORCE INSTITUTE OF TECHNOLOGY**

Wright-Patterson Air Force Base, Ohio

DTIC QUALITY INSPECTED 1

AFIT/GEE/ENP/95D-04

DETERMINING THE EFFECTS OF WASTE COAL ASH  
ON LANDFILL RADON LEVELS

THESIS

Richard S. Krysiak Jr., Captain, USAF

AFIT/GEE/ENP/95D-04

Approved for public release; distribution unlimited

DETERMINING THE EFFECTS OF WASTE COAL  
ASH ON LANDFILL RADON LEVELS

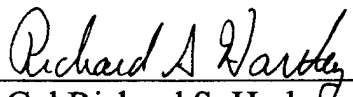
Richard S. Krysiak Jr., B.S.I.E., M.P.A.

Captain, USAF

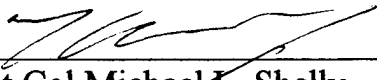
Approved:

  
\_\_\_\_\_  
Captain Jeff Martin, Chairman

28 Nov '95  
Date

  
\_\_\_\_\_  
Lt Col Richard S. Harley

November 29, 1995  
Date

  
\_\_\_\_\_  
Lt Col Michael L. Shelly

29 Nov 95  
Date

AFIT/GEE/ENP/95D-04

DETERMINING THE EFFECTS OF WASTE COAL ASH  
ON LANDFILL RADON LEVELS

THESIS

Presented to the Faculty of the School of Engineering of the

Air Force Institute of Technology

Air University

In Partial Fulfillment of the

Requirements for the Degree of

Master of Science in

Engineering and Environmental management

Richard S. Krysiak Jr., B.S.I.E., M.P.A

Captain, USAF

November 1995

Approved for public release; distribution unlimited

## Acknowledgments

Sincere gratitude is extended to all the people who so willingly supported and showed interest in this thesis. To Captain Jeff Martin, thesis advisor, for his professional advice, constructive criticism, and encouragement which were particularly inspirational to me. I would also like to thank Lt. Col. Richard Hartley and Professor Dan Reynolds who expertly guided the sampling and geostatistical efforts. Their probing questions resulted in thorough and complete product. Also, to O.J. for keeping the world at home watching the trial and out of the computer lab.

Special thanks to Mr. Leroy Cannon for the support he provided at the laboratory. His patience and understanding coupled with his willingness to help made the long hours spent analyzing samples possible and more enjoyable.

Finally, I would like to express my sincerest appreciation to my wife Tina, and children Ricky, Jacob, and Samantha for putting up with me during this demanding program.

## Table of Contents

	Page
Acknowledgments.....	ii
List of Figures.....	v
List of Tables.....	vi
Abstract.....	vii
1.0 INTRODUCTION .....	1
1.1 General Issue.....	1
1.2 Problem Statement.....	6
1.3 Scope of the Problem.....	6
1.4 Specific Research.....	7
1.5 Research Objectives.....	9
1.6 Thesis Organization .....	10
2.0 BACKGROUND .....	11
2.1 Coal Consumption and Ash Generation .....	11
2.2 Past Research .....	12
2.3 Radon Health Effects .....	14
2.4 Radon Migration .....	16
3.0 METHODOLOGY .....	19
3.1 Introduction.....	19
3.2 Sampling and Analysis Plan (SAP) .....	19
3.3 Pilot Study.....	21
3.3.1 Sample Collection.....	23
3.3.2 Sample Analysis .....	26
3.3.3 Geostatistical Analysis.....	34
3.3.3.1 Univariate Description.....	35
3.3.3.2 Spatial Description.....	40
3.3.3.3 Descriptive Structural Analysis .....	42
3.4 Regular Study.....	45
3.4.1 Sample Collection.....	45
3.4.2 Statistical Analysis.....	46
3.5 Background Study.....	47
3.5.1 Sample Collection.....	47
3.5.2 Sample Analysis .....	50
3.6 Radon Source Potential Comparison .....	50
3.7 Outdoor Radon Emanation .....	53
3.8 Indoor Radon Emanation Calculations .....	54
4.0 DATA DESCRIPTION AND ANALYSIS .....	57
4.1 Introduction.....	57

## Table of Contents (con't)

	Page
4.2 Pilot Study Results.....	57
4.2.1 Univariate Analysis.....	63
4.2.2 Spatial Description.....	68
4.2.3 Descriptive Structural Analysis .....	71
4.3 Regular Study Results.....	73
4.4 Radon Source Potential Comparison .....	74
4.5 Outdoor Radon Emanation Calculations .....	75
4.6 Indoor Radon Calculations .....	76
5.0 CONCLUSIONS AND RECOMMENDATIONS .....	78
5.1 Sampling Technique .....	78
5.2 Radon Source Potential.....	78
5.3 Outdoor Radon Emanation .....	79
5.4 Indoor Radon Emanation .....	81
5.5 Recommendations.....	82
Appendix A: Sampling and Analysis Plan.....	85
Appendix B: Statistical Analysis Figures.....	126
Bibliography.....	151
Vita.....	154

## List of Figures

	Page
1.0 $^{238}\text{U}$ Decay Chain.....	3
1.1 Comparison of Radiation Sources.....	5
2.0 Radon Movement Characteristics.....	16
2.1 Radon Entry Routes.....	18
3.0 Data Quality Objective Process.....	20
3.1 Sampling Grid.....	23
3.2 Base Ash Landfill Location Map.....	25
3.3 Box and Whisker Plot.....	37
3.4 Histogram Showing Skewed Data and Extreme Values.....	38
3.5 Rankit Plot and WS Normality Statistic.....	40
3.6 Variogram.....	43
3.7 Behavior Near the Origin of a Variogram.....	44
3.8 Background Sample Locations.....	49
4.0 Nuclide Box and Whiskers Plot.....	64
4.1 Histogram of $^{226}\text{Ra}$ Data.....	65
4.2 Wilk-Shapiro Rankit Plot of $^{226}\text{Ra}$ Data.....	66
4.3 Patch Plot and Contour Plot of $^{226}\text{Ra}$ Data.....	68
4.4 Location of Extreme $^{226}\text{Ra}$ Data Values.....	69
4.5 Moving Window Means for $^{226}\text{Ra}$ .....	70
4.6 Variogram for $^{226}\text{Ra}$ Data.....	72
5.0 Mean $^{226}\text{Ra}$ Activity Level Comparison.....	79
5.1 Radon Flux Density Versus Soil Moisture Content.....	80



## List of Tables

	Page
3.0 $^{235}\text{U}$ Energies and Yields.....	33
3.1 Number of Samples Required for the Regular Study.....	46
4.0 Nuclide Activity Results.....	58
4.1 Nuclide Uncertainty Results.....	60
4.2 Uncertainty in Mean Activity Measurements.....	62
4.3 Summary Statistics.....	63
4.4 Wilk-Shapiro Normality Statistics.....	67
4.5 Omnidirectional Variogram Results for $^{226}\text{Ra}$ .....	71
4.6 Summary of Landfill and Background Activity and.....	73
Standard Deviation Calculations	
4.7 Radon Flux Density From Uncovered Soil.....	76
4.8 Indoor Radon Concentration Results.....	77

## Abstract

Coal contains trace amounts of the primary radionuclides  $^{40}\text{K}$ , and elements of the  $4n$  ( $^{232}\text{Th}$ ),  $4n+2$  ( $^{238}\text{U}$ ), and  $4n+3$  ( $^{235}\text{U}$ ) series including  $^{220}\text{Rn}$  and  $^{222}\text{Rn}$ . Combustion of coal by electric power and heat plants result in concentration of noncombustible mineral matter, including most of the radionuclides, in the coal ash. The increased radiation due to the concentration of radionuclides is known as technologically enhanced natural radiation.

The purpose of this research was to determine the effects of landfilled coal ash on one specific aspect of technologically enhanced natural radiation, radon levels. Soil samples were collected from the ash landfill at Wright Patterson AFB and from several background locations, analyzed using gamma spectroscopy, and the  $^{226}\text{Ra}$  activities compared. The landfill  $^{226}\text{Ra}$  activity ( $4.78 \pm 1.58$  pCi/g) was 2.95 times higher than background ( $1.62 \pm 0.04$  pCi/g). Estimated outdoor and indoor radon emanation at the landfill are predicted to be enhanced by the same factor compared to background. Additionally, the indoor radon concentration calculated in a hypothetical structure built on the landfill (11.48 pCi/l) was above the Environmental Protection Agency's action level of 4.0 pCi/l.

Finally, lifetime occupancy of a home with the previously stated indoor radon concentrations resulted in a 2.83 times greater lifetime risk of early death at the landfill (4.1%) than at background (1.2%). The increase in risk is due to the inhalation of radon emanating from the landfilled coal ash.

# DETERMINING THE EFFECTS OF WASTE COAL ASH ON LANDFILL RADON LEVELS

## 1.0 Introduction

### 1.1 General Issue

Earth's inhabitants have always been exposed to low levels of naturally occurring radiation from the many radionuclides found in the earth's atmosphere and crust as a result of cosmogenic (bombardment from space) or primordial (in the earth's crust from the beginning) sources. Coal in particular contains trace amounts of the primary radionuclides  $^{40}\text{K}$ , and elements of the  $4n$  ( $^{232}\text{Th}$ ),  $4n+2$  ( $^{238}\text{U}$ ), and  $4n+3$  ( $^{235}\text{U}$ ) series as well as their daughter products including  $^{220}\text{Rn}$  and  $^{222}\text{Rn}$ . Additionally, the direct combustion of coal by power and heat plants result in concentration of noncombustible mineral matter, including most of the radionuclides, in waste by-products commonly referred to as coal ash (6: 231). The increased radiation in the coal ash due to the concentration of radionuclides is known as technologically-enhanced natural radiation.

Coal ash generally falls into two categories: fly ash and bottom ash. Fly ash is a powdery particulate that travels up the stack with the flue gases. While some of the fly ash escapes into the atmosphere, most of it is collected from flue gases by stack filters and scrubbers. Bottom ash consists of heavier particles that fall to the bottom of the furnace during the combustion process. The fly ash captured by the filters and scrubbers and the bottom ash are both collected and disposed of in one of two places: settling

ponds or landfills. These disposal practices result in a redistribution of radionuclides from coal deposits located deep in the earth to surface environments. Consequently, there may be changes in local ambient natural radiation levels and hence an increase in natural radiation exposure.

The dominant component of natural radiation exposure for the general population is the radiation dose from inhaled decay products of  $^{220}\text{Rn}$  and  $^{222}\text{Rn}$  (23:1). However, since the half life of  $^{220}\text{Rn}$  is only 55 seconds compared to 3.8 days for  $^{222}\text{Rn}$ , its ability to migrate through soil before decaying is limited. This makes  $^{220}\text{Rn}$  a less important source of radon exposure because it is less likely to reach the atmosphere where it can be inhaled by humans. In fact,  $^{220}\text{Rn}$  makes up less than 20 percent of the total human radon exposure (25: 2-2). Therefore, only the effects of  $^{222}\text{Rn}$  will be addressed in this thesis.

$^{222}\text{Rn}$  is a noble gas formed in the  $^{238}\text{U}$  chain from the decay of its parent  $^{226}\text{Ra}$ . Because it is a nonreactive noble gas, once a radon atom is formed it is relatively free to move. Also, as previously stated,  $^{222}\text{Rn}$  is the most important radon isotope because it has the longest half-life (3.8 days). This is long enough that much of the radon formed within about one meter below the earth's surface can reach the atmosphere where it can be inhaled by humans (23: 1).

As seen in Figure 1.0,  $^{222}\text{Rn}$  and its decay products are members of the  $^{238}\text{U}$  decay series.  $^{222}\text{Rn}$  decays to a series of daughter products that are chemically active and relatively short lived. Of prime concern are airborne concentrations of  $^{218}\text{Po}$ ,  $^{214}\text{Pb}$ , and  $^{214}\text{Bi}$  due to their potential for retention in the lung if inhaled. Once in the lung,  $^{214}\text{Pb}$  and  $^{214}\text{Bi}$  decay to  $^{214}\text{Po}$  which, with  $^{218}\text{Po}$ , emit alpha particles when they in turn decay.

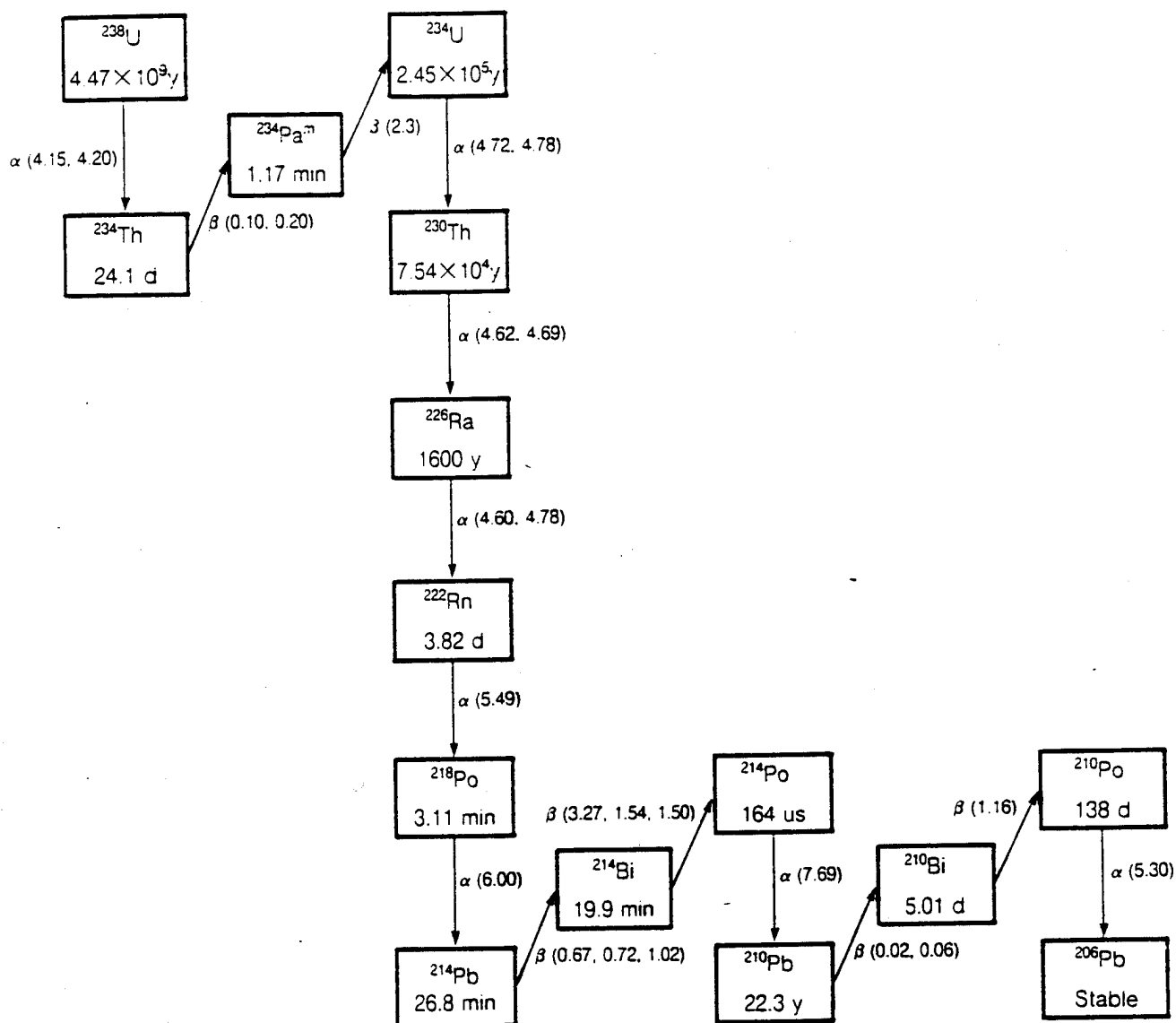


Figure 1.0  $^{238}\text{U}$  Decay Chain. Ref 23.

Although these alpha particles can't travel very far, they have the potential to cause damage by penetrating epithelial cells and depositing enough energy to kill or transform them (22: 9). The transformed cells, either by themselves or through interaction with another agent, have the potential to develop into lung cancer. The average lifetime risk of lung cancer caused by exposure to radon decay products is estimated to be about 0.3%, causing on the order of 10,000 additional cases of lung cancer annually among the US population of 235 million (23: 1). Figure 1.1 shows that the dose received by humans from radon sources is more significant than that received from medical procedures and from nuclear power operations.

Also, as the amount of coal usage increases at Air Force installations so does the amount of ash generated as a result of the coal combustion process. If the coal ash has been disposed of in a landfill on base, the landfill may be a significant source of increased radon production due to technologically enhanced natural radiation.

Additionally, as a result of military base closures, missions and personnel are being transferred to bases that are remaining open. If the facilities at the gaining bases are inadequate to support the mission or personnel, new ones may be built. Currently no consideration is given to technologically enhanced natural radiation when deciding on post closure land use scenarios for ash landfills. Therefore, the potential exists for locating a structure in an area which will generate potentially high levels of radon.

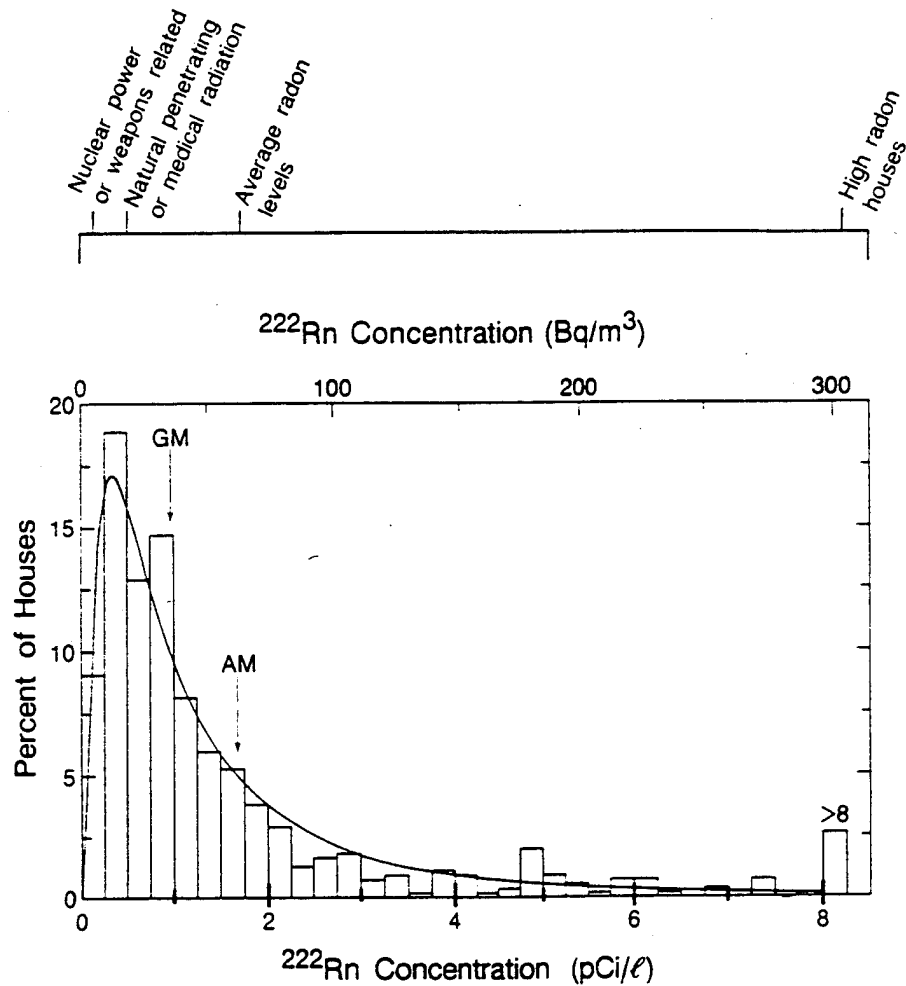


Figure 1.1 Comparison of Radiation Sources. The smooth curve is a lognormal function with the indicated parameters. The upper scale indicates approximately the relative doses from radon and other sources of exposure. From Ref 23.

The increased activity of the naturally occurring radionuclides due to the combustion of coal combined with past disposal practices of landfilling the waste ash on base, may present a radiation exposure source to base population in the form of increased radon production due to an increase in its “source potential”,  $^{226}\text{Ra}$  activity.

## **1.2 Problem Statement**

This research determined the effects of waste coal ash on landfill radon source potential and associated changes in radon emanation. The effects were determined by estimating mean source potentials for the Wright Patterson AFB base ash landfill (landfill #5) and background locations via sampling and analysis and comparing them to see if they were significantly different.

Changes in radon emanation resulting from the observed changes in source potentials were also determined. This was accomplished by using the source potentials at the landfill and background locations to calculate radon emanation into the atmosphere and into a hypothetical structure. Standard radon soil diffusion equations were used to calculate the emanation into the atmosphere from uncovered soil, while the indoor radon emanation was calculated using equations that modeled radon emanation through building materials.

## **1.3 Scope of the Problem**

In determining the effects of waste coal ash on landfill radon source potential, the scope of this research was limited to analyzing the top 24 inches of landfill soil because studies have shown that radon generated at greater depths than this is not likely to reach the atmosphere (23: 6). Also, there was no need to go deeper because the solubility of the radionuclides bound in coal ash were limited (.001 to .003 percent) so they were not expected to leach downward (18: 56).



Once the radon source potential was determined, the transport equations for calculating radon emanation into the atmosphere and into a structure were presented. The scope of the indoor radon emanation calculation was limited to the basement of a typical single unit concrete slab structure.

The health effects due to direct gamma radiation (ground shine) were neglected because radon is generally the most significant source of radiation exposure from naturally occurring alpha decay chains.

#### **1.4 Specific Research**

The base ash disposal area located at Wright Patterson AFB landfill #5 was chosen as the site for the experiment to determine the effects of waste coal ash on landfill radon levels. The six acre site operated as a coal ash disposal landfill from 1945 to 1991 and is estimated to contain over 136 tons of coal ash (27: 1-1). Because the landfill contains a large quantity of coal ash and was operated for a long period of time, it was an ideal location for the experiment.

A sampling and analysis plan employing geostatistical and classical regression sampling techniques were used to estimate the mean activity levels of  $^{226}\text{Ra}$  (radon source potential) at the landfill and background locations.

Gamma spectroscopy was used as the laboratory analysis method. This method provided several advantages over alternative methods considered, but its main advantage was that it could be used to determine several radionuclides simultaneously (19: 64). Consequently, sample preparation was greatly simplified and costs held to a minimum.

Individual gamma peaks of each radionuclide were identified by placing the sample into a high resolution and high efficiency germanium detector for a two hour count time. Because the samples were presented to the detector in a constant geometry, preparations such as fusion, acid digestion, or ashing were not required.

The source potentials were compared using a two-sample t test with a 95% confidence level to determine if the landfill source potential was significantly higher than background.

Outdoor and indoor radon emanation levels were calculated using radon transport equations and the mean radon source potentials at the landfill and background locations. The resulting emanation levels at the landfill were compared to background emanation to determine the effects of the two source potentials.

Additionally, the indoor radon emanation concentrations resulting from the landfill and background source potentials were compared to established EPA guidelines. The same comparison was not be made for outdoor radon levels since there are no EPA guidelines for outdoor radon.

## **1.5 Research Objectives**

The purpose of this research is to determine the effects of landfilled waste coal ash on  $^{222}\text{Rn}$  source potential by sampling an ash landfill and measuring the source potential at the site. The landfill source potential was compared to the background source potential to determine if they were significantly different. Also, radon emanation into the atmosphere and into a structure, using the two source potentials, was calculated and compared. The research was accomplished through the following research objectives:

### **Objective 1**

Conduct an experiment that will facilitate accurate estimation and comparison of the radon source potentials at the ash landfill and background locations.

### **Research Question**

Which sampling technique will ensure the most accurate estimation of the source potential due to the technologically enhanced natural radiation?

### **Objective 2**

Determine the increased source potential, if any, due to the effects discovered in objective number one.

### **Research Question**

How does the radon source potential at the coal ash landfill compare to the source potential in background soil?

### **Objective 3**

Calculate radon emanation into the atmosphere and into a structure for the landfill and background source potentials.

### Research Questions

1. What equations can be used to calculate radon emanation into the atmosphere from uncovered soil?
2. What equations can be used to calculate radon emanation into a structure from the surrounding soil?

### **1.6 Thesis Organization**

Five chapters detail the development of an experiment that determined the effects of waste coal ash on radon source potential at a coal ash landfill and the associated radon emanation into the atmosphere and structure. Chapter 1 provides background on the subject of technologically enhanced natural radiation and coal combustion. Chapter 2 provides relevant background information and a review of past research in the subject area. Chapter 3 presents the methodology used to meet the stated research objectives. Chapter 4 shows the data collected and the analysis performed on the data. Finally, Chapter 5 presents the conclusions and recommendations.

## **2.0 Background**

### **2.1 Coal Consumption and Ash Generation**

In the early and mid 1970s, coal consumption in the US rose due to increased oil prices and growing shortages of oil and natural gas. In 1979, 680 million tons of coal were consumed which provided 20 percent of the heat and energy in the US (21: 63). This resulted in the generation and disposal of approximately 54.4 million tons of coal ash. In 1988, 69 million tons of coal ash were produced, and by the year 2000 the United States Environmental Protection Agency (USEPA) projects that the generation of coal ash will reach 108.8 million tons (8: 227). Presently, only 20% of the coal ash is re-utilized, primarily as an ingredient in Portland cement mixtures, with the remaining 80% disposed of in landfills or surface impoundments. Therefore, these disposal sites represent the greatest potential environmental impact of technologically enhanced natural radiation.

Increased coal consumption was also seen in the Department of Defense and the Air Force. In July 1977, Presidential Executive Order 12003 required each federal agency to adopt a 10 year agency energy management plan. As part of this plan, each agency was required to derive at least 10 percent of its energy from sources other than petroleum and natural gas (26: 2). As a result, the Air Force focused on converting its heat plants fueled by oil or natural gas to coal and completed a total of 12 coal-conversion projects during the 1980s. At present, the Air Force has 22 bases that utilize coal-fired heat plants, some of which have been in operation for over 40 years, each generating and

disposing of coal ash (16:109). For example, Wright Patterson AFB has three coal-fired heat plants that have been in operation since 1945 and over the last 10 years have generated and disposed of an average of 10,100 pounds of coal ash per year (16: 72). The ash was disposed of in an on base landfill until 1991 when the base obtained a contract to have the ash hauled off-site for disposal.

## **2.2 Past Research**

In an effort to determine the radiation hazard from coal burning plants, the radioactivity of coal and its byproducts must be obtained. Past research focused on accomplishing this task. In the late 1970's and early 1980's extensive research was conducted to determine the radioactivity in coals from various areas of the US. The results of the research revealed that the level of natural activity found in coal depends on the geographical area from which it was mined (3: 1523). For example, coal mined from areas in the northeast quarter of the US, such as Pennsylvania, Illinois, and Appalachia, had natural activity levels of uranium 238 ( $^{238}\text{U}$ ) that ranged from 1.7 to 1.9 pCi/g, while coal mined from areas in the southwestern quarter of the US, such as New Mexico and Utah, had natural activity levels of  $^{238}\text{U}$  that ranged from 0.20 to 0.281 pCi/g (19: 40).

Other research during this time focused on analyzing coal ash itself, the by-product of the coal combustion process. The resulting research, as previously mentioned, concluded that the combustion process concentrates the activities of naturally occurring radionuclides in the coal. Average increases range from 4 to 10 times original activity

levels found in the coal; however, the exact amount of increase depends on the type of coal used and the particular combustion process (19: 41).

Large amounts of coal ash are introduced into the environment by stack emissions. Several researchers have looked at the radiological effects of coal ash particles that escape from smoke stacks and deposit themselves in the top few inches of soil in the vicinity of the plant. Researchers have concluded that there is a significant increase in the concentration of naturally occurring radionuclides in the soil compared to background concentrations, mainly due to particles escaping from the stack (3: 1524, 14: 48). This increase is small, and at present does not pose an environmental hazard because the amount of particulate that actually reaches the atmosphere is small and what little escapes is dispersed over a large area. The small amount of particulate matter that escapes from the stack is usually about 0.5% to 1% of total coal ash produced (4: 689). Once released, it is usually dispersed over a large geographical area by winds. Depending on the wind speed and direction, the geographical area of dispersion can be as large as 625 square kilometers (14: 46). The result is little accumulation and relatively small activity levels.

While most of the research has focused on analyzing the ash itself and the ash that is released to the environment from the stacks, little research has been conducted to assess the radiological effects of coal ash that has been disposed of in landfills. Landfills store large amounts of coal ash for long periods of time. In fact, some landfills have been used as a burial place for waste coal ash for several decades and contain several hundred tons of the waste (26: 57). Disposing of a large amount of coal ash, coupled with the long

storage time, provides excellent opportunities for further research. One such opportunity encompasses determining the effects of waste coal ash on radon source potential at a landfill.

### **2.3 Radon Health Effects**

The effects of exposure to radon and its decay products was first mentioned relative to lung cancer mortality in Bohemian uranium miners in the early 1900s (22: 55). Since then, epidemiological studies of underground miners have provided consistent data on health risks associated with radon and its decay products. The major concern when discussing health risks of radon doesn't come from exposure to the radon gas itself, but from its decay products. As previously mentioned,  $^{222}\text{Rn}$  decays to a series of radionuclides that are chemically active, relatively short lived, and emit alpha particles upon decay. For example,  $^{218}\text{Po}$  has a half life of 3.11 minutes. This is long enough for the electrically charged polonium atoms to attach themselves to microscopic dust particles which can be inhaled. Once inhaled, these particles are usually deposited in the epithelial lining of the bronchi (25: 5-1).

Most of the inhaled dust particles are eventually cleared by mucus, but not quickly enough to keep  $^{218}\text{Po}$  and  $^{214}\text{Po}$  from decaying and emitting alpha particles. These particles penetrate the epithelial cells and can deposit enough ionizing energy to transform or kill them (25: 5-2). The transformed cell then has the potential to develop into lung cancer.



Even though the initial focus of environmental concern has been on indoor radon levels, outdoor radon levels still have potential for posing a health risk to humans. It also can contribute to the total amount of radon detected indoors. Recent studies have shown that of the total amount of radon found in a single family home, approximately 20% enters from outside air (23: 43). This percentage was found to be even larger in other types of buildings.

Also, outdoor radon levels are be a good indicator of radon sources beneath the soil. Assuming similar soil types (permeability, moisture, etc.) in a specific area, high levels of radon leaving the soil indicate a stronger radon source beneath the surface. This is important when deciding land use scenarios for closed coal ash landfills. High levels of radon may either preclude the building of family housing units or a day care center at the site or indicate the need for radon mitigation strategies (increased ventilation, etc.).

Several key characteristics of the soil affect the amount of radon that emanates from it. They can be grouped into two categories: radon availability and radon migration (23: 58). The first category, radon availability, includes those characteristics that influence the concentration of radon in the soil. The second category, radon migration, includes those characteristics that determine the movement of the radon from the soil into the atmosphere.

Figure 2.0 shows a schematic representation of these characteristics. The boxes represent the major states of radon from its generation in soil to its entry into structures. The labels on the horizontal arrows indicate a characteristic of the soil that is a measure of how readily the radon moves from one state to the next one. The labels on the vertical

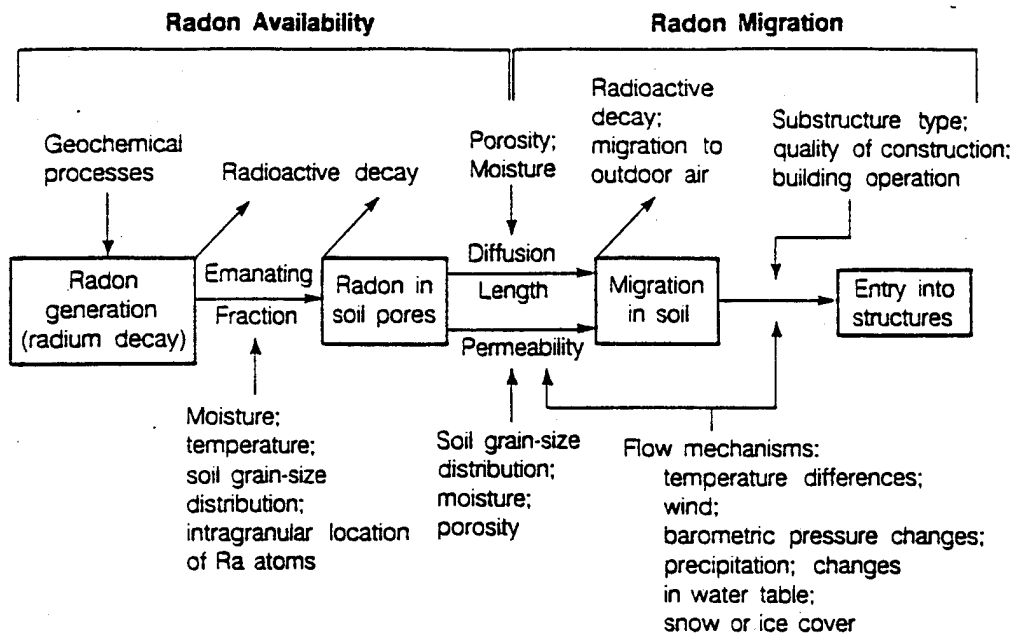


Figure 2.0 Radon Movement Characteristics. Ref 23.

arrows show the parameters and processes that influence the rate of transition from one state to the next. Finally, the labels on the diagonal arrows indicate the alternate paths of radon generated in the soil.

## 2.4 Radon Migration

There are two transport mechanisms that effect the emanation of radon from uncovered soil, forced convection and molecular diffusion. The forced convection

mechanism plays a major role in determining the amount of radon that enters a building, but only has a small effect on outdoor emanation calculations (22: 93). This is due to the fact that outdoor pressure gradients necessary for convective flow are relatively small. These gradients, which occur between the soil and the walls of the building, are generated by winds blowing on the side of building walls, temperature differences between the inside and outside building walls, and building ventilation systems.

Scientific investigations have indicated that diffusion alone cannot account for the high levels of indoor radon discovered in buildings, pressure differences between indoor and outdoor air seem to be the major determinant (25: 8-1). These pressure differences actually cause radon to be drawn into the structure through the structure floor and walls and any opening between the structure and the soil.

Even in well built structures, openings will exist. Generally, the openings are in the form of cracks in concrete floors and walls, floor drains, sumps, joints, and pores and cracks in hollow block and concrete floors and walls. The major entry routes are shown in Figure 2.1.

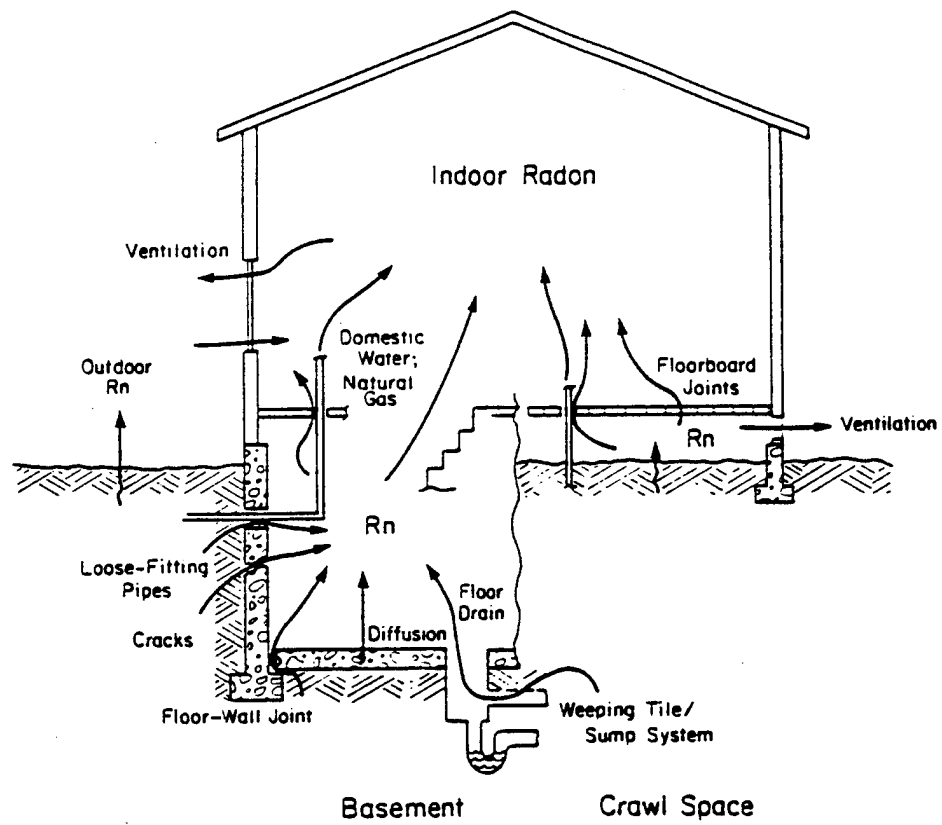


Figure 2.1 Radon Entry Routes. Ref 25.

## **3.0 Methodology**

### **3.1 Introduction**

This chapter includes the methods used to determine the effects of waste coal ash on radon source potential at the coal ash disposal area of landfill #5, Wright-Patterson AFB, and the associated amount of radon emanated into the atmosphere and into a structure. It begins with a description of the data collection and analysis strategy used to determine the source potential for radon production at the landfill. The chapter then shows the steps taken to collect and analyze background samples and compares the landfill radon source to the background radon source. Finally, it includes the methods and equations used to calculate the amount of radon emanating from the soil and into a structure.

### **3.2 Sampling and Analysis Plan (SAP)**

The Data Quality Objectives (DQO) process designed by the Environmental Protection Agency (EPA), coupled with the application of geostatistical analysis techniques, was used to develop the sampling and analysis plan (SAP). Although the DQO process was originally designed for Superfund sites, it is applicable to all collection activities. It consists of a series of planning steps shown in Figure 3.0 that are based on scientific methods designed to ensure that the type, quantity, and quality of environmental data used in decision making were appropriate for the intended application (23: 1).

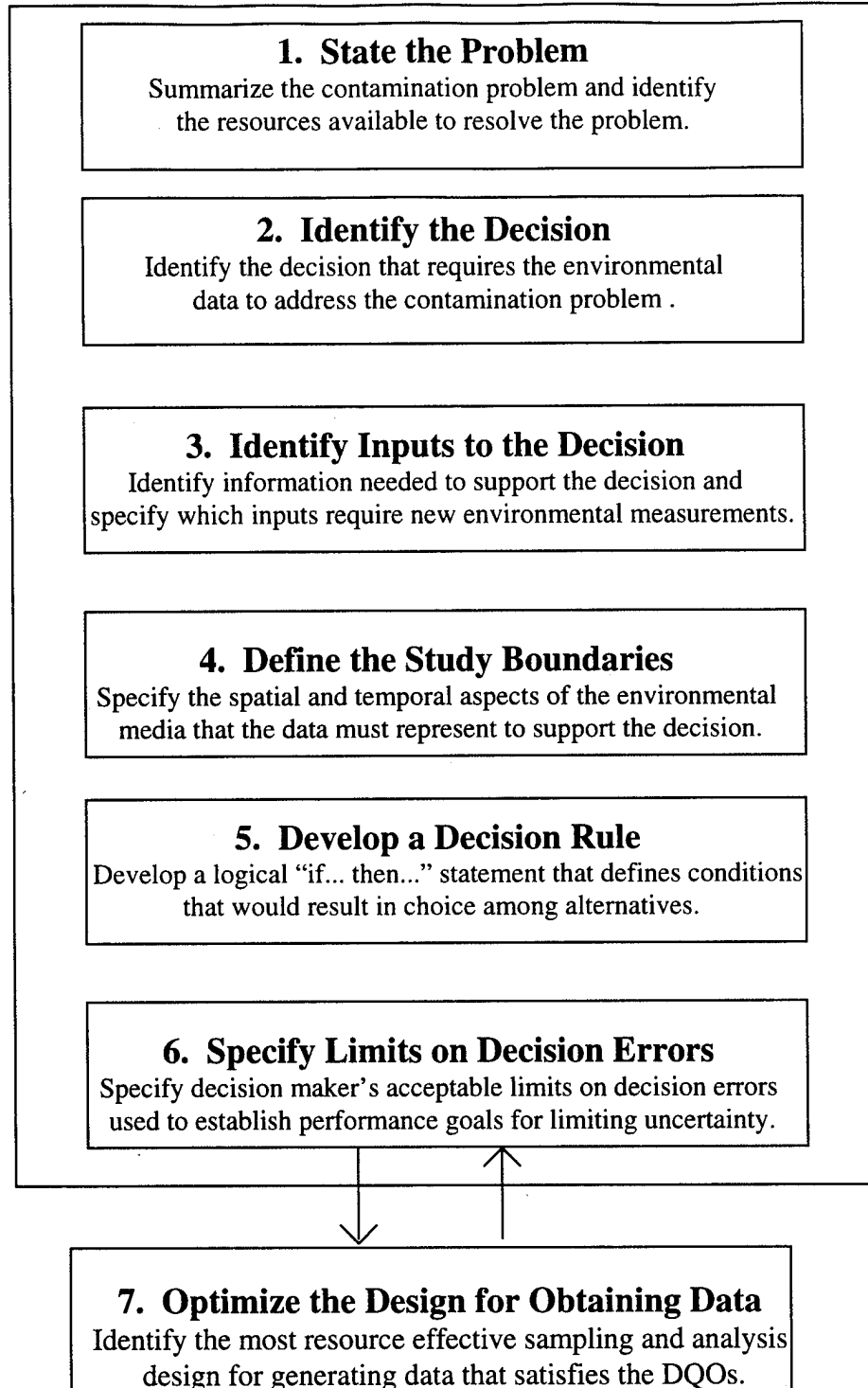


Figure 3.0 The Data Quality Objectives Process. Ref 24.

Geostatistical analysis techniques have been used for many years in the mining industry to efficiently characterize the distribution of one or more variables, such as mineral grades, in three dimensional space. These techniques can also be used in the environmental area to develop a more efficient soil sampling design, resulting in more precise data analysis. They do this by offering a way of describing the spatial correlation that is an essential feature of many natural phenomena found in soil and by providing adaptations of classical regression techniques to take advantage of this correlation (13: 1). However, if no spatial correlation exists, classical regression techniques are preferred because of their simplicity. A more detailed explanation of how this is accomplished can be found in Section 3.3.3, Geostatistical Analysis.

As a result of the DQO process and the use of geostatistical techniques, the data collection portion of the SAP was divided into two phases. The first phase consisted of a pilot study used to collect enough data to define the range of influence and correlative structure of the distribution of radionuclides in the landfill. Based on the results of the pilot study, which showed no spatial correlation (see Section 4.2, Pilot Study Results), traditional regression techniques were used in the second phase of the data collection. This phase, called the regular study, consisted of a survey of the area defined by the pilot study.

### **3.3 Pilot Study**

The pilot study consisted of three main processes. First, samples representative of the site were collected. Proper quality assurance/quality control measures coupled with

the fact that the nuclides of interest were non-volatile and fairly insoluble ensured accurate representation.

Next, the samples were analyzed using gamma spectroscopy to determine the types and activities of radionuclides present. Five nuclides were of particular interest;  $^{226}\text{Ra}$ ,  $^{214}\text{Pb}$ ,  $^{214}\text{Bi}$ ,  $^{40}\text{K}$ , and  $^{234\text{m}}\text{Pa}$ . The  $^{226}\text{Ra}$ ,  $^{214}\text{Pb}$ , and  $^{214}\text{Bi}$  nuclides were important because of their relationship to radon (parent and two daughters respectively).  $^{234\text{m}}\text{Pa}$  was important because of its possible secular equilibrium relationship with  $^{226}\text{Ra}$ . It may be in secular equilibrium with  $^{226}\text{Ra}$  if there was no segregation of the different elements during combustion. Although  $^{40}\text{K}$  is not in the  $^{238}\text{U}$  decay chain, it was important because its previous measurement in coal ash was well documented in literature. Comparisons with the literature values could easily be made if necessary.

Finally, geostatistical analysis techniques were used to check for and define any spatial correlation that might have existed. The use of geostatistical techniques is beneficial if spatial correlation in the data exists. However, the ash disposal techniques at the landfill consisted of dumping the ash and spreading it out with a bulldozer. This was suspected to result in a homogeneous layer of ash that would show no spatial correlation in the nuclide data and therefore render the geostatistical techniques less effective than traditional regression techniques. This information obtained in the pilot study was used to determine a course of action for the regular study.



### **3.3.1 Sample Collection**

A 500 x 500 foot square sampling grid was constructed to cover the ash disposal area. An aligned grid system shown in Figure 3.1 was used to determine 36 initial sampling points 100 feet apart, one at each node of the grid. This method was selected over random sampling and stratified sampling because it ensured complete coverage of the site shown in Figure 3.2, and was easier to implement under field conditions. Also, its randomly selected starting point ensured unbiased selection of sampling points (9: 89). However, since the ash landfill area was not exactly square, the four sampling points (#25, 26, 31, and 32) fell outside of the ash landfill area. These four points were not used as sampling locations. An additional 32 sampling points were located at 5, 10, and 20 foot intervals along a 200 foot transect extending north and a 200 foot transect extending east of grid location #22. (see Figure 3.1) The samples collected at these shorter intervals were required to provide the structure needed for geostatistical analysis.

After the grid was established at the site, a sample of the soil was taken at each designated location. A shovel was used to collect the samples down to 24 inches below the surface. This method has previously been proved to be most effective in collecting non-volatile soil samples at a depth of less than 5 feet (5: 85). The samples were placed in a 2.0 liter Marinelli beaker, sealed, properly labeled, and transported to the laboratory for analysis. Specific procedures for sample collection including decontamination procedures, quality assurance/quality control (QA/QC) measures, and safety plans can be found in Appendix A, Sampling and Analysis Plan.

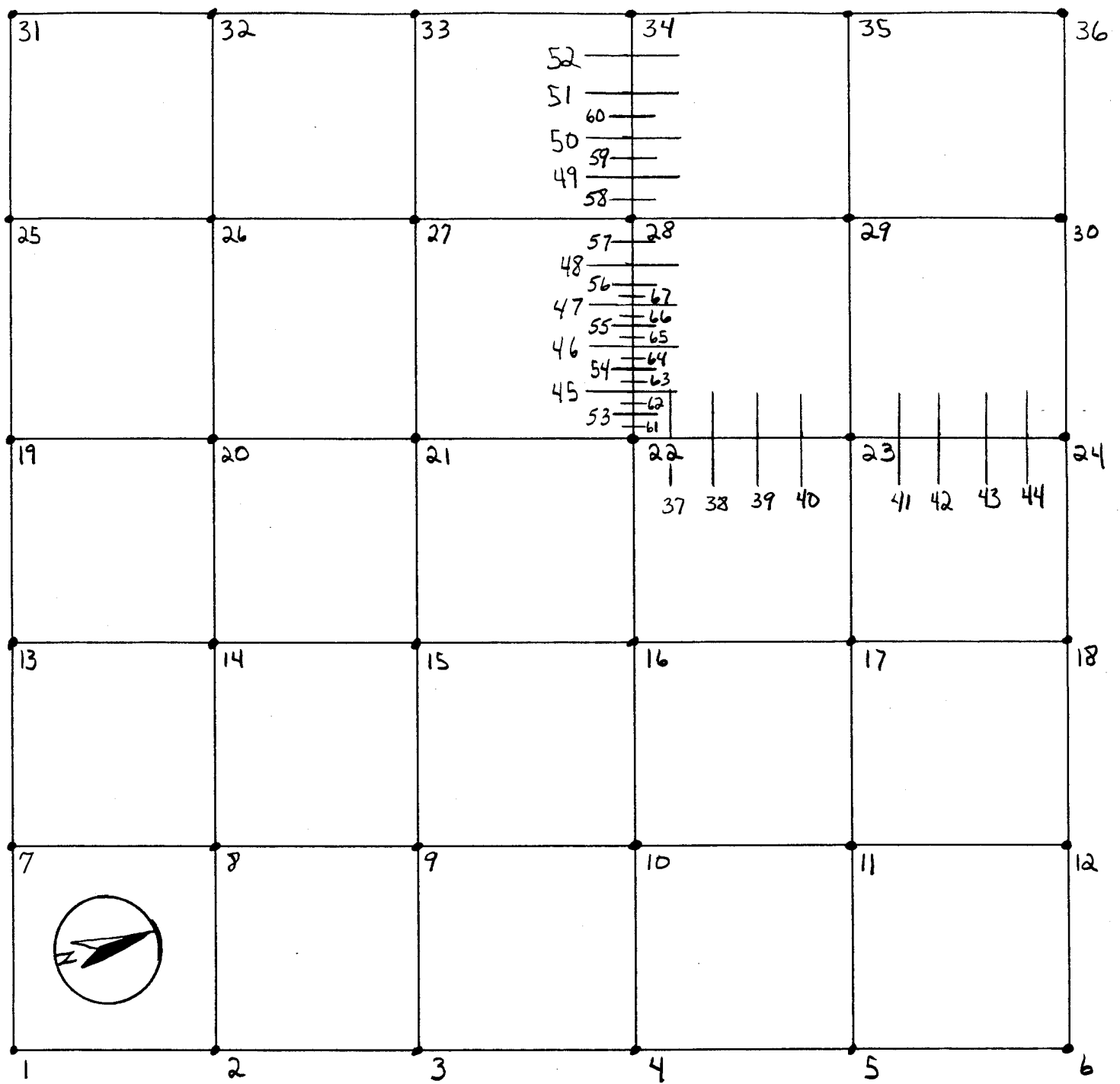


Figure 3.1 Sampling Grid Showing Pilot Study Sample Locations.

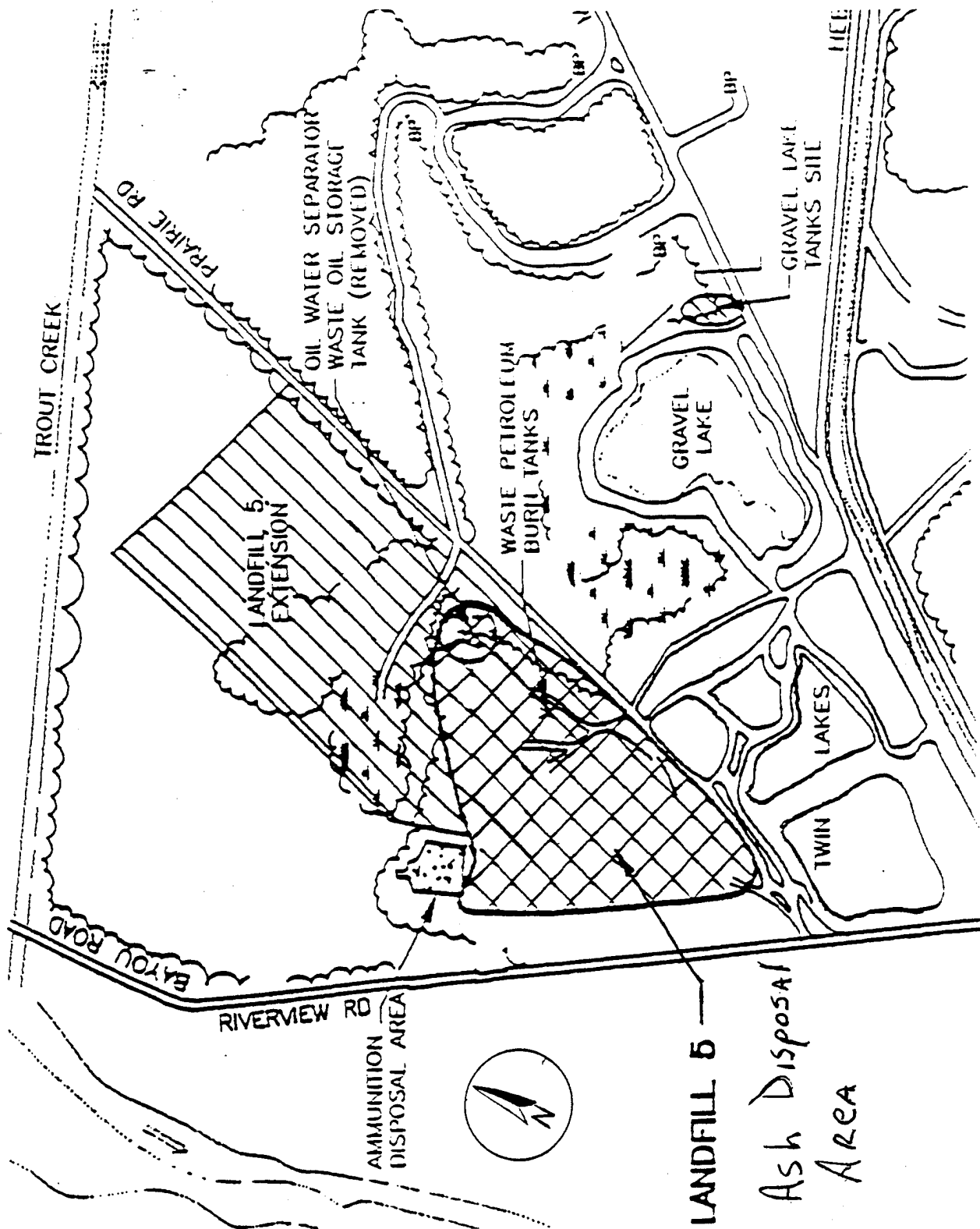


Figure 3.2 Base Ash Landfill Location Map

### **3.3.2 Sample Analysis**

Once at the lab, the samples were weighed and then analyzed using gamma spectroscopy. Gamma spectroscopy provided several advantages over alternative methods available. Its main advantage was that it required minimal sample preparation before presentation to the detector (19: 64).

A high-resolution/high-efficiency germanium detector built by the Canberra Corp. was used for the analysis. The detector is a semiconductor diode having a P-I-N structure in which the intrinsic (I) region is sensitive to ionizing radiation, particularly gamma rays (7: 1-1). Under reverse bias, an electric field extends across the intrinsic or depleted region of the semiconductor. When electrons produced by one of the three major types of gamma-ray interaction mechanisms (photoelectric absorption, Compton scattering, and pair production) interact with the material within the depleted region, charge carriers (holes and electrons) are produced and are swept by the electric field to the P and N electrodes (18: 50). The charge, which is proportional to the energy deposited in the detector, is converted into a voltage pulse by an integral charge sensitive preamplifier. The amplitude of the voltage pulse is proportional to the energy deposited. The pulses are fed to an analog-to-digital converter (ADC), from which the digitized pulses are passed to Canberra's GENIE-PC software. The software develops a histogram from the pulses and displays them as a spectrum.

Radionuclides in samples can be identified from the characteristic energies of gamma rays that they emitted. Also, the amount of each nuclide present in the sample

can be determined by the number of gamma rays depositing their full energy in the detector.

Before the energy of gamma rays and quantities of nuclides present in the samples can be determined, the pulse height scale of the detector must be calibrated in terms of absolute gamma-ray energy. To do this, a standard source with known quantities of several gamma-emitting nuclides was measured. The radionuclides in the source were uniformly dispersed in a matrix designed to simulate soil.

After calibrating the energy scale, the detector efficiency was calculated as a function of gamma-ray energy for each sample using the peak efficiency algorithm in the GENIE-PC software. After the efficiency was determined for each calibration peak, a least-squares fit was made to the polynomial expression shown in Equation 3.1.

$$\ln(\epsilon) = \sum_{i=0}^n (b_i) \cdot \ln(E)^i \quad (3.1)$$

Where  $\epsilon$  is the photopeak efficiency at energy  $E$ ,  $n$  is the degree of the polynomial,  $b_i$  is the number of counts, and  $E$  is the photopeak energy.

Landfill sample measurement consisted of placing the filled Marinelli beaker on the detector for a two hour count time. Also, a laboratory background measurement was made to identify spectral peaks resulting from the environment. This background

component will be subtracted from the sample measurement to give a corrected net peak area.

Peaks in the landfill sample and background spectra were identified using the peak locate algorithm in the GENIE-PC software. Many of the identified peaks in the spectra corresponded to full-energy depositions in the detector. The energies were assigned to the centroid of each peak using the measured energy calibration.

The area of each identified peak in both the landfill sample and background spectra was calculated using a non-linear least squares fit algorithm in GENIE-PC. The algorithm fit the identified peaks to a Gaussian function which yielded peak height and width. From this fit, the gross peak area (A) was determined by Equation 3.2 (7: B-39).

$$A = h \cdot Z \cdot \sqrt{\pi} \quad (3.2)$$

Where h is the height of the peak and Z is a measure of the peak width ( $Z^2 = 2\sigma^2$ , where  $\sigma$  is the Gaussian standard deviation).

For any of the peaks in the landfill sample spectrum, that matched peaks in the background, the area of the background peak was corrected for live time and then was subtracted from the landfill sample peak using Equation 3.3 to obtain the corrected net peak area.

$$A_{\text{net}} = A_s - \left( \frac{T_{Ls}}{T_{Lb}} \right) \cdot A_b \quad (3.3)$$

Where  $A_{\text{net}}$  is the corrected net peak area,  $A_s$  is the peak area of the landfill sample,  $A_b$  is the background peak area,  $T_{Ls}$  is the live time of the landfill sample, and  $T_{Lb}$  is the live time of the background sample.

The uncertainty in the sample and background peak areas ( $\sigma_s$  and  $\sigma_b$ ) are related to the square root of the peak areas. These uncertainties can be propagated to the uncertainty in the net area using Equation 3.4.

$$\sigma_{\text{net}}^2 = \sigma_s^2 + \left( \frac{T_{Ls}}{T_{Lb}} \right)^2 \cdot \sigma_b^2 \quad (3.4)$$

Where  $\sigma_{\text{net}}^2$  is the uncertainty in the net peak area,  $\sigma_s^2$  is the uncertainty in the landfill sample peak area, and  $\sigma_b^2$  is the uncertainty in the background peak area.

The net area of each peak was divided by its efficiency to give a best estimate of the number of gamma rays that were emitted by the sample at that energy. The efficiency was assigned to each peak using the efficiency calibration previously discussed. Equation 3.5 shows the calculation of the number of gamma rays emitted.

$$N_j = \frac{A_{netj}}{\epsilon_j} \quad (3.5)$$

Where  $N_j$  is the number of gamma rays emitted by the sample at the energy of peak  $j$ ,  $A_{netj}$  is the net area of peak  $j$ , and  $\epsilon_j$  is the efficiency of peak  $j$ . Also, the uncertainty in the number of gamma rays emitted can be computed using Equation 3.6.

$$\sigma_{Nj}^2 = \left( \frac{\sigma_{netj}}{A_{netj}} \right)^2 + \left( \frac{\sigma_{\epsilon j}}{\epsilon_j} \right)^2 \quad (3.6)$$

Where  $\sigma_{Nj}$  is the uncertainty in the number of gamma rays emitted at energy  $j$ ,  $\sigma_{netj}$  is the uncertainty in the net area at energy  $j$ , and  $\sigma_{\epsilon j}$  is the error in efficiency at energy  $j$ .

The gamma-ray emission rate for a particular energy  $j$ , was found by dividing the number of emitted gamma rays at energy  $j$  by the live time for the sample measurement (see Equation 3.7).

$$R_j = \frac{N_j}{T_{Ls}} \quad (3.7)$$

Where  $R_j$  is the gamma ray emission rate at energy  $j$ . Also, the uncertainty in the emission rate was found using Equation 3.8.



$$\sigma_{Rj}^2 = \left( \frac{\sigma_{Nj}}{T_{Ls}} \right)^2 \quad (3.8)$$

Where  $\sigma_{Rj}$  is the uncertainty in the gamma ray emission rate at energy j.

To identify the radionuclides detected, the energy for each peak in the sample spectrum was compared to a data base of radionuclides by the GENIE-PC nuclide identification algorithm. The data base includes the energies and intensities (the number of photons emitted per decay) of all known gamma rays emitted by the bulk of the known radionuclides.

The activity of every identified radionuclide was estimated from each corresponding gamma-ray energy found in the sample spectrum using Equation 3.9.

$$Act_{kl} = \frac{R_{kl}}{I_{kl}} \quad (3.9)$$

Where  $Act_{kl}$  is the activity of the  $k^{th}$  identified radionuclide computed from its  $l^{th}$  gamma energy,  $R_{kl}$  is the emission rate of the  $l^{th}$  gamma energy of that radionuclide, and  $I_{kl}$  is the intensity of the  $l^{th}$  gamma energy for that radionuclide. Also, the uncertainty of the activity was estimated using Equation 3.10.

$$\sigma_{\text{Actkl}}^2 = \left( \frac{\sigma_{\text{Rkl}}}{I_{\text{kl}}} \right)^2 \quad (3.10)$$

Where  $\sigma_{\text{Actkl}}$  is the uncertainty of the activity of the  $l^{\text{th}}$  gamma energy of the  $k^{\text{th}}$  identified radionuclide,  $\sigma_{\text{Rkl}}$  is the uncertainty of the emission rate of the  $l^{\text{th}}$  gamma energy of the  $k^{\text{th}}$  identified radionuclide, and  $I_{\text{kl}}$  is the intensity of the  $l^{\text{th}}$  gamma energy for the  $k^{\text{th}}$  identified radionuclide.

Finally, a penalty function is assigned for each gamma energy of a nuclide that is near an observed gamma peak based on the difference between the reference and measured energy,  $\Delta E_i$ . The confidence value, which starts out as 1.0, is multiplied by the penalty function shown in Equation 3.11 to obtain the final nuclide identification confidence (7: B-57).

$$f(\Delta E_i) = \exp \left[ \frac{-\frac{0.16}{\text{ETOL}} \cdot \Delta E_i^2 \cdot y_i}{\sum_i y_i} \right] \quad (3.11)$$

Where ETOL is a user-selected energy tolerance,  $\Delta E_i$  is the difference between the reference energy and the measured energy for the  $i^{\text{th}}$  peak, 0.16 is an empirical constant, and  $y_i$  is the branching ratio. Also, if at least one matching energy has been found for a radionuclide, the confidence value is further reduced by Equation 3.12.

$$\text{Confidence}_{\text{new}} = \text{Confidence} - 1.6 \frac{u}{T} \quad (3.12)$$

Where  $\text{Confidence}_{\text{new}}$  is the resulting confidence value, Confidence is the old confidence value, 1.6 is an empirical constant,  $u$  is the sum of gamma yields of all the lines that did not have a matching observed energy, and  $T$  is the sum of all gamma yields reported in the library for the nuclide in question.

It should be noted that the GENIE-PC software doesn't determine contributions of two radionuclides to a single peak. This determination must be done manually. For example,  $^{235}\text{U}$  has been identified with the following energies and percent yields:

Table 3.0  $^{235}\text{U}$  Energies and Yields

Energy (keV)	Yield (%)
89.96*	1.50
93.35*	2.50
105.00	1.00
109.14	1.50
143.76	10.50
163.35	4.70
185.71*	54.00
202.12	1.00
205.31	4.70

\* = Energy line found in spectrum.

Three peaks were found in the  $^{235}\text{U}$  spectrum. The peaks at 89.96 keV and 93.35 keV were also found in  $^{228}\text{Ac}$ . Rather than determining the contribution of each nuclide to the 89.96 keV and 93.35 keV peaks, GENIE-PC assigned the full activity detected to each peak in both nuclides. It was up to the user to determine the individual contributions of each nuclide. This was done by analyzing the GENIE-PC output.

The output showed that  $^{228}\text{Ac}$  had 14 peaks, all of which were found resulting in an overall identification confidence of 0.994.  $^{235}\text{U}$  had 9 peaks, of which only three were found resulting in an overall identification confidence of 0.527. Two of the three  $^{235}\text{U}$  peaks were found in  $^{228}\text{Ac}$ . The other  $^{235}\text{U}$  peak (185.71keV), was found in  $^{226}\text{Ra}$  which had an overall identification confidence of 1.00. The fact that the only peaks found in  $^{235}\text{U}$  were also found in other nuclides ( both of which had higher identification confidences), indicated that the existence of  $^{235}\text{U}$  in the sample was suspect.

Further analysis of the energies in the  $^{235}\text{U}$  spectrum supports the idea that  $^{235}\text{U}$  is below detectable limits. The 143.76 keV energy has a 10.5% yield compared to 1.5% and 2.5% for the 89.96 keV and 93.35 keV energies. If  $^{235}\text{U}$  was present in the sample, the 143.76 keV line would be expected to be identified before the 89.96 keV and 93.35 keV lines because of its higher yield, and it was not.

### **3.3.3 Geostatistical Analysis**

Geostatistical techniques were used to perform structural analysis of the radionuclides of interest. The analysis was divided into in three steps. The first step, univariate description, was conducted to determine any indications of aberrant data (to

include skewness), the shape of the distribution, and the number of underlying distributions, if any. The second step, spatial description, was used to obtain an understanding of any spatial features such as location of extreme values and overall trend. Finally, step three, descriptive structural analysis, was conducted to obtain the best empirical semivariogram to allow formal modeling and generation of the covariance matrix needed to perform estimation.

### **3.3.3.1 Univariate Description**

Step one of the geostatistical analysis involved using STATISTIX 4.0 analytical software package to conduct the univariate description of the five radionuclides of interest (2:1). Descriptive statistics were calculated for each radionuclide to include the mean, median, standard deviation, and coefficient of variation (CV). The mean  $m$ , is the arithmetic average of the data values and was calculated using Equation 3.13.

$$m = \frac{1}{n} \cdot \sum_{i=1}^n x_i \quad (3.13)$$

Where  $m$  is the mean,  $n$  is the number of data points, and  $x_i$  is an individual data value.

The median  $M$  is the midpoint of the observed values arranged in increasing order. Half the values are below the median and half the values are above the median. It was calculated using either Equation 3.14 or 3.15.

$$M = x_{\frac{n+1}{2}} \quad \text{if } n \text{ is odd} \quad (3.14)$$

$$M = x_{\frac{n}{2}} + x_{\frac{n}{2} + 1} \quad \text{if } n \text{ is even} \quad (3.15)$$

Both the mean and median were used as measures of the location of the center of the distribution.

The standard deviation  $\sigma$  is the average difference of the observed values from their mean was calculated using Equation 3.16.

$$\sigma = \sqrt{\frac{1}{n} \sum_{i=1}^n (x_i - m)^2} \quad (3.16)$$

Finally, the covariance (CV) is the ratio of the standard deviation to the mean. It was primarily used to detect skewness of the distribution and was calculated using Equation 3.17.

$$CV = \frac{\sigma}{m} \quad (3.17)$$

These statistics were used to develop three checks for outliers and skewness. The CV was used in the first check. A CV greater than one indicated the presence of erratic values which could impact later estimation. The second check used a box and whiskers plot to give visual indication of both skewness and presence of outliers. The box plot consists of a box and two whiskers. The box encloses the data between the first and third quartiles (the middle half of the data). The box is bisected by a line at the median value.

The whiskers are vertical lines at the top and bottom of the box and they show the range of typical data values. Extreme values are shown as either an asterisk or the letter "O". For example, Figure 3.3 shows a box and whisker plot that displays both skewness and the presence of extreme values. The skewness is represented by the position of the

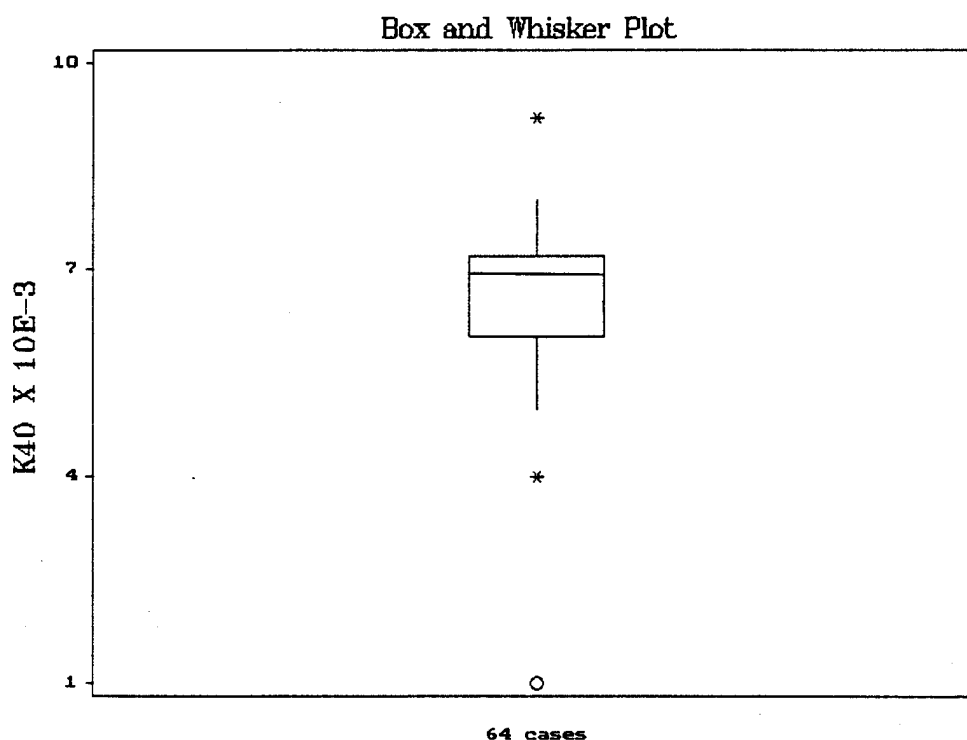


Figure 3. 3 Box and Whisker Plot Showing Skewed Data and Extreme Values.

median line. The median line within the top or bottom quarter of the box, as shown, indicates the possibility of skewed data. The extreme values are represented by the asterisk and circle located away from the box and whisker plot.

The third check used a histogram as another visual indicator of skewness and outliers. A visual check of the histogram data of each nuclide was conducted for skewness and extreme values. Figure 3.4 shows an example of a histogram of data that is skewed and has extreme values. The data appears to be slightly skewed to the right of the

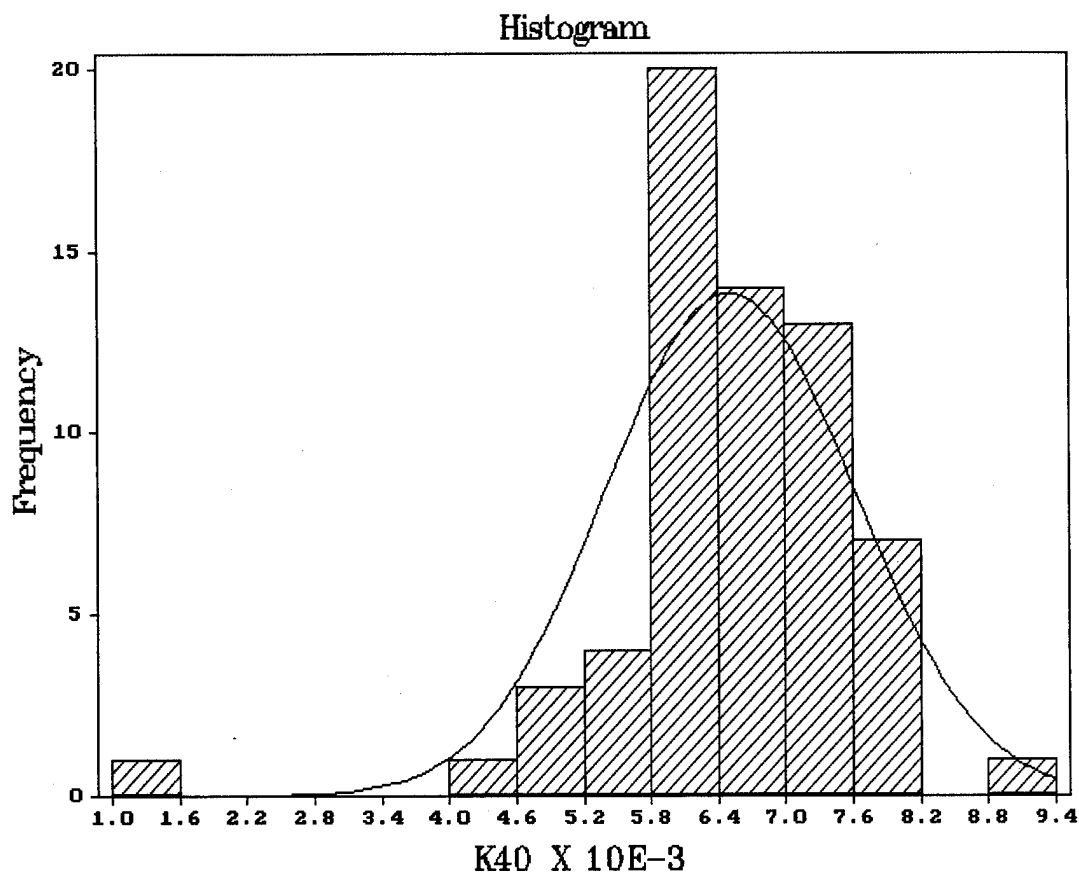


Figure 3.4 Histogram Showing Skewed Data and Extreme Values.



normal curve superimposed over the histogram and an extreme value appears outside the curve. Each of the radionuclides of interest were subjected to the three tests described in this section. The results of the tests are discussed in Section 4.2, Univariate Analysis Results.

The shape of the distribution of each radionuclide of interest was also observed. The histograms and box and whiskers plots generated using the statistical software package STATISTIX 4.0 were used to test the data for symmetry. Since the data appeared to be symmetric (see Section 4.2.1), a rankit plot and Wilk-Shapiro (WS) normality statistic, also generated using STATISTIX 4.0, were constructed to check for normality. If the distribution on which the rankit plot is based is normally distributed, the points in the plot will fall close to a straight line (9: 171). The WS normality statistic is the square of the linear correlation between the rankit plot points (2: 246).

If the rankit plot resembled a straight line and the WS number was greater than 0.90, then the data was considered to have a single normal distribution. If the WS number was less than 0.90, the distribution was considered to be other than normal and nonparametric techniques would be used for later estimation. For example, Figure 3.5 shows the rankit plot and WS normality statistic for a hypothetical data set that is not normally distributed. While the center portion of the plot resembles a straight line, the extreme values at either end indicate other than a straight line fit. Also, the WS normality statistic value of 0.84 is less than 0.90 which also indicates non-normality.

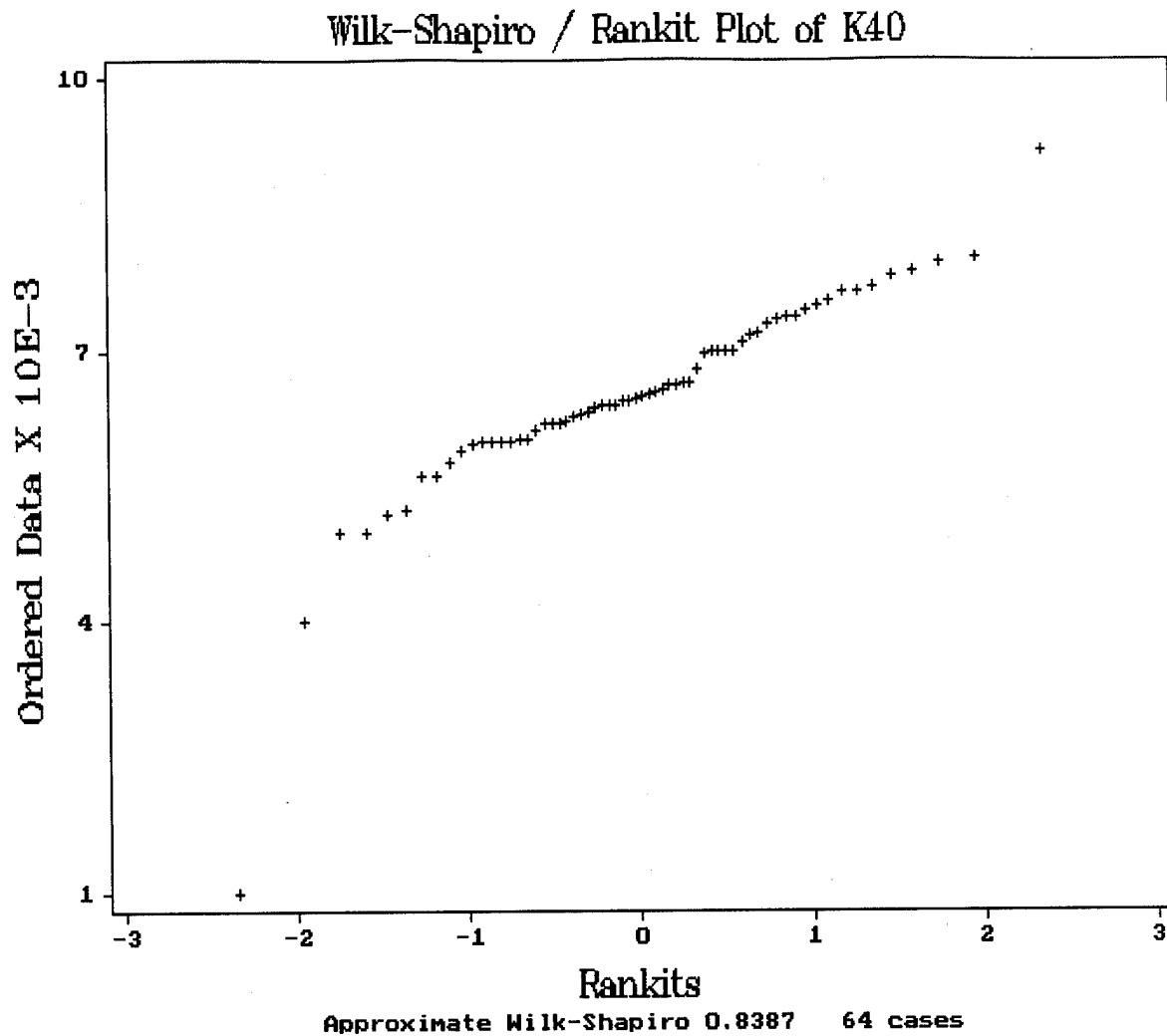


Figure 3.5 Rankit Plot and WS Normality Statistic.

### **3.3.3.2 Spatial Description**

In this step, spatial correlation of the data was determined and described. If correlation exists, the spatial description will be used to determine any anisotropies which

will be used to perform structural analysis. If no spatial correlation exists, then traditional statistical methods will be used to estimate the mean concentrations of the radionuclides at the landfill.

The spatial description step began with another look at the results of the univariate study to try to describe any aberrant data. Aberrant data located sporadically around the site might indicate mistakes in data entry or transcription. On the other hand, aberrant data located together might indicate quality control problems such as cross contamination or the data may be real, but it may be from different populations. In order to determine if the aberrant data was sporadically located or located together, surface plots were used. The data values obtained at each grid location for each radionuclide were plotted using MATHCAD 5.0 to relate outliers with spatial locations. The surface plots were visually analyzed to determine any of the conditions discussed above. Any abnormally large peaks or valleys in the surface plots were noted.

Next, spatial description of any trends present was conducted. Again, the surface plots were used, but this time overall trends in the data were analyzed. Any trends in data values versus location were studied to determine the existence of gradual gradients. Presence of the gradients would indicate a natural physical environmental process operating.

Also, the location of the highest and lowest values were analyzed to determine any possible trends in the data. Extreme values located close to each other could be an indicator of high spatial variability. If they were not located close to each other, the locations should be compared to any trends observed in the data.

Overlapping moving window statistics was another tool used to determine trends in the data. In overlapping moving window statistics, the gridded area was divided into windows of equal size. In this case, the window was a two by two grid point square (100 ft by 100ft). The mean of the four corner values in the window were calculated. Also, in order to identify anomalous localities and to give more data points for analysis, the windows overlapped each other. For example, the first two points in the succeeding window are the last two points in the previous window. This resulted in 25 windows, each containing four data points. Surface plots of the window values were developed using MATHCAD 5.0 and visually analyzed to determine any trends across the grid.

#### **3.3.3.3 Descriptive Structural Analysis**

In this step, variogram analysis of the data was performed to describe any spatial continuity that might have existed. It involved comparing pairs of data values at various distances apart and in various directions. More specifically, the variogram value  $\gamma(h)$ , which is half the average squared difference between the paired data values at a separation distance  $h$ , was calculated using Equation 3.18 (13:142).

$$\gamma(h) = \frac{1}{2 \cdot N(h)} \sum_{h_{i,j}} (v_i - v_j)^2 \quad (3.18)$$

Where  $N$  is the number of pairs of data points at that distance  $h$  and  $v_i$  and  $v_j$  are the data points associated with the pair being evaluated.

The variogram has certain properties that need to be presented before further discussion continues. The definition of the variogram as the variance of increments entails the following properties:

$$\gamma(0) = 0, \text{ and } \gamma(h) = \gamma(-h) \geq 0$$

Which means that at a separation distance of zero feet, you should be evaluating the same point and therefore should see no difference in the points which results in a  $\gamma(0)$  value of zero. Also, as the distance  $h$  increases, the variance of the two points being evaluated tends to increase so  $\gamma(h)$  increases from its initial value of zero as shown in Figure 3.6. The semi-variogram stops increasing beyond a certain distance and becomes stable around a limit value  $\gamma(\infty)$  called a “sill” value (15:12Q).

Finally, the variogram discontinuity at the origin is called the “nugget effect” and is due to both measurement errors and to micro-variability in the soil (15: 12S).

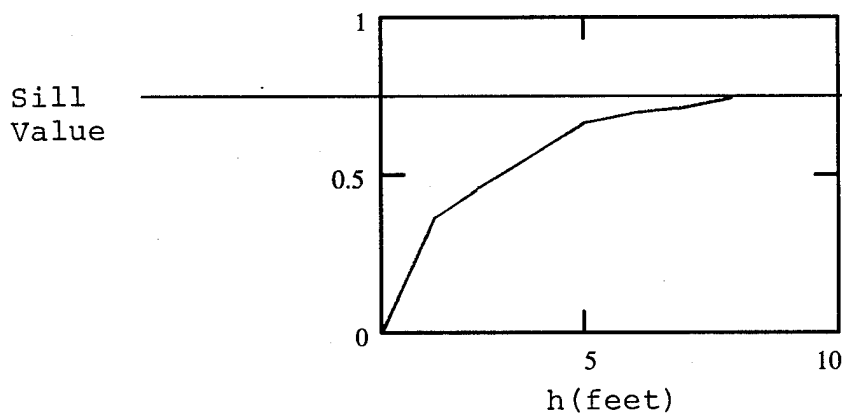


Figure 3.6 . Semivariogram.

Figure 3.7 (a) shows a nugget effect. The  $\gamma(h)$  value at  $h$  equal to zero should be zero, but due to measurement errors and to micro-variability in the soil it is actually 0.30. Figure 3.7 (b) shows a pure nugget effect. A “pure nugget effect” occurs when  $\gamma(h)$  appears solely as a discontinuity at the origin and corresponds to total absence of correlation. A pure nugget effect indicates that no matter how small the distances between the evaluated pairs, the corresponding  $\gamma(h)$  value will be at its sill value.

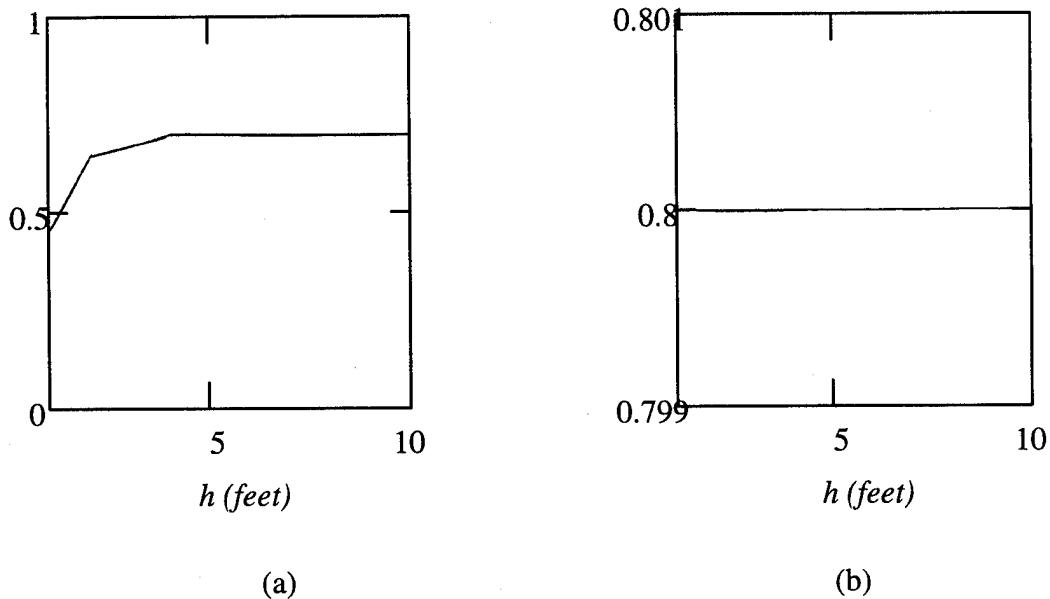


Figure 3.7 Behavior Near the Origin. (a) Nugget Effect; (b) Pure Nugget Effect.

For this thesis an omnidirectional variogram was developed using GSLIB software program. It was used because it had a large directional tolerance which, in effect, combined all possible directions into one variogram where only the magnitude of  $h$  was important. It can be thought of as an average of various directional variograms, which are variograms with small tolerances along the directional anisotropies (13: 143).

Also, since it contained more sample pairs than any directional variogram, it was more likely to show a clearly interpretable structure.

### **3.4 Regular Study**

Based on the results of the pilot study (see Section 4.2, Pilot Study Results), which showed no spatial correlation in the data, traditional regression techniques were used in the second phase of the data collection. This phase, called the regular study, consisted of a survey of the area defined by the pilot study.

#### **3.4.1 Sample Collection**

The pilot study data was used to determine the number of samples  $n$  required to estimate the mean levels of the radionuclides at the site. Using a prespecified relative error ( $d_r$ ) of 10 percent, Equation 3.19 was used to calculate the number of samples required.

$$n = \left[ \frac{Z_{1-\frac{\alpha}{2}} \cdot \left( \frac{s}{\bar{x}} \right)}{d_r} \right]^2 \quad (3.19)$$

Where  $Z_{1-\alpha/2}$  is the standard normal deviate or critical value using an  $\alpha$  of .05 (corresponding to a 95% confidence level),  $s$  is the standard deviation of the sampling

distribution, and  $\bar{x}$  is the mean of the sampling distribution. The following table shows the results of the calculations.

TABLE 3.1  
The Number of Samples Required for the Regular Study.

Radionuclide	Sample Size $n$
$^{40}\text{K}$	15
$^{214}\text{Bi}$	47
$^{214}\text{Pb}$	49
$^{234\text{m}}\text{Pa}$	48
$^{226}\text{Ra}$	43

Since 64 samples were collected in the pilot study, therefore no more samples were collected and analyzed in the regular study.

### **3.4.2 Statistical Analysis**

Since the data was uncorrelated, the Equation 3.20 was used to calculate an unbiased estimator of the mean activity of each nuclide of interest.

$$\bar{x} = \frac{1}{n} \sum_{i=1}^n x_i \quad (3.20)$$

Also, the unbiased estimator of the variance of the mean activity level ( $s^2$ ) was calculated using Equation 3.21.



$$s^2 = \frac{1}{n-1} \sum_{i=1}^n (x_i - \bar{x})^2 \quad (3.21)$$

These values were used to calculate the radon emanation from the uncovered landfill soil and radon emanation into a structure.

### **3.5 Background Study**

In order to determine the relationship between the radon source potential at the landfill and normal levels found in the soil, background samples were collected and analyzed. The samples were collected from undisturbed areas that were near the ash landfill to ensure that the soil would exhibit levels of the radionuclides representative of the natural surrounding area.

#### **3.5.1 Sample Collection**

Three samples were collected, one from each location shown on the map in Figure 3.8. The samples were collected and handled in the same manner as the pilot study samples. After the sampling location was established, a shovel was used to collect a sample down to 24 inches below the surface. The sample was placed in a 2.0 liter Marinelli beaker, sealed, properly labeled, and transported to the laboratory for analysis. Specific procedures for sample collection including decontamination procedures, quality

assurance/quality control (QA/QC) measures, and safety plans can be found in Appendix A, Sampling and Analysis Plan.

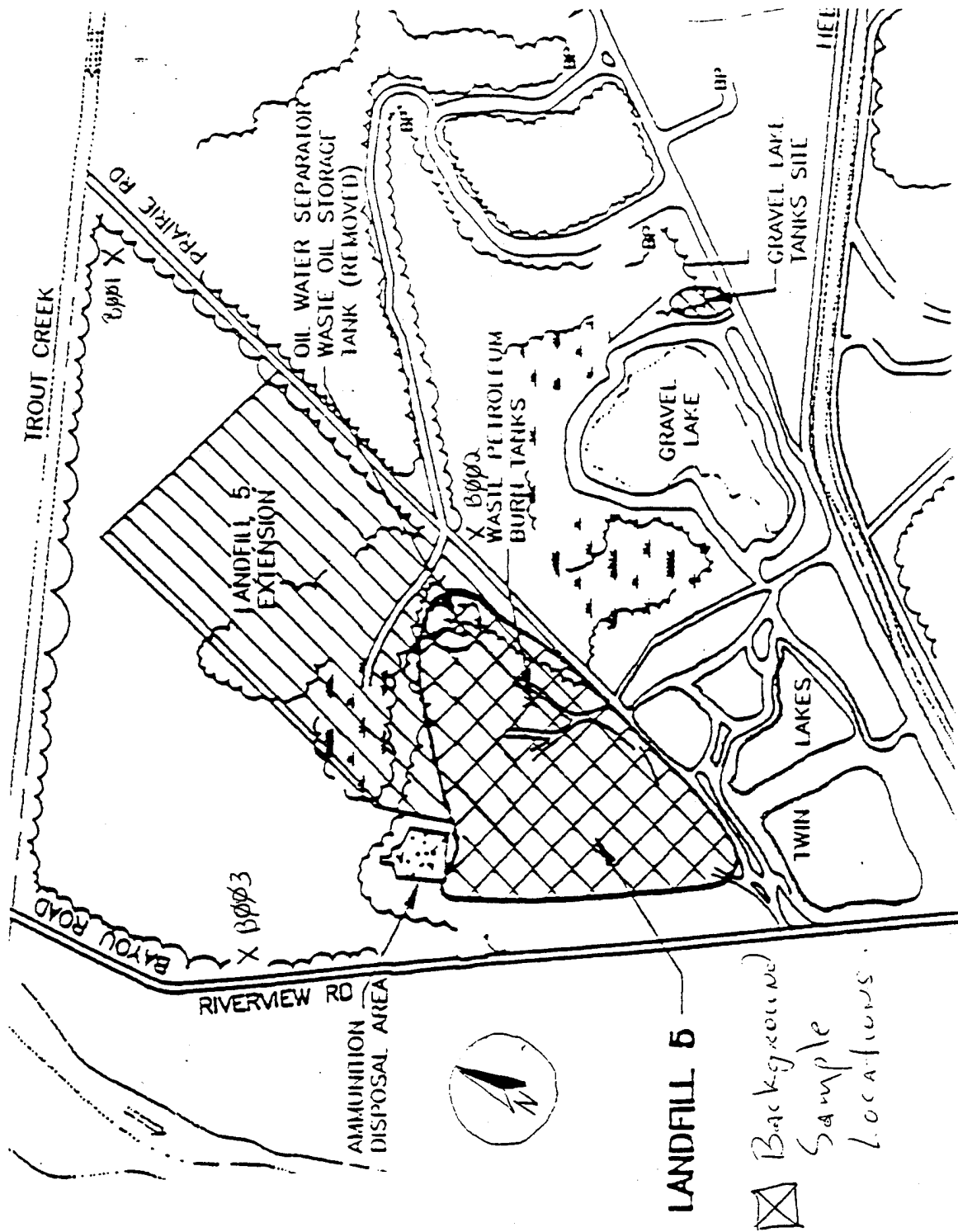


Figure 3.8 Background Sample Locations.

### **3.5.2 Sample Analysis**

Once at the lab, the samples were weighed and analyzed using gamma spectroscopy. Individual gamma peaks of each radionuclide of interest were identified by placing the sample directly onto the detector for a two hour count time. The same procedures followed in the pilot study were used here for analysis of the background samples (see Section 3.3.2, Sample Analysis).

### **3.6 Radon Source Potential Comparison**

After determining the mean radon source potential of the ash landfill and background locations, the two were compared using a two-sample t test to determine if the source at the ash landfill was significantly higher than background. A two-sample t test was applied to the landfill and background mean  $^{226}\text{Ra}$  activities. The two-sample t test was used because the sample size of the background sampling effort was small (less than 30) and the variance of the population was unknown. This test was also chosen because it offered a minimum beta ( $\beta$ ) value which is the probability of not rejecting  $H_0$  when  $H_0$  is false (Type II error).

In order to use the two sample t, two assumptions had to be made. First, both populations were assumed to be normal, so that  $X_1, X_2, \dots, X_m$  (regular study) was a random sample from a normal distribution and so was  $Y_1, Y_2, \dots, Y_n$  (background study) with the X's and Y's independent of one another. The second assumption made was that the value of the two population variances  $\sigma_1^2$  and  $\sigma_2^2$  were equal, so that their common

value could be denoted by  $\sigma^2$  (which is unknown) (9: 338). Since  $\sigma^2$  was unknown it was estimated using equation 3.22.

$$S_p^2 = \frac{(m-1) \cdot S_1^2 + (n-1) \cdot S_2^2}{m+n-2} \quad (3.22)$$

Where  $S_p^2$  is the pooled estimator of the population variance,  $S_1^2$  and  $S_2^2$  are the two sample variances (regular study and background study), and  $m$  and  $n$  are the sample sizes for the regular study and background study respectively. This estimate, commonly known as the pooled estimator, depends on both the  $X_i$ s and the  $Y_i$ s. As might be expected, more weight was given to the sample that corresponded to the larger of the two sample sizes.

Once the estimator of the population variance was calculated, the following two-sample t test was derived for testing.

$$H_0: \mu_1 - \mu_2 = 0$$

$$H_a: \mu_1 - \mu_2 > 0$$

The null hypothesis ( $H_0$ ) was that the mean  $^{226}\text{Ra}$  activities of the landfill and background study populations ( $\mu_1$  and  $\mu_2$  respectively) were equal. If they were equal, then  $\mu_1 - \mu_2$  would equal zero. The alternate hypothesis ( $H_a$ ) was that the mean  $^{226}\text{Ra}$  activity of the landfill population was greater than the background study population. If this were true,  $\mu_1 - \mu_2$  would be greater than zero.

A test statistic was calculated using Equation 3.23 to test the hypothesis.

$$t = \frac{\bar{X} - \bar{Y}}{S_p \sqrt{\frac{1}{m} + \frac{1}{n}}} \quad (3.23)$$

Where  $S_p$  is the pooled estimator of the population variance,  $\bar{X}$  and  $\bar{Y}$  are estimators of  $\mu_1$  and  $\mu_2$  respectively, and  $m$  and  $n$  are the regular study and background study sample sizes respectively.

If the  $t$  statistic was greater than the  $t$  critical value then the null hypothesis would be rejected. The  $t$  critical value was obtained from a table of critical values for  $t_{\alpha, m+n-2}$ . Where  $t_{\alpha, m+n-2}$  is the  $100(1-\alpha)$ th percentile of the  $t$  distribution with  $m+n-2$  degrees of freedom and  $\alpha$  equal to 0.05. Therefore, the rejection region would be:

$$t \geq t_{\alpha, m+n-2}$$

The test was set up so that if the null hypothesis was accepted it would mean that  $\mu_1$  and  $\mu_2$  were equal and the landfilled coal ash had no effect on the  $^{226}\text{Ra}$  activity. The alternative, or researcher's hypothesis was set up so that if the null hypothesis was rejected in favor of the alternate, it would indicate that the regular study  $^{226}\text{Ra}$  mean activity was statistically significantly greater than the background study  $^{226}\text{Ra}$  mean

activity. In other words, the landfilled coal ash resulted in a statistically significant increase in  $^{226}\text{Ra}$  activity.

### **3.7 Outdoor Radon Emanation**

Transport Equation 3.24 was used to model the molecular diffusion mechanism for outdoor radon emanation (23: 86). Once radon atoms are produced by radium decay in soil, they fill the soil pore spaces and can diffuse through the soil and reach the atmosphere. However, not all the radon produced will be available to fill the pore spaces. The amount that is available is a function of certain soil characteristics, radon source potential, and radioactive decay. Equation 3.24 shows the relationship between these factors and was used to determine the flux density of radon ( $J_{\text{Rn}}$ ) from uncovered soil entirely due to diffusion:

$$J_{\text{Rn}} = \left( D \cdot \lambda_{\text{Rn}} \right)^{\frac{1}{2}} \cdot \rho_s \cdot A_{\text{Ra}} \cdot (1 - \epsilon) \cdot f_w \quad (3.24)$$

Where  $(D \cdot \lambda_{\text{Rn}})^{1/2}$  is the distance through which radon diffuses (diffusion length),  $\rho_s$  is the density of the soil grains,  $A_{\text{Ra}}$  is the activity concentration of  $^{226}\text{Ra}$  in the soil, and  $\epsilon$  is the total soil porosity. The emanation factor  $f_w$  is the amount of radon generated in the soil that leaves the soil grains and enters the pore volume. This variable is dependent on the moisture content of the soil and was calculated using Equation 3.25.

$$f_w := f \cdot \left[ \frac{\epsilon_a}{(\epsilon_a + k \cdot \epsilon_w) \cdot \epsilon} \right]^{\frac{1}{2}} \quad (3.25)$$

Where  $f$  (emanation fraction) is the fraction of radon that enters the pore volume,  $\epsilon_w$  is the fraction of soil pore space occupied by water (water porosity),  $\epsilon_a$  is the fraction of soil pore space occupied by air (air porosity), and  $k$  is the ratio of radon concentrations between water and air at equilibrium (coefficient of solubility).

### **3.8 Indoor Radon Emanation Calculations**

Two transport equations were used as a check to determine the radon concentration inside a structure due to the  $^{226}\text{Ra}$  activity in the soil. Because there are many radon entry routes into a facility, each of which may vary in number and extent for an individual structure, a rigorous calculation of the indoor radon concentration would be very complicated. Therefore, a simplified scenario was developed that could be applied across all structures with minimal effort.

The simplified scenario involves using four principle variables to determine indoor radon concentration. These variables are radon entrance rate, volume of the structure, effective ventilation rate, and radiological decay. The major simplification made is that the only source of entry considered is through the walls and floor of the structure's basement. Equation 3.26, presented by Guimond and Wingham, calculates



the radon concentration in a structure resulting from radon migration through its foundation (12: 1460).

$$C_I = \frac{F_s}{V \cdot (\lambda_v + \lambda_r)} \cdot \frac{1}{1000} \quad (3.26)$$

Where  $C_I$  (pCi/l) is the concentration of radon in the structure,  $F_s$  (pCi/sec) is the rate of radon entering the structure through the walls and floor of the structure,  $V$  ( $m^3$ ) is the structure volume,  $\lambda_v$  ( $sec^{-1}$ ) is the number of air changes per second (effective ventilation rate), and  $\lambda_r$  ( $2.11 \times 10^{-6} sec^{-1}$ ) is the radiological decay constant for radon.

The values for  $V$ ,  $\lambda_v$ , and  $\lambda_r$  were easily obtained, but the value for  $F_s$  had to be calculated using Equation 3.27. This equation was used by Moeller, Underhill, and Gulezian to determine the rate of radon entry through the structure due to the radon source potential ( $^{226}Ra$ ) in the soil (20: 1427).

$$F_s = P \cdot A \cdot \left( f \cdot \rho_s \cdot A_{Ra} \cdot \frac{1 - \epsilon}{\epsilon} \right) \cdot (\lambda_m \cdot D)^{\frac{1}{2}} \cdot \text{csch} \left[ L \cdot \left( \frac{\lambda_m}{D} \right)^{\frac{1}{2}} \right] \quad (3.27)$$

Where  $P$  is the fractional wall volume consisting of interparticle pore volume,  $A$  ( $m^2$ ) is the wall and floor area,  $f$  is the emanation fraction,  $\rho_s$  ( $kg m^{-3}$ ) is the density of the soil grains,  $A_{Ra}$  (pCi/kg) is the radium activity in the soil (or radon source potential),  $\epsilon$  is

the soil porosity,  $\lambda_r$  ( $\text{sec}^{-1}$ ) is the decay constant for radon,  $D$  ( $\text{sec}^{-1}$ ) is the diffusion coefficient for radon through the building material, and  $L$  (m) is the wall/floor thickness.

These Equations (3.26 and 3.27) can be used to determine if a potential indoor radon problem exists by comparing the calculated indoor radon concentration to EPA indoor radon limits. If the calculated indoor concentration is above the 4 pCi/l action level set by EPA, then a potential indoor radon problem exists.

## **4.0 Data Description and Analysis**

### **4.1 Introduction**

This chapter presents the data obtained by using the methodology described in Chapter 3 and its analysis. It begins with a discussion of the results obtained in the pilot and regular studies, to include the results of the radon emanation calculations. Next, the results of the hypothesis testing are presented. This testing was used to determine if the ash landfill radon source potential was significantly higher than background. The chapter concludes with the results of the radon emanation calculations and comparisons.

### **4.2 Pilot Study Results**

The pilot study was conducted to obtain enough data to determine the course of action of the regular study. A total of 64 soil samples were collected and analyzed using the methods described in Section 3.0. The results of the gamma spectroscopy analysis were normalized on a per kilogram of sample basis by dividing the detector output by the net weight. The net weight was calculated by taking the actual weight of the sample and subtracting the weight of the empty Marinelli beaker and its lid. The normalized results for the five nuclides of interest, in pCi/g, are shown in Table 4.0 and Table 4.1.

An uncertainty associated with each measurement was calculated using the GENIE-PC software. Measurement uncertainties result from uncertainties in determining spectral peak area which include uncertainty in peak height and uncertainty associated

TABLE 4.0  
Nuclide Activity Results

Sample #	Grid Location		Activity in pCi/g				
	X Coord	Y Coord	K-40	Bi-214	Pb-214	Pa-234m	Ra-226
1	300	300	7.65	1.38	1.10	3.71	5.91
2	300	320	6.28	3.62	3.25	7.13	7.41
3	300	340	6.31	2.89	2.39	4.55	5.69
4	300	360	5.28	2.11	1.84	5.89	4.47
5	300	380	6.55	2.48	2.20	4.61	4.63
6	300	400	7.53	3.17	2.69	5.06	6.78
7	320	300	8.41	0.84	0.71	1.53	2.19
8	340	300	5.61	2.03	1.80	3.96	4.28
9	360	300	5.25	1.94	1.72	4.57	4.29
10	380	300	6.55	2.80	2.37	4.37	6.13
12	400	300	5.81	2.56	2.39	4.89	5.91
13	300	420	6.35	2.59	2.36	3.75	5.39
14	300	440	7.25	2.55	2.42	5.15	5.60
15	300	460	6.40	2.41	2.26	5.15	4.68
16	300	480	6.99	2.67	2.50	4.67	5.54
17	300	500	7.09	1.37	1.28	1.40	3.08
18	420	300	0.54	2.31	2.24	5.69	5.08
19	440	300	5.07	2.29	2.20	3.92	4.97
20	460	300	4.98	1.93	1.82	4.97	4.27
21	480	300	5.96	2.16	1.80	5.84	4.54
22	500	300	6.57	2.52	2.31	5.47	5.14
23	0	0	6.27	0.87	0.83	2.12	2.14
24	100	0	7.37	1.03	0.95	1.73	2.40
25	200	0	6.49	1.05	0.82	2.02	2.41
26	300	0	6.02	1.82	1.69	4.77	4.23
27	400	0	6.52	2.77	2.56	7.69	6.33
28	500	0	6.96	2.36	2.15	4.64	5.27
29	0	100	5.17	1.52	1.29	2.69	3.01
30	100	100	7.50	1.01	0.90	1.41	2.44
31	200	100	6.32	2.45	2.32	5.84	5.08
32	300	100	6.20	2.37	2.35	4.88	5.09
34	400	100	7.19	3.24	3.03	3.64	6.68
35	500	100	7.97	2.82	2.92	2.17	6.13
36	500	110	8.83	2.97	2.85	4.56	7.30
37	0	200	6.65	2.39	2.20	4.21	4.91
38	100	200	8.02	0.77	0.68	1.57	1.86
39	200	200	6.38	2.62	2.51	4.06	5.39
40	300	200	5.98	2.40	2.27	5.83	5.50
41	400	200	7.69	2.94	2.79	6.48	6.33
42	500	200	4.99	1.14	1.00	1.32	2.39
43	0	300	6.43	0.38	0.41	1.07	1.13
44	100	300	2.93	0.75	0.68	1.56	1.31
45	200	300	5.77	1.63	1.59	2.75	3.35
46	200	400	7.18	2.32	2.12	3.39	4.67
47	400	400	6.38	2.25	2.26	3.41	5.18
48	500	400	6.38	2.82	2.69	5.76	6.39
49	200	500	8.32	1.11	1.07	2.35	2.61
50	400	500	5.23	1.65	1.50	3.39	3.43

TABLE 4.0 (con't)  
Nuclide Activity Results

Sample #	X Coord	Y Coord	Activity in pCi/g				
			K-40	Bi-214	Pb-214	Pa-234M	Ra-226
51	500	500	6.54	1.91	1.80	5.34	4.11
53	300	310	5.89	2.33	2.14	3.69	4.72
54	300	330	6.22	3.10	2.88	4.43	6.45
55	300	350	5.61	3.35	3.13	7.37	7.28
56	300	370	6.45	2.19	2.32	1.68	4.68
57	300	390	6.30	2.15	2.06	3.21	4.52
58	300	410	5.20	2.16	2.16	3.34	4.78
59	300	430	6.62	2.21	2.29	4.78	4.52
60	300	450	6.61	2.35	2.40	2.97	4.93
61	300	305	5.62	1.65	1.56	2.98	3.70
62	300	315	6.64	1.74	1.62	5.16	3.78
63	300	325	6.01	3.07	2.94	6.59	6.53
64	300	335	7.44	3.29	3.38	4.98	6.82
65	300	345	5.95	2.45	2.54	5.37	5.47
66	310	310	8.01	3.49	3.26	5.83	7.03
67	320	320	7.29	3.64	3.42	6.07	7.65

TABLE 4.1  
Nuclide Uncertainty Results

Sample#	K-40	Uncertainty in pCi/g				Sample Weight (kg)
		Bi-214	Pb-214	Pa-234m	Ra-226	
1	0.21	0.02	0.05	0.56	0.21	2.959
2	0.19	0.04	0.12	0.90	0.32	2.461
3	0.19	0.03	0.09	0.68	0.27	2.553
4	0.16	0.03	0.07	0.69	0.23	2.722
5	0.19	0.03	0.08	0.69	0.24	2.612
6	0.22	0.04	0.26	0.65	0.32	2.54
7	0.24	0.02	0.04	0.68	0.16	2.519
8	0.17	0.03	0.07	0.63	0.22	2.854
9	0.17	0.03	0.07	0.64	0.23	2.497
10	0.20	0.04	0.09	0.69	0.31	2.112
12	0.19	0.04	0.09	0.78	0.30	2.048
13	0.19	0.03	0.09	0.68	0.27	2.497
14	0.21	0.04	0.09	0.68	0.27	2.201
15	0.20	0.03	0.08	0.75	0.26	2.238
16	0.21	0.03	0.09	0.81	0.28	2.116
17	0.20	0.02	0.05	0.63	0.19	2.729
18	0.18	0.03	0.08	0.79	0.28	1.969
19	0.17	0.03	0.08	0.66	0.26	1.998
20	0.16	0.03	0.07	0.69	0.23	2.327
21	0.19	0.03	0.07	0.79	0.25	2.112
22	0.20	0.03	0.09	0.89	0.26	2.05
23	0.20	0.02	0.04	0.91	0.19	1.873
24	0.21	0.02	0.04	0.48	0.16	2.763
25	0.19	0.02	0.04	0.49	0.16	2.95
26	0.19	0.03	0.07	0.81	0.25	1.99
27	0.21	0.03	0.09	0.79	0.30	1.932
28	0.21	0.03	0.08	0.77	0.27	2.031
29	0.16	0.02	0.05	0.52	0.17	3.089
30	0.21	0.02	0.04	0.63	0.17	2.706
31	0.20	0.04	0.09	0.85	0.26	2.081
32	0.20	0.03	0.08	0.70	0.27	2.064
34	0.22	0.04	0.11	0.91	0.33	1.824
35	0.24	0.04	0.07	0.93	0.32	1.832
36	0.26	0.04	0.10	0.85	0.35	1.799
37	0.20	0.03	0.08	0.70	0.26	2.423
38	0.22	0.01	0.03	0.43	0.14	2.99
39	0.20	0.03	0.09	0.78	0.27	2.059
40	0.19	0.03	0.09	0.83	0.28	2.041
41	0.23	0.04	0.10	0.76	0.32	1.964
42	0.16	0.02	0.04	0.54	0.16	2.664
43	0.18	0.01	0.01	0.49	0.11	3.503
44	0.12	0.01	0.01	0.25	0.08	2.75
45	0.17	0.02	0.06	0.57	0.20	2.832
46	0.21	0.03	0.08	0.66	0.27	2.447
47	0.20	0.03	0.08	0.84	0.27	1.966
48	0.20	0.04	0.10	0.83	0.32	2.028
49	0.23	0.02	0.05	0.60	0.23	2.599
50	0.17	0.02	0.06	0.72	0.22	2.078

TABLE 4.1 (con't)  
Nuclide Uncertainty Results

Sample#	K-40	Uncertainty in pCi/g				Sample Weight (kg)
		Bi-214	Pb-214	Pa-234m	Ra-226	
51	0.20	0.03	0.07	0.82	0.23	2.063
53	0.18	0.03	0.08	0.63	0.24	2.588
54	0.19	0.04	0.10	0.68	0.30	2.455
55	0.18	0.03	0.05	0.71	0.34	2.402
56	0.20	0.04	0.11	0.80	0.26	2.308
57	0.19	0.03	0.07	0.70	0.25	2.486
58	0.17	0.03	0.05	0.63	0.26	2.344
59	0.20	0.03	0.05	0.73	0.24	2.487
60	0.20	0.03	0.06	0.68	0.26	2.347
61	0.17	0.02	0.06	0.60	0.21	2.803
62	0.19	0.02	0.06	0.64	0.21	2.734
63	0.18	0.04	0.10	0.74	0.31	2.417
64	0.22	0.04	0.08	0.70	0.33	2.281
65	0.19	0.03	0.06	0.74	0.28	2.31
66	0.23	0.04	0.11	0.76	0.33	2.264
67	0.21	0.04	0.12	0.72	0.35	2.33

with interfering peaks. Table 4.2 shows the uncertainty for the mean of each nuclide measured and the sample standard deviation. The percent uncertainty in the mean was used as an indicator of detector

TABLE 4.2

Uncertainty in the Mean Activity Measurements

Nuclide	Mean (pCi/g)	Uncert. in the Mean (pCi/g)	% Uncert. of the Mean	Sample Std Deviation (pCi/g)
<sup>40</sup> K	6.48	0.025	0.39	0.91
<sup>214</sup> Bi	2.20	0.004	0.18	0.77
<sup>214</sup> Pb	2.06	0.010	0.48	0.74
<sup>234m</sup> Pa	4.15	0.089	2.14	1.65
<sup>226</sup> Ra	4.78	0.032	0.67	1.58

performance. A value of 15 percent or less was deemed acceptable before the measurements were performed. This level of uncertainty was assumed to be negligible compared to uncertainties associated with the health effects of radon.

Also, six samples were dried in an effort to determine the soil moisture content (by weight). Six samples were dried in an oven for 48 hours at 103° C. The weights of the samples were recorded before and after drying. The soil moisture content was calculated by taking the change in weight of the sample. The average sample moisture content was 21 percent by weight.

Spectra of the six samples were measured before and after drying. The same procedures followed in the pilot study were used here for sample analysis (see Section



3.3.2, Sample Analysis). The dried samples showed an average 14 percent increase in activity over the moist samples. However, the measured activity of the moist samples were considered more accurate because the density of the moist samples better matched the density of the calibration standard.

#### **4.2.1 Univariate Analysis**

Next, summary statistics were calculated for each nuclide in order to conduct univariate analysis of the data. These statistics are shown in Table 4.3. The first check described in Chapter 3 was conducted to see if the CV was greater than one for any nuclide. A CV of greater than one would indicate presence of erratic values which could impact later estimation. A simple check of the table shows that none of the radionuclides of interest have a CV of greater than one.

TABLE 4.3  
Summary Statistics of Sample Activity Densities

Nuclide	Mean (pCi/g)	Median (pCi/g)	Std Dev. (pCi/g)	Coeff. of Variation
<sup>40</sup> K	6.48	6.50	0.91	0.14
<sup>214</sup> Bi	2.20	2.32	0.77	0.35
<sup>214</sup> Pb	2.06	2.22	0.74	0.36
<sup>234m</sup> Pa	4.15	4.49	1.65	0.40
<sup>226</sup> Ra	4.78	4.92	1.58	0.33

Next, a box and whiskers plot was developed for each nuclide using STATISTIX 4.0 software. Figure 4.0 shows the box and whiskers plots of all five nuclides of interest.

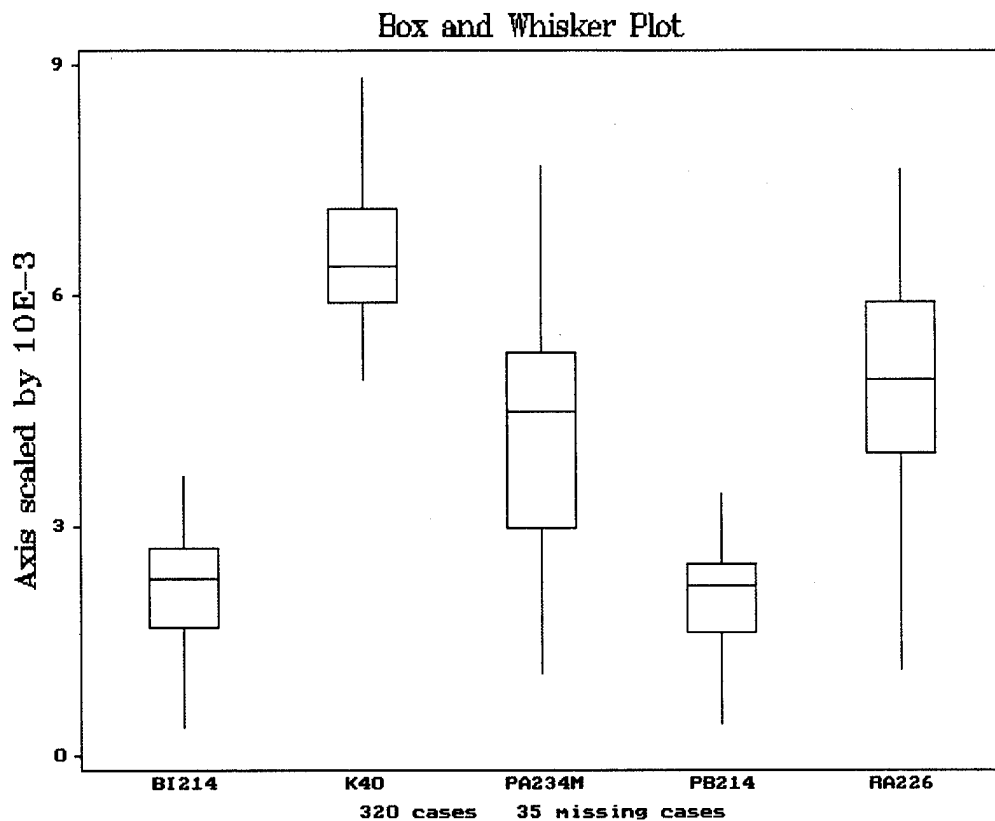


Figure 4.0 Nuclide Box and Whiskers Plot.

A visual check of the plots gives no indication of outlier or erratic values for any of the radionuclides. These values would show up as asterisks or circles located either above or below the box and whiskers plot for each nuclide. Also, a visual check of the horizontal line in each box, which represents the average of the data values, was conducted to check for indications of skewed data. Skewed data would be illustrated by a horizontal line located within the top or bottom quarter of the box. Only one plot,  $^{214}\text{Pb}$ ,

showed the possibility of skewed data. The horizontal line was close to the top quarter of the box, but not in it. A check of the histogrammed  $^{214}\text{Pb}$  data, presented later, was used to confirm that it was not skewed.

The histograms for each radionuclide were visually analyzed. Figure 4.1 shows an example of a histogram for the  $^{226}\text{Ra}$  data. Again, as with the box and whiskers plot, the histogram gives no indication of outliers or erratic values. This also holds true for the other nuclides of interest, their histograms can be found in Appendix B, Statistical Analysis Figures.

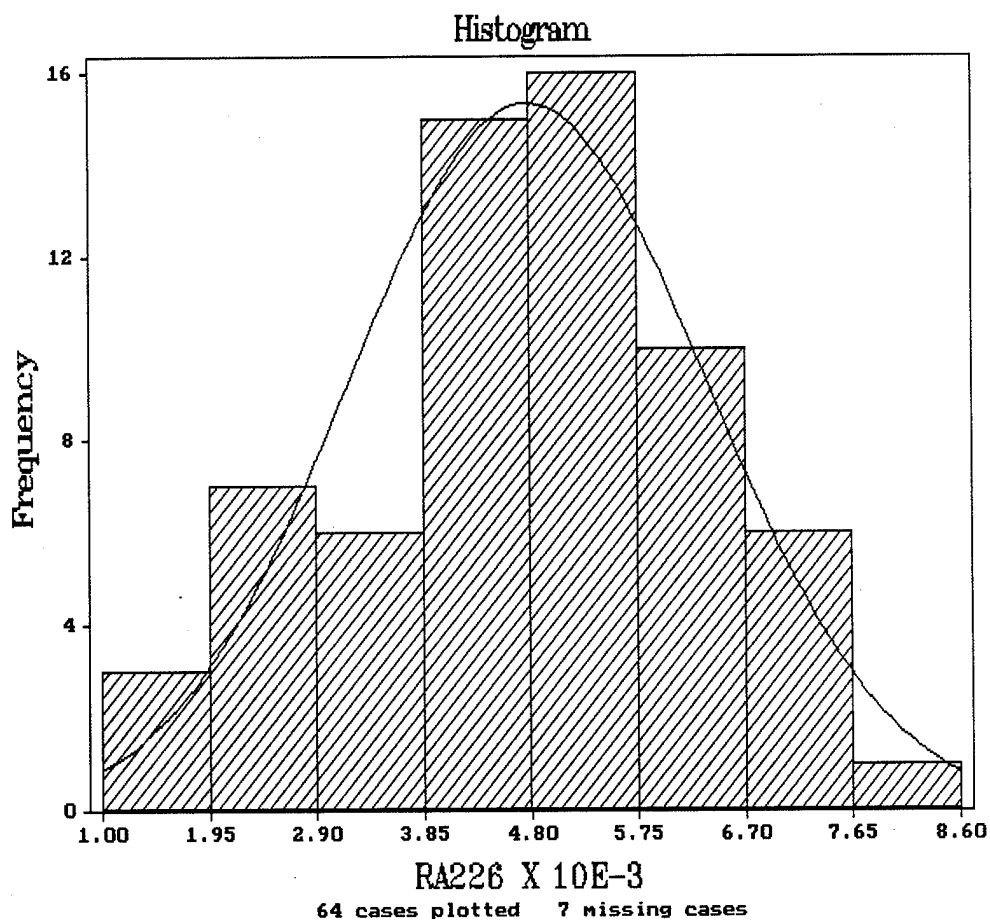


Figure 4.1 Histogram of  $^{226}\text{Ra}$  Data.

The shape of each histogram was visually analyzed to determine possible distributions. Each of the histograms showed that the data appeared to be symmetric and not skewed. Given this indication, a rankit plot along with an approximate Wilk-Shapiro normality statistic was developed to see if the data conformed to a normal distribution. An example of the individual rankit plot for  $^{226}\text{Ra}$  data is shown in Figure 4.2. The data appeared to follow a straight line, with no outliers or erratic values. This indicated that

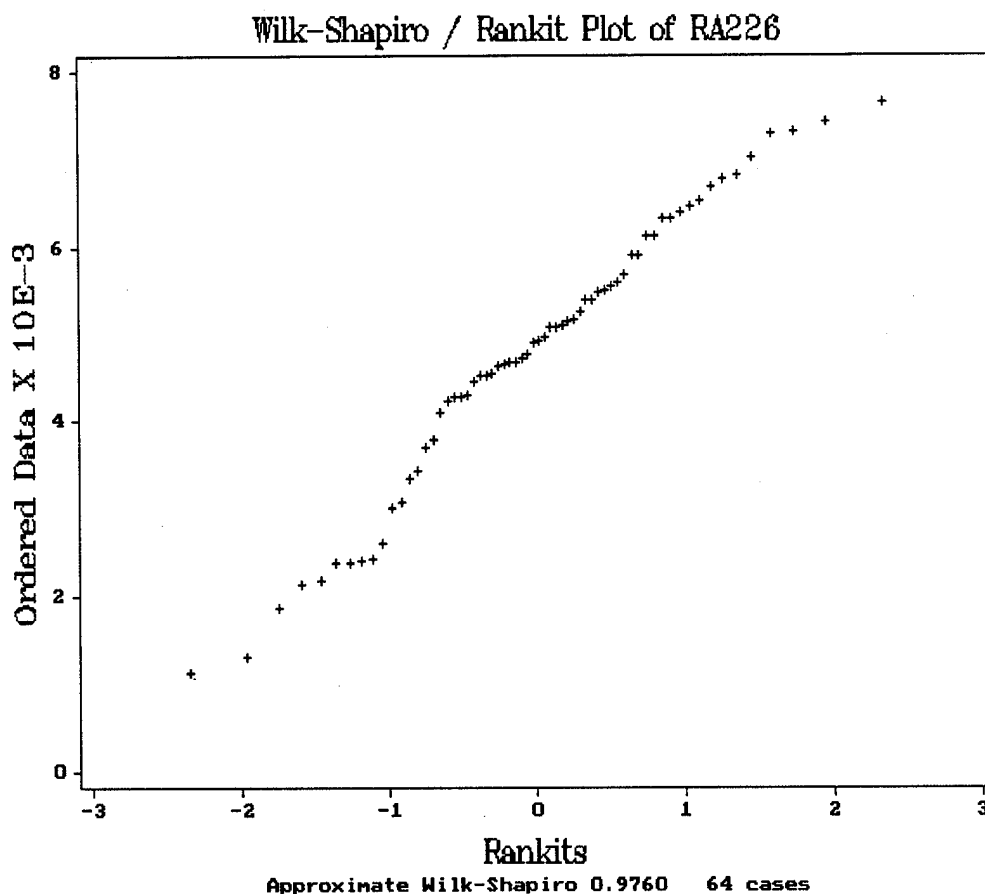


Figure 4.2 Wilk-Shapiro Rankit Plot for  $^{226}\text{Ra}$  Data.

the data conformed to a normal distribution. The plots for each of the other nuclides also appeared to resemble a straight line. These plots can be found in Appendix B.

The Wilk-Shapiro normality statistics were calculated using STATISTIX 4.0 and are summarized in Table 4.4. Based on the data in the table and the criteria established in section 3.2.3.1, which stated that a WS statistic greater than 0.90 indicated normality, the data for each nuclide is assumed to be normally distributed.

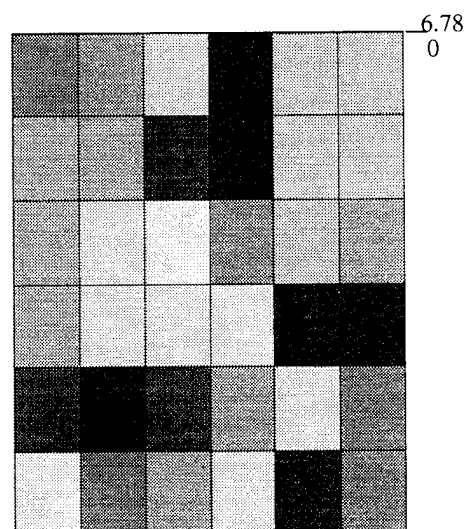
TABLE 4.4  
Summary of the Wilk-Shapiro Normality Statistics

Radionuclide	Normality Statistic
<sup>40</sup> K	0.9729
<sup>214</sup> Bi	0.9759
<sup>214</sup> Pb	0.9669
<sup>234m</sup> Pa	0.9764
<sup>226</sup> Ra	0.9760

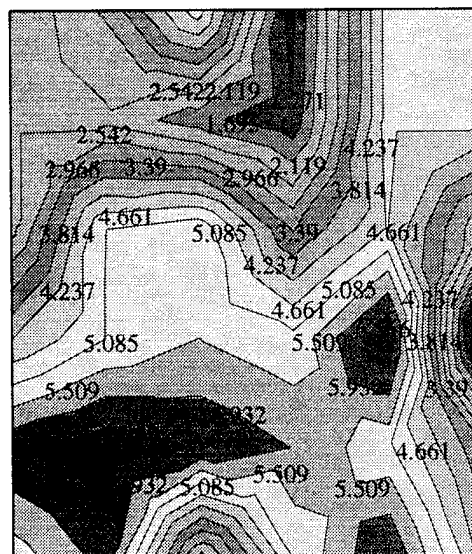
To summarize the findings of the univariate analysis section, none of the tests conducted indicated the presence of outliers or erratic values. However, the box and whiskers plot of <sup>214</sup>Pb data showed the possibility of slightly skewed data. A check of the histogram of the <sup>214</sup>Pb data, in Appendix B, revealed that the data was in fact symmetric. Since the data for all the nuclides showed symmetry, rankit plots and Wilk-Shapiro statistics for each nuclide were developed to check for normality. Both the rankit plots and Wilk-Shapiro statistics confirmed that the data for all nuclides were normally distributed.

### 4.2.2 Spatial Description

Since no aberrant data was found in the univariate study, the spatial description analysis started with analysis of trends in the data. The analysis was conducted using surface plots generated in MATHCAD 5.0 Plus. Specifically, the presence of gradual gradients in the data for each radionuclide was determined by plotting the data values obtained at each grid point versus location and visually checking for trends across the site. Figures 4.3 (a) and (b) show a patch plot and contour plot of the  $^{226}\text{Ra}$  data, respectively. A visual check of the plots revealed no gradient across the entire site for the



reg



wdscv

(a)

(b)

Figure 4.3 Plot of the Individual Data Values. (a) Patch Plot of  $^{226}\text{Ra}$  Data; (b) Contour Plot of  $^{226}\text{Ra}$  Data.

$^{226}\text{Ra}$  data. A check of the plots of the  $^{214}\text{Bi}$  and  $^{214}\text{Pb}$  data gave the same indications as the  $^{226}\text{Ra}$  data. The data values at the top and bottom of the plots decreased indicating no single gradient across the site. The plots of the  $^{234\text{m}}\text{Pa}$  and  $^{40}\text{K}$  data showed no gradients. The plots can be found in Appendix B.

Also, a check on the location of the two extreme values was conducted as a possible indicator of high spatial variability. Figure 4.4 shows the patch plot of  $^{226}\text{Ra}$  data values with the location of the highest and lowest values identified. The patches with two values are relatively close to each other (separated by only 200 feet) indicating high spatial variability. This coupled with the fact that a gradient was not seen in the contour plot, indicates high spatial variability within the data for  $^{226}\text{Ra}$ . Only one other nuclide ( $^{234\text{m}}\text{Pa}$ ) had extreme values located close to each other.

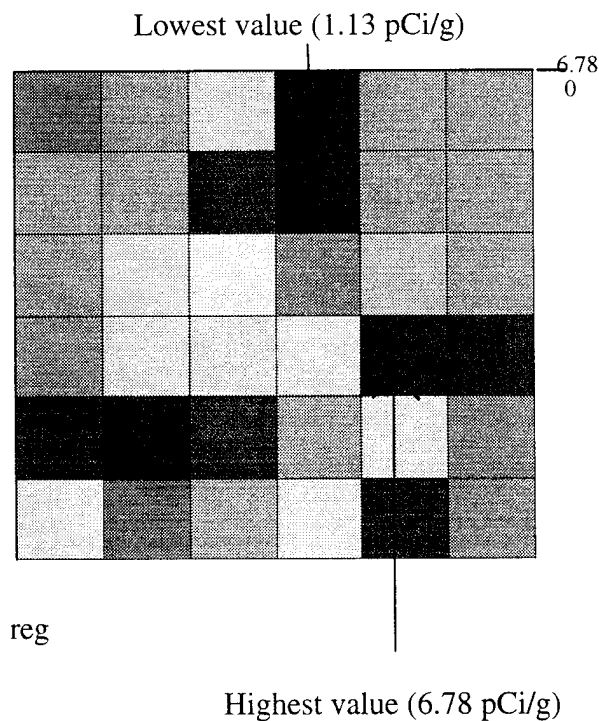


Figure 4.4 Patch Plot Showing Extreme Values for  $^{226}\text{Ra}$ .





and the moving window plots for all the nuclides, except  $^{40}\text{K}$ , showed a slight trend across the site from left to right.

The spatial description checks did not show conclusively that there was no spatial correlation in the data. Therefore, a more rigorous geostatistical technique, variogram analysis, was used to determine if there was spatial correlation.

#### **4.2.3 Descriptive Structural Analysis**

Since the spatial description analysis did not show conclusively that the data for the nuclides was not correlated, variogram analysis was conducted as a final check for correlation. If correlation exists, variogram analysis quantify it. An omnidirectional variogram was constructed for each nuclide. Table 4.5 show the results obtained for the

TABLE 4.5 Omnidirectional Variogram Results for  $^{226}\text{Ra}$ .

No. of Pairs	Distance (ft)	$\gamma(h)$ Value	No. of Pairs	Distance (ft)	$\gamma(h)$ Value
20	5.0	1.891	128	259.58	2.137
186	17.83	2.424	114	281.26	2.297
146	37.56	2.644	188	300.13	3.441
130	57.72	3.107	230	318.29	2.581
126	78.06	1.995	112	339.80	2.450
310	100.52	2.064	154	360.52	1.994
230	119.12	1.647	92	378.88	3.495
244	139.98	2.142	102	397.50	2.910
146	158.93	2.351	142	417.13	2.564
150	179.76	2.491	96	442.78	2.494
298	201.38	2.492	50	458.93	2.716
286	220.72	2.225	30	478.90	2.482
132	238.64	2.643	102	501.24	2.717

omnidirectional variogram of  $^{226}\text{Ra}$ . The results are shown visually by plotting the  $\gamma(h)$  values versus distance (see Figure 4.6). The  $\gamma(h)$  value reaches its sill at a relatively short distance, approximately 27 feet, which causes a discontinuity at the origin. This effect closely resembles a pure nugget effect, and indicates no spatial correlation in the data. Omnidirectional variograms for the other four nuclides can be found in Appendix B. Visual analysis of the variograms also indicate close to pure nugget effect for all the nuclides, and therefore no spatial correlation in the data.

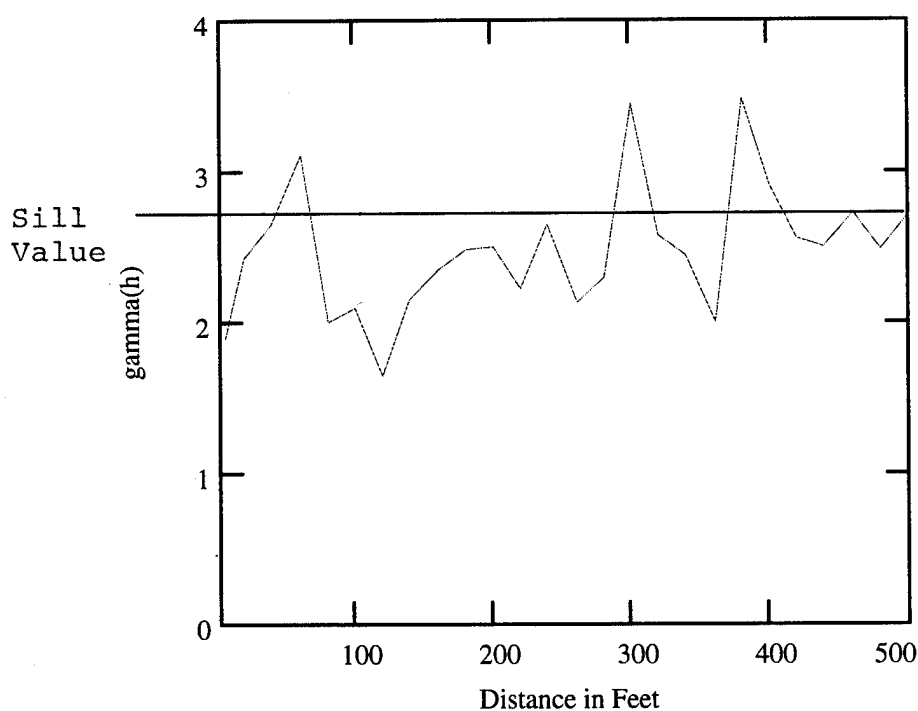


Figure 4.6 A Plot of the  $\gamma(h)$  Values Versus Distance for  $^{226}\text{Ra}$ .

### 4.3 Regular Study Results

Since no additional samples were required for the regular study, estimates of the mean activity and standard deviation of each nuclide at the landfill and background locations were calculated using samples collected in the pilot study. Table 4.6 shows a summary of the results. The sample standard deviations shown in the table are large compared to the measurement uncertainties shown in Table 4.2, indicating that the measurement technique provided better than adequate uncertainties.

TABLE 4.6 Summary of Landfill and Background Mean Activity and Standard Deviation Calculations

Nuclide	Regular Study Results		Background Results	
	Mean (pCi/g)	Std. Dev (pCi/g)	Mean (pCi/g)	Std. Dev. (pCi/g)
$^{40}\text{K}$	6.48	0.91	7.76	0.35
$^{214}\text{Bi}$	2.20	0.77	0.53	0.03
$^{214}\text{Pb}$	2.06	0.74	0.49	0.01
$^{234\text{m}}\text{Pa}$	4.15	1.65	1.67	0.05
$^{226}\text{Ra}$	4.78	1.58	1.62	0.04

The activities of the two radionuclides ( $^{214}\text{Pb}$  and  $^{214}\text{Bi}$ ) that are below  $^{222}\text{Rn}$  in the  $^{238}\text{U}$  decay chain should have the same activities based on the secular equilibrium that is quickly established due to their short half lives. This does agree with the measurements shown in Table 4.6. Also, the activities of the two radionuclides ( $^{234\text{m}}\text{Pa}$  and  $^{226}\text{Ra}$ ) that are above  $^{222}\text{Rn}$  in the decay chain, should be equal. Again, the measurements in the table show agreement. The difference between the activities of the nuclides above and below  $^{222}\text{Rn}$  indicates that a large fraction of  $^{222}\text{Rn}$  escapes the soil.

#### **4.4 Radon Source Potential Comparison**

The two-sample t test described in Section 3.6 was applied to the mean landfill and background  $^{226}\text{Ra}$  activities to determine if the landfill radon source potential was significantly higher than the background radon source potential. The following null and alternate hypotheses were tested:

$$H_0: \mu_1 - \mu_2 = 0$$

$$H_a: \mu_1 - \mu_2 > 0$$

Where  $\mu_1$  and  $\mu_2$  are the mean  $^{226}\text{Ra}$  activities of the regular study and background study populations, respectively. A test statistic was calculated using Equation 3.22 and compared to a t critical value. If the test statistic was greater than the t critical value then the null hypothesis would be rejected. The t critical value was obtained from a table of critical values for  $t_{\alpha, m+n-2}$ , where  $t_{\alpha, m+n-2}$  is the  $100(1-\alpha)$ th percentile of the t distribution with  $m+n-2$  degrees of freedom. The test statistic was equal to 4.31, and for an  $\alpha$  of 0.05, the t critical value was 2.0. Since the test statistic was greater than the t critical value, the null hypothesis was rejected in favor of the alternate, in effect establishing that the  $^{226}\text{Ra}$  activity in the landfill is significantly higher than background with 95% confidence.

#### **4.5 Outdoor Radon Emanation Calculations**

Flux densities at the landfill and background locations were calculated using Equation 3.16. Typical values for  $^{222}\text{Rn}$ , which were experimentally obtained by Nazaroff and Nero, were used for the following variables:  $D_e = 4 \times 10^{-6} \text{ m}^2 \text{ s}^{-1}$ ,  $\lambda_{\text{Rn}} = .0076 \text{ hr}^{-1}$ , and  $f = 0.25$  (23: 68, 85). Nazaroff and Nero also published typical soil values for several variables in the equation. These values were based on the diameter of the grains in the soil. For soil with a 30 micron diameter grain size, the following values for the equations were obtained:  $\rho_s = 2.65 \times 10^3 \text{ kg m}^{-3}$ ,  $\epsilon = .5$ , and  $k = .25$  (23: 60, 84). The values for the remaining variables were obtained experimentally.

The mean landfill and background  $^{226}\text{Ra}$  activities were obtained by the sampling and analysis experiment, and the water porosity  $\epsilon_w$  and the air porosity  $\epsilon_a$  values were obtained by drying several samples and determining the fraction of the soil volume taken up by the water.

Six samples were dried in an oven for 48 hours at 103 C. The weights of the samples were measured before and after drying. The water porosity was calculated by taking the change in weight and multiplying it by the density of water to get the volume of water driven off. This volume was then used to calculate the fraction of sample pore volume occupied by water. This value (.21) used with the relationship shown in Equation 4.1 and a value of 0.5 for  $\epsilon$  to determine the air porosity value.

$$\epsilon = \epsilon_w + \epsilon_a \quad (4.1)$$

This result was an air porosity value of 0.29. Table 4.7 shows the calculated radon flux densities for radon emanating from uncovered soil at the landfill and background areas using Equation 3.16 with error propagation.

TABLE 4.7  
Radon Flux Densities From Uncovered Soil.

Location	<sup>222</sup> Rn Flux Density (pCi/m <sup>2</sup> s)	Error (pCi/m <sup>2</sup> s)
Landfill	9.36	0.04
Background	3.17	0.12

#### **4.6 Indoor Radon Calculations**

In order to illustrate the effects of the increased radon source potential, Equations 3.17 and 3.18 introduced in Section 3.7.2 were used to calculate radon concentrations in the basement of a two identical hypothetical structures, one built on the ash landfill and one built on normal background soil. The structures were assumed to have a 40 ft by 20 ft basement with 8 ft tall concrete slab walls that were 6 inches thick. The floor in the basement was assumed to also be 6 inch thick concrete slab. The typical soil values obtained and used in the previous section were used again. However, typical values for the construction materials had to be obtained. Typical values for the following concrete slab variables were used: the fractional wall volume  $P$  consisting of interparticle pore volume was 0.05 and the diffusion coefficient  $D$  for radon through building material was  $9.75 \times 10^{-5} \text{ m}^2/\text{sec}$  (12: 1460, 23: 60, 67, 68). One other value, effective ventilation rate

$\lambda_v$ , was obtained from a list of typical values for a single family dwelling published by Guimond and Windham. The value used for the variable was  $1.4 \times 10^{-3}/\text{sec}$  (12: 1460).

The remaining values were calculated using the dimensions given in the first paragraph: total wall and floor area was  $163.44 \text{ m}^2$ , the wall/floor thickness was  $.152 \text{ m}$ , and the volume of the basement was  $181.14 \text{ m}^3$ .

The indoor concentrations resulting from the landfill source and background source were calculated. Table 4.8 shows the results including propagation of error..

TABLE 4.8  
Indoor Radon Concentration Calculations

Source Location	$^{222}\text{Rn}$ Conc. (pCi/l)	Error (pCi/l)
Landfill	11.48	0.05
Background	3.89	0.15

The implications of these results are discussed in Section 5.4, Indoor Radon Emanation Conclusions.

## **5.0 Conclusions and Recommendations**

### **5.1 Sampling Technique**

The geostatistical analysis of the data for all five nuclides of interest indicated that there was no spatial correlation present in the data sets. Therefore, no advantage was gained by using the geostatistical techniques (which relies on spatial correlation) when developing a sampling and analysis plan for implementation at a coal ash landfill. In fact, the use of these geostatistical techniques in this situation would result in higher costs because a higher number of samples would be required to characterize the site.

Since the process being measured showed no spatial trends, the systematic sampling technique was adequate for estimating the mean activities of the nuclides at the site. This technique had two advantages over other traditional sampling techniques like random sampling and stratified random sampling. While estimating the true mean activity levels with the same precision as simple random and stratified random sampling, it provided uniform coverage of the site and was easier to implement under field conditions.

### **5.2 Radon Source Potential**

The mean  $^{226}\text{Ra}$  activity level at the ash landfill was found with 95% confidence to be significantly higher than background by using a two-sample t test. This increase in the radon source potential is attributed to the landfilled coal ash. Figure 5.0 shows a



graphical comparison of the landfill and background source potentials. The landfill mean  $^{226}\text{Ra}$  activity is 2.95 times higher than the mean background level.

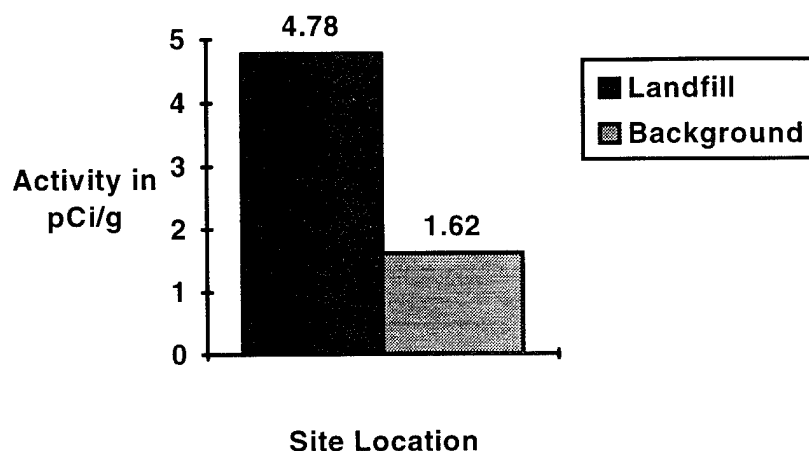


Figure 5.0 Mean  $^{226}\text{Ra}$  Activity Levels Comparison.

### 5.3 Outdoor Radon Emanation

The radon emanation into the atmosphere at the landfill was greater than background emanation,  $9.36 \pm 0.04 \text{ pCi/m}^2\text{-s}$  compared to  $3.17 \pm 0.12 \text{ pCi/m}^2\text{-s}$ . The flux density at the ash landfill is 2.95 times higher than the background flux density. This was expected given that the source potential at the landfill was significantly higher (2.95 times) than background.

It should also be noted that these results show the emanation only during one particular time of the year, spring. The samples were taken in March of 1995, just after

Two of the variables ( $D_e$ , the diffusion coefficient and  $f_w$ , the emanation factor) used in the outdoor emanation equation are effected by the moisture content of the soil. As the amount of water in the sample decreases, the value for  $D_e$  increases and the value for  $f_w$  decreases. Figure 5.2 shows the change in radon flux density at the landfill given a decrease in moisture content of the soil. The moisture content was reduced from 25 to 0 percent in 5 percent increments. The values for  $D_e$  and  $f_w$  at the specific water contents were used in the emanation equation to create the graph. It shows a decrease in radon emanation as moisture content decreases. Therefore, the radon flux density should be lower in the summer months when the soil contains less moisture.

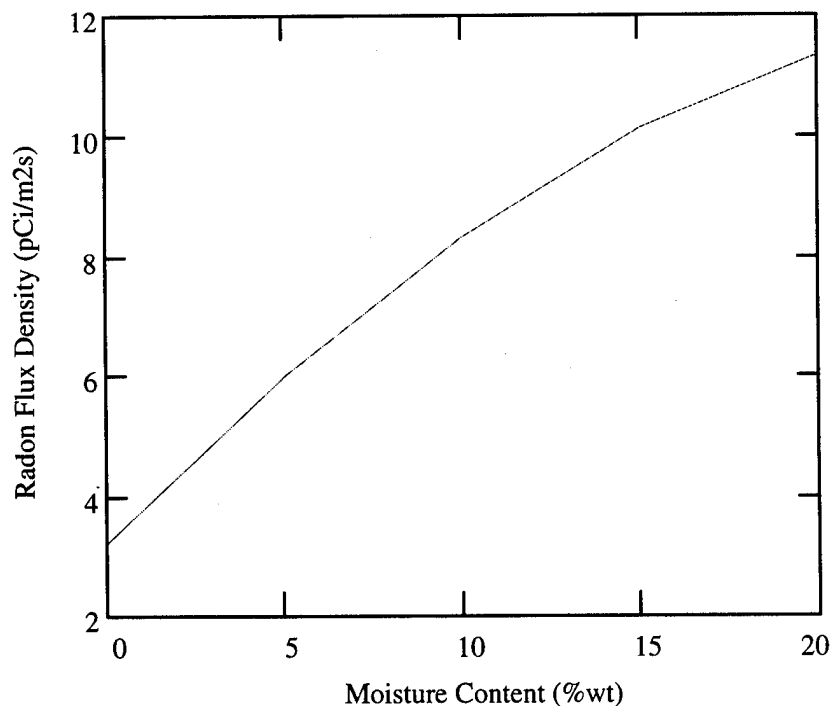


Figure 5.1 Radon Flux Density Versus Soil Moisture Content.

## **5.4 Indoor Radon Emanation**

The radon emanation into a hypothetical structure due to the landfill and background source potentials resulted in an indoor radon concentration of  $11.48 \pm 0.05$  pCi/l due to the landfill source potential compared to  $3.89 \pm 0.15$  pCi/l for the background source potential. The increased indoor concentration was expected given that the source potential at the landfill was 2.95 times higher than background.

The 11.48 pCi/l indoor radon concentration due to the landfill source exceeds the EPA action level of 4 pCi/l. Currently, an indoor level of 11.48 pCi/l requires mitigation within four years (25:16-3).

Also, a comparison of lifetime risk of premature death due to the two indoor radon concentrations can be made using values obtained from a radon exposure chart published by DuPont and Morrill. Assuming 20 year occupancy of a home with the previously stated 11.48 and 3.89 pCi/l concentrations, the associated lifetime risk of early death is 3.4% (about 1 in 30) and 1.2% (about 1 in 83) respectively (11: 72). The risk of premature death due to the landfill source potential is 2.83 times greater than that of the background source potential. To put these estimates in perspective, the lifetime risk of dying in an automobile accident in the United States is 2.0% (about 1 in 50) and the lifetime risk of early death from smoking two packs of cigarettes a day is 25% (about 1 in 4) (11: 70).

This risk from radon is quite high compared to the amount of risk built into regulations for chemicals in the environment. For example, the EPA sets a standard for exposure to a chemical so that the lifetime risk of early death does not exceed 1 in a

million ( $10^{-6}$ ) (11:73). The risk from their guideline threshold level of 4.0 pCi/l for radon is 1 in 83, which is much higher than the socially accepted threshold for chemicals.

These results have a significant impact on future landfill land use scenarios that involve construction on the site. Even though the simplified calculation only considered one source of radon entry into the structure, the indoor radon concentration exceeded the EPA guideline of 4.0 pCi/l. Therefore, construction design of similar structures should include radon mitigation strategies such as upgrading the ventilation system to increase the air exchange rate.

## **5.5 Recommendations**

When considering construction on a base coal ash landfill, determine the radon source potential and radon emanation at the site before the construction design begins. If the indoor radon concentrations exceed EPA guidelines, radon mitigation strategies can be integrated into the design usually at a lower cost as opposed to applying them as a corrective action.

The techniques used for this research can easily be adapted to any base ash landfill. Just adjust the size of the grid to cover the site and follow the steps in the sampling and analysis plan to determine the radon source potential and soil moisture content, with the exception of the geostatistical analysis portion. The use of geostatistical techniques does not provide an advantage over the systematic sampling techniques used because no spatial correlation exists in the data. This is expected at ash landfills, because

the ash is usually bulldozed after it is dumped at the site. Bulldozing the ash tends to homogenize it.

After determining the radon source potential and soil moisture content, the emanation equations can be used to determine the indoor radon concentration based on specific facility characteristics (volume, construction material, etc.).

Currently there are no EPA guidelines for outdoor radon concentrations. However if the ash landfill is located close to a recreation area, the outdoor radon emanation results can be used to determine the radon concentration reaching the users of the area. For example, the Twin Lakes Recreation area at Wright Patterson AFB is located approximately 50 feet from the base ash landfill boundary. The Gaussian Plume Model, with the flux densities as inputs, can be used to calculate the radon concentration reaching the users of the recreation area.

Finally, one method of closing ash landfills involves placing an impermeable liner, or cap, over the landfill. The cap usually contains several vents that release subsurface gases into the atmosphere. Research into the effects of the cap and vents on radon emanation is recommended.

## **APPENDIX A**

### **SAMPLING AND ANALYSIS PLAN**

## TABLE OF CONTENTS

	<u>Page</u>
1.0 Introduction.....	86
1.1 Historical Information.....	86
1.2 Geological Information.....	86
1.3 Previous Studies.....	91
2.0 Site Conceptual Model.....	94
2.1 Geology.....	94
2.2 Hydrology.....	94
2.3 Topography.....	94
2.4 Meteorological Conditions.....	96
3.0 Contaminant Information.....	96
3.1 Contaminants of Interest.....	96
3.2 Contaminant Transport.....	96
4.0 Data Quality Objectives (DQOs).....	96
4.1 State the Problem.....	96
4.2 Identify the Decision.....	99
4.3 Identify the Inputs Into the Decision.....	99
4.4 Define the Boundaries of the Study.....	100
4.5 Develop a Decision Rule.....	100
4.6 Specify limits On Decision Errors.....	100
5.0 Field Approach.....	102
5.1 Available Resources.....	102
5.2 Phase 1 (Pilot Study).....	103
5.3 Phase 2.....	106
6.0 Quality Assurance/ Quality Control.....	106
7.0 Waste Handling.....	106
8.0 Health and Safety.....	107
8.1 Site Responsibility.....	107
8.2 Contamination.....	107
8.3 Levels of Protection.....	108
8.4 Emergency Response.....	109

## LIST OF FIGURES

	<u>Page</u>
1-1 Area Map Location.....	87
1-2 Location of Wright Patterson AFB.....	88
1-3 Location of Operable Unit 5 (OU5).....	89
1-4 South-North Geologic Cross Section.....	92
1-5 West-East Geologic Cross Section.....	93
2-1 Potentiometric Map.....	95
2-2 Conceptual Site Model NW-SE Orientation.....	97
2-3 Conceptual Site Model SW-NE Orientation.....	98

## LIST OF TABLES

	<u>Page</u>
1-1 Estimated Quantities of Hazardous Materials Landfilled.....	90

## ATTACHMENTS

	<u>Page</u>
A. Field Sampling Protocol (FSP).....	110
B. Quality Assurance Project Plan (QAPP).....	120



## **SAMPLING AND ANALYSIS PLAN**

### **1.0 INTRODUCTION:**

#### **1.1 HISTORICAL INFORMATION:**

Wright Patterson Air Force Base (WPAFB) lies between the Cities of Dayton, OH and Fairborn, OH and occupies about 8,500 acres of Green and Montgomery Counties (Figure 1-1). The base is divided into three areas: A, B, C (Figure 1-2). Areas A and C encompass 5,711 acres and are part of Patterson Field, an active United States Air Force (USAF) airfield. Area A is primarily comprised of building complexes and area C is primarily comprised of active runways and flight facilities. Area B encompasses approximately 2,800 acres and is located southwest of areas A and C. It contains a complex of buildings and three runways that are no longer utilized for flying, except occasionally when aircraft are flown in for exhibition at the Air Force Museum.

In the southwest corner of area C is a collection of discrete sites that have, or may have, been used for handling or disposing of hazardous chemical materials in the past. The discrete sites include Landfill 5 (LF5) and Landfill 5 Extension, Fire Training Area 1 (FTA1), Gravel Lake Tanks Site (GLTS), and Burial Site 4 (BS4). LF5 is a 23 acre site located north of the Twin Lakes area between Riverview Road and Prairie Road (Figure 1-3). General refuse from areas A and C were reportedly disposed of at this landfill during the period of 1945 to 1991. The refuse is suspected to have consisted of unknown quantities of oily wastes, solvents, and organic and inorganic chemicals. The actual type, quantities, and hazardous constituents are not known however, estimated quantities of hazardous materials disposed of in all the base landfills are presented in Table 1-1. These are estimated of the total volume of material disposed of at LF-5.

From 1940 to 1991, LF5 was used as a coal ash disposal area for waste generated at the base heating plants. It was also the site of a waste oil collection, separation, burning, and recycling operation. These activities took place over a 20 year period ending in 1978. The northwest portion of LF5 was also used for explosive ordinance disposal (EOD) and EOD ash disposal for an unknown period of time.

#### **1.2 GEOLOGICAL INFORMATION:**

Geographically, WPAFB is located within the till plains section of the central lowlands physiographic province. The land surface of the region is generally flat to gently rolling with streams and rivers forming level flood plains. Topographic relief in the area is the result of glacial deposition activity from the Wisconsin glaciation of the Pleistocene age. Glacial tills consist of a heterogeneous, unsorted mixture of cobble, gravel, sand, silt, and clay sized particles. The till ranges from 1 to 80 feet thick and can contain sand and gravel stringers.

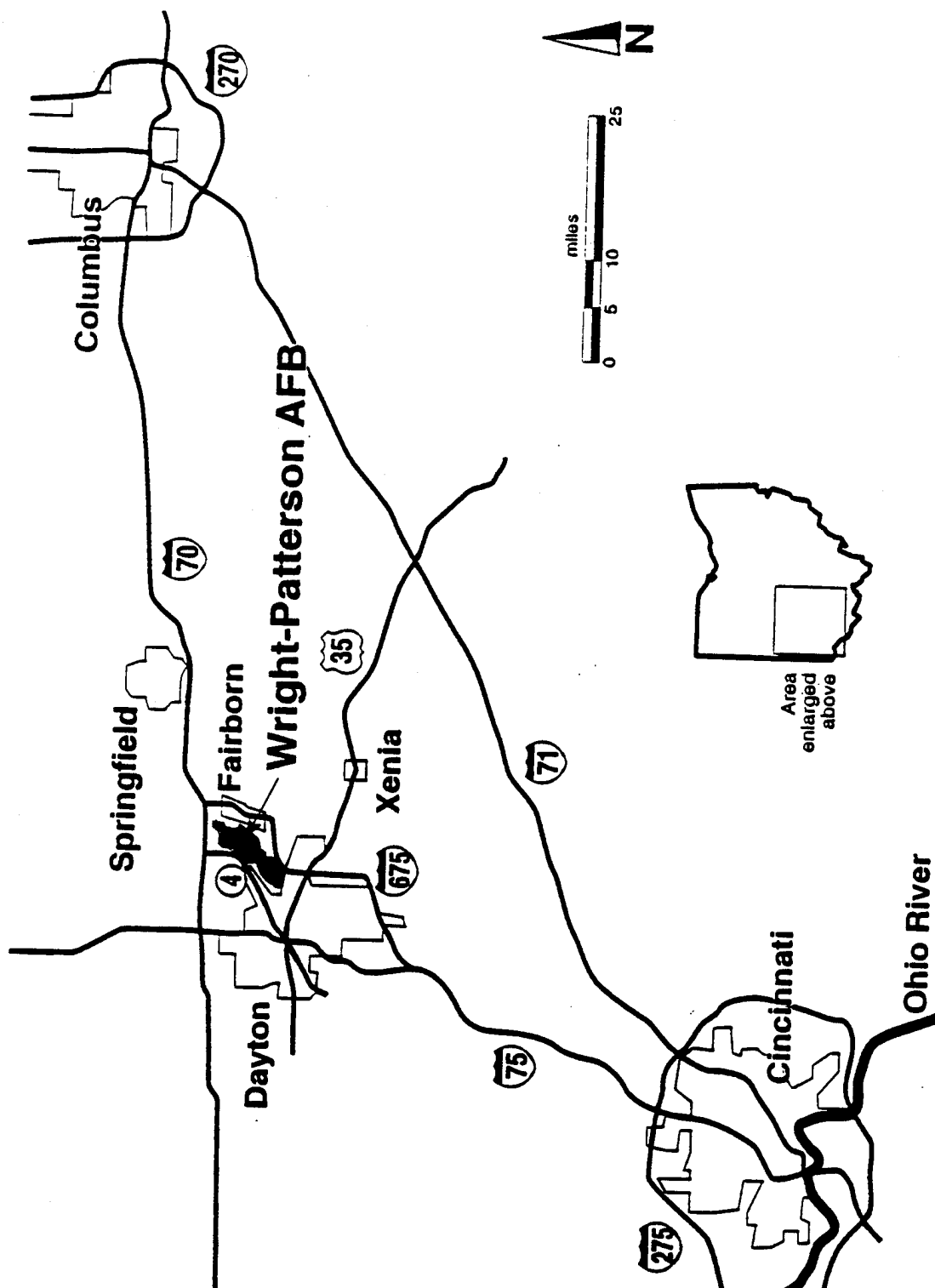


Figure 1-1 Area Location Map

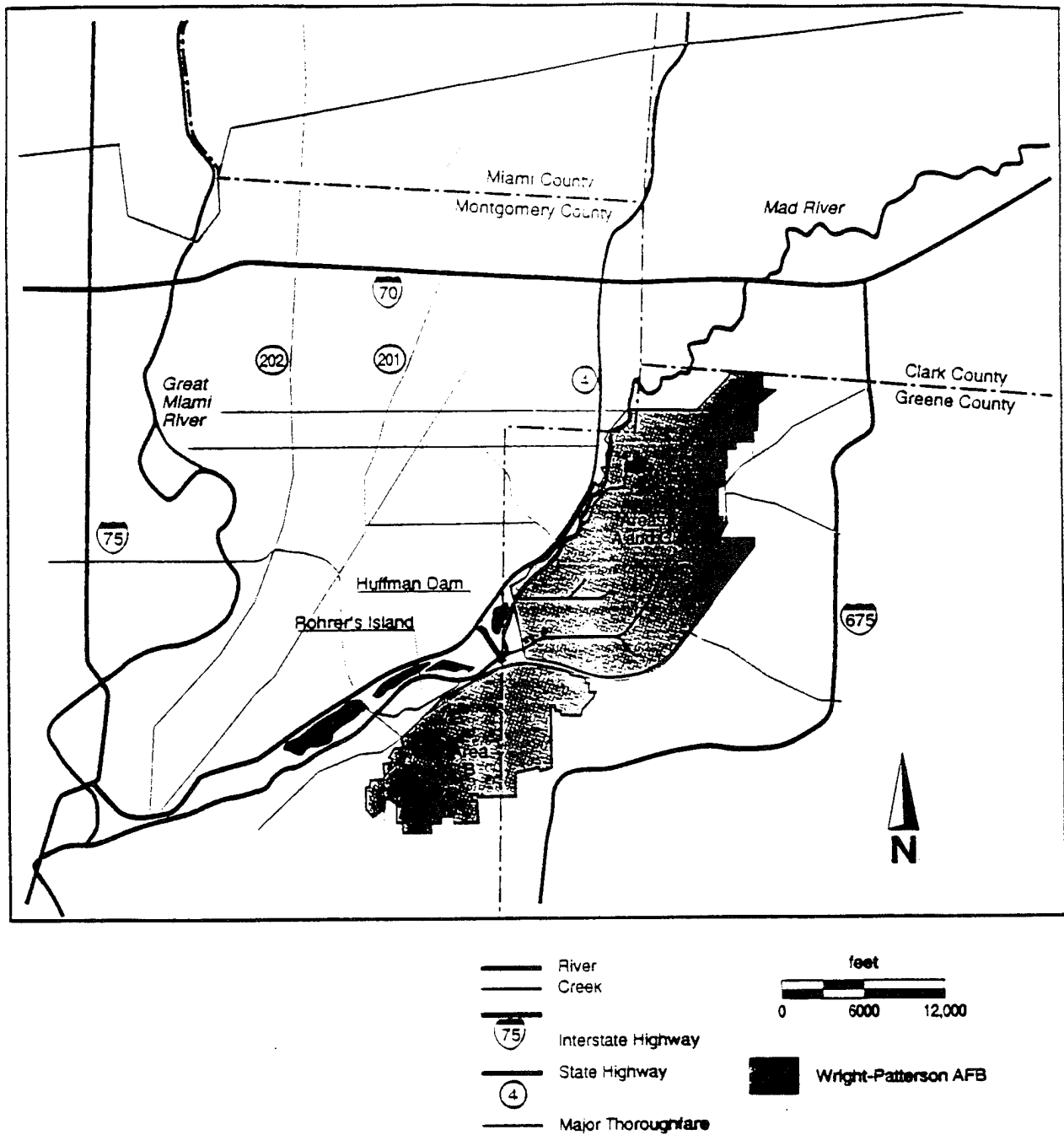


Figure 1-2 Location of Wright Patterson AFB.

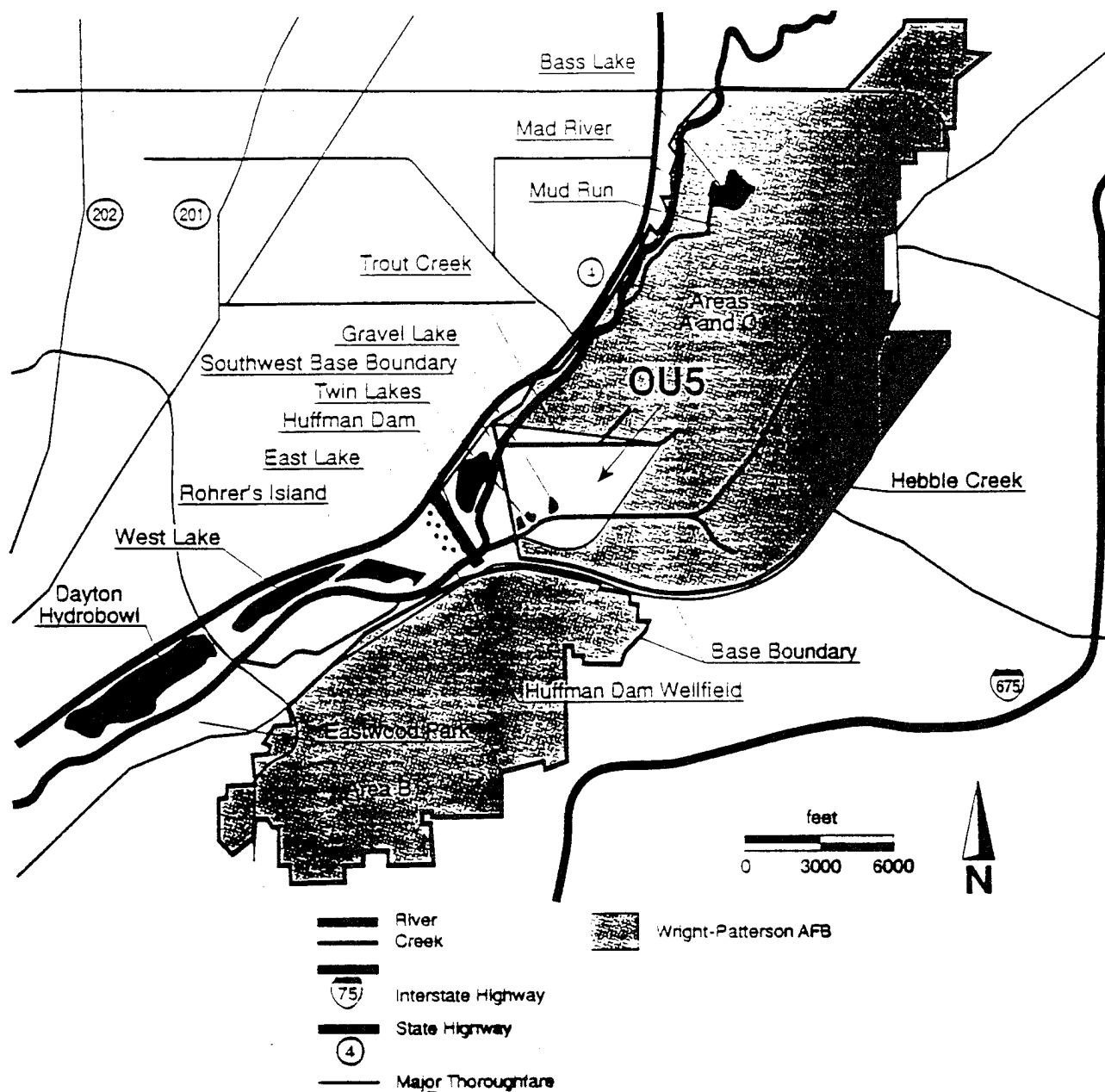


Figure 1-3 Location of Landfill #5.

TABLE 1-1  
Estimated Quantities of HM

Material	Estimated Quantity Landfilled
Nickel acetate	6,400 gallons
Cadmium oxide powder, sodium cyanide, caustic soda	25,740 gallons
Trichloroethene (TCE)	520 gallons
TCE degreaser sludge	8.25 drums
Paint strippers, contaminated thinners, waste paint	1,540 gallons
Paint remover	40,600 gallons
Carbon remover, PD-680, hydraulic fluid, paint thinner	20,300 gallons
Paint strippings	9,075 gallons
Enamel paints	370 drums
Solvent wastes, paint wastes, thinners	66 drums
Miscellaneous chemicals	8,400 pounds
Plating solutions	1,500-2,300 gallons

Source: Preliminary Assessments (ES, 1988)

More specifically, the geological conditions of the actual ash disposal site are depicted in South-North and West-East geologic cross sections shown in Figures 1-4 and 1-5. The predominant stratigraphic intervals observed in these sections consist of flyash, landfill debris, and native soils. A previous study of the area indicated that the area is comprised of loose sands (flyash), silts, gravels, some clay intervals, and various amounts and distributions of general refuse and hardfill.

### **1.3 PREVIOUS STUDIES:**

Since the ash disposal area is an Installation Restoration Program (IRP) site, several previous studies have been conducted to characterize the site. A summary of the studies is discussed below.

A. PHASE 1 - Initial activities consisted of a Phase 1 Records Search Report. This document identifies LF5 as a potentially contaminated site and included it in the IRP.

B. PHASE 2, STAGE 1 - Phase 2, Stage 1 IRP Confirmation/Quantification activities were conducted during 1982 through 1984 and the results were reported by Weston in 1985. The activities during this phase included drilling of soil borings and installation of monitoring wells.

C. PHASE 2, STAGE 2 - Phase 2, Stage 2 investigations were undertaken to more fully determine the types of contaminants present and potential exposure pathways. Phase 2, Stage 2 work was initiated in 1986 and was completed in 1989 as reported by Weston in 1989.

D. SOIL GAS AND GEOPHYSICAL INVESTIGATIONS - A soil gas survey was performed at LF5 between the Autumn 1989 and Summer 1990 to screen for locations of potential contaminant sources. During the same period, a geophysical investigation of LF5 was also conducted to identify potential sources of contamination.

E. REMEDIAL INVESTIGATION/FEASIBILITY STUDY (RI/FS) - A RI/FS was conducted in the summer of 1992 and was submitted to the EPA for approval in September 1992.

F. AERIAL RADIOLOGICAL SURVEY OF WPAFB - An aerial survey was conducted over WPAFB and the immediate surrounding during the period of July 7 through July 20, 1994. The survey was conducted to measure and map gamma radiation in the area. The ash disposal area was detected as a source of localized gamma radiation.

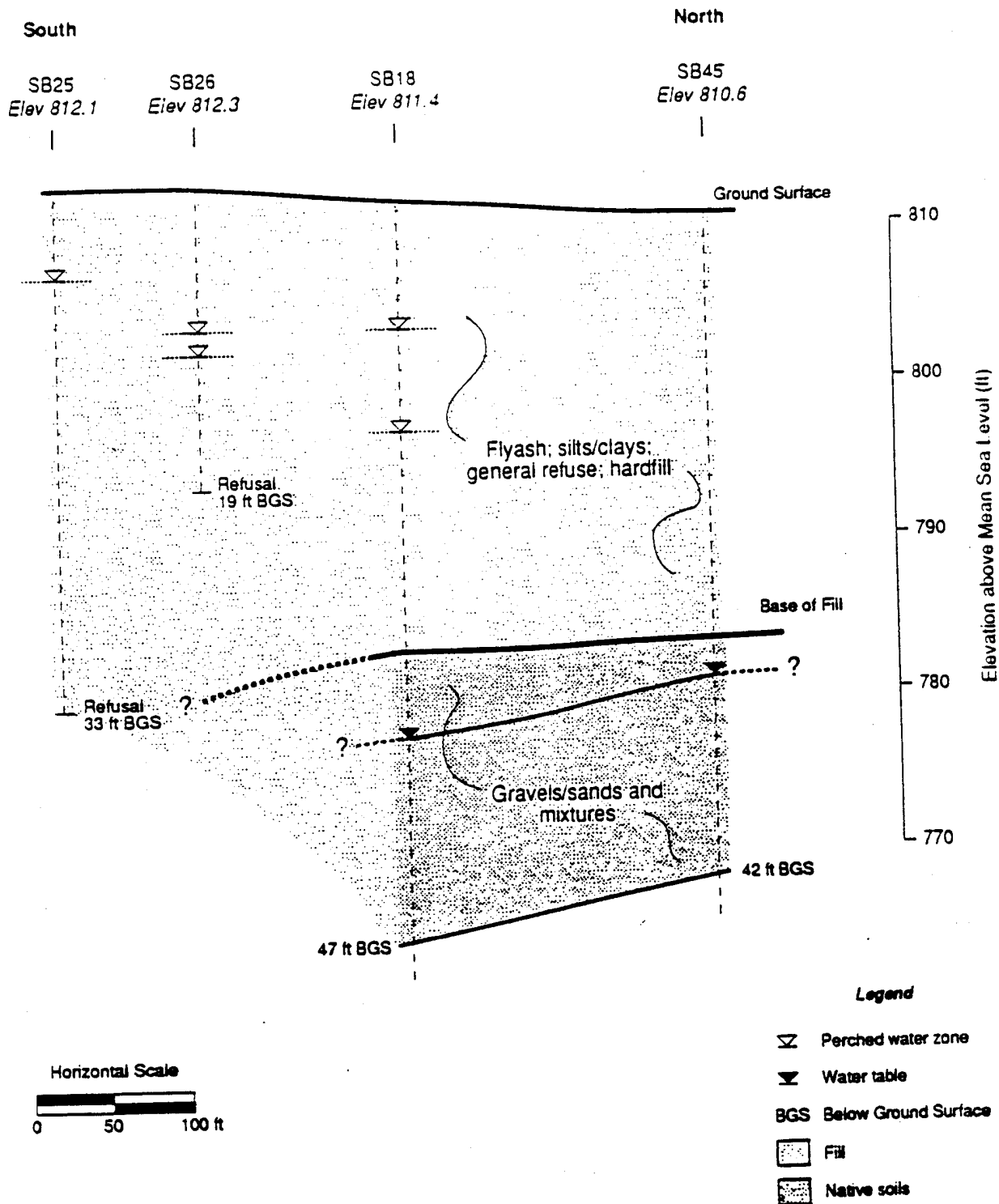


Figure 1-4 North - South Geologic Cross Section.

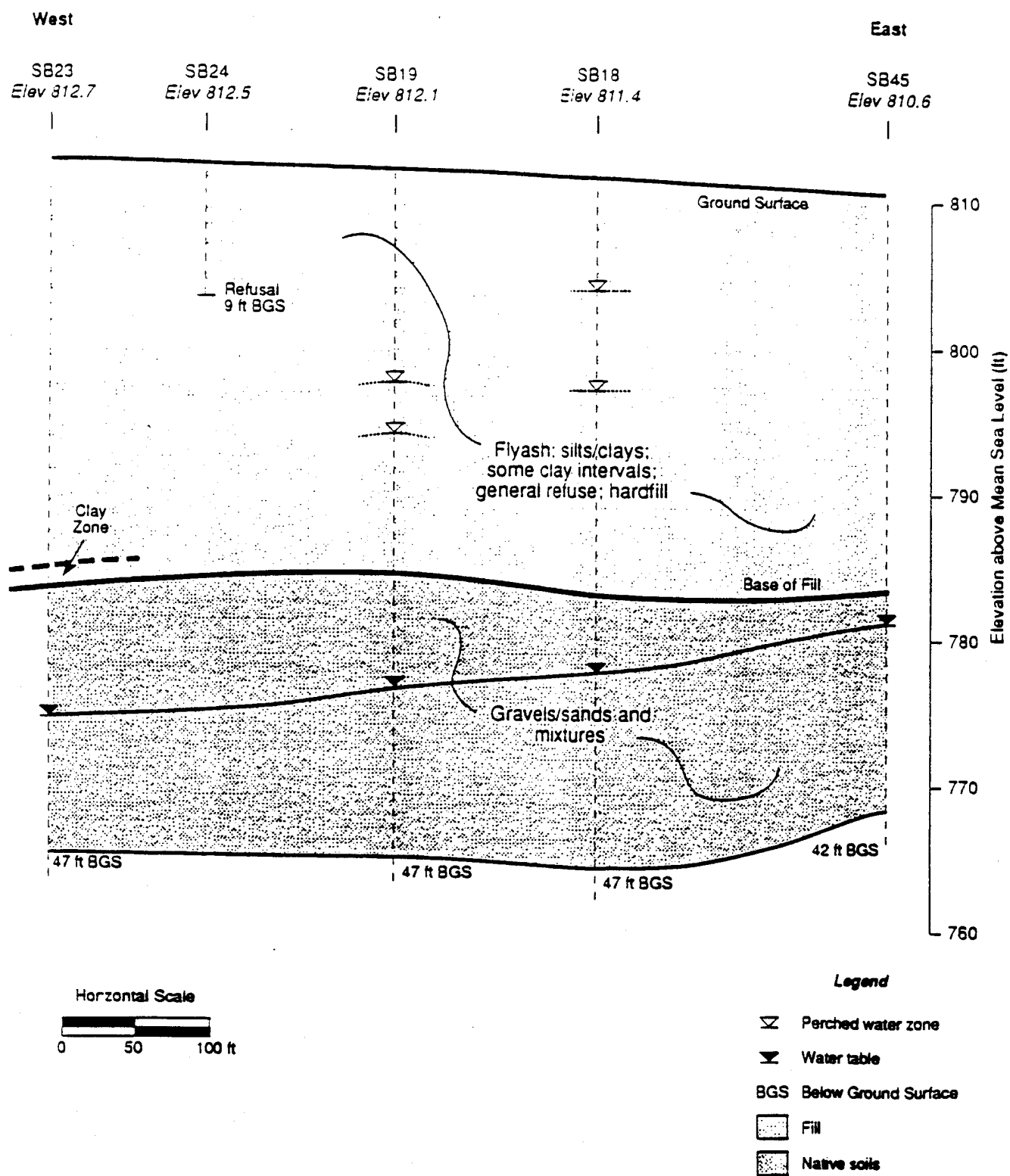


Figure 1-5 East - West Geologic Cross Section.



## **2.0 CONCEPTUAL SITE MODEL:**

The conceptual model is a tool that is used to understand the site dynamics and link potential sources of release with existing or potential receptors. Since the base ash disposal area is a part of the base LF-5, the conceptual model will be developed for the whole landfill.

### **2.1 Geology:**

LF-5 is located over unconsolidated alluvial deposits consisting of gravel, sand, silt, and clay of variable thickness. This thickness ranges from near zero at the basin borders to over 225 feet at the City of Dayton (COD) well # 3 located west of the base boundary. Alluvial deposits overlay dense gray clay layer which in turn overlays shale bedrock at a depth of 32 feet near Fire Training Area 1 (FTA-1).

### **2.2 Hydrology:**

Groundwater occurs in alluvial deposits at a depth of approximately ten feet below the ground surface in the area near and west of LF-5 under unconfined conditions. The alluvial aquifer does not contain laterally continuous clay layers above the aquifer base and is conceptualized to be a single aquifer containing discontinuous minor clay bed microstructure. Groundwater flow is generally to the southwest toward the Mad River. Figure 2-1 presents a potentiometric surface map of a portion of LF-5.

Surface water in LF-5 consists primarily of three drainages and three small lakes. The Mad River is the dominant drainage in the area. Huffman Dam was constructed on the Mad River in 1921 to control downstream flooding. The average flow of the river at Huffman Dam is reported to be approximately 630 cubic feet per second as reported by Weston, 1989. Two tributaries to Mad River occur near LF-5: Trout Creek, located north of LF-5 and Hubble Creek, located south of LF-5. Twin Lakes and Gravel Lake constitute the remainder of the surface water. The lakes are reported to be former gravel quarries and are currently used for recreational activities.

### **2.3 Topography:**

LF-5 Lies within the floodplain of the Mad River and is characterized by relative flat to slightly rolling topography. Land surface elevations range from approximately 815 feet above mean sea level (MSL) on top of LF-5, to 780 feet above MSL in the area west of LF-5.

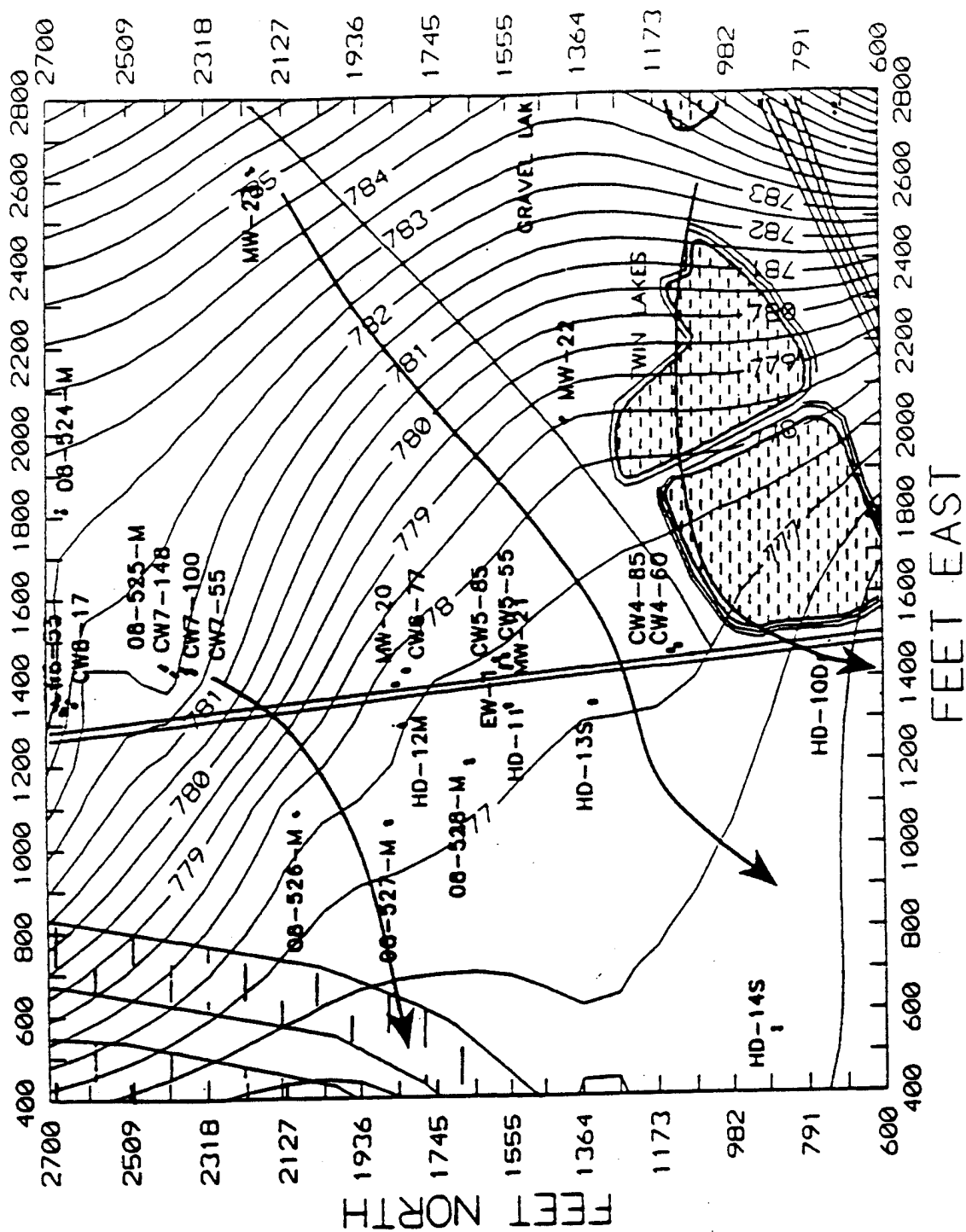


Figure 2-1 Potentiometric Surface Map

## **2.4 Meteorological Conditions:**

The climate of WPAFB and surrounding areas is humid and temperate with a mean annual temperature of 52.5 degrees F. Recorded temperatures during the winter period indicate a mean monthly minimum of 21.4 degrees F. The recorded mean monthly maximum in the summer is 85.2 degrees F. Annual precipitation ranges from 2.17 inches in February to 3.73 inches in May. Average annual lake evaporation is estimated to be 33 inches (3:1-3).

Figures 2-2 and 2-3 depict the conceptual model in graphical format.

## **3.0 CONTAMINANT INFORMATION:**

### **3.1 CONTAMINANTS OF INTEREST:**

This study is interested in detecting the levels of radionuclides in the  $4n$ ,  $4n+2$  and  $4n+3$  decay chains. More specifically, since gamma spectroscopy is going to be used to analyze the samples, the interest lies in those radionuclides that emit gamma radiation. The nuclides specifically selected for this study are  $^{40}\text{K}$ ,  $^{214}\text{BI}$ ,  $^{214}\text{PB}$ ,  $^{234\text{m}}\text{PA}$ , and  $^{226}\text{RA}$ .

### **3.2 CONTAMINANT TRANSPORT:**

One possible pathway of radionuclide escape into the environment could occur from the leaching of the flyash in the disposal pit, but research has shown that the radionuclides bound in fly ash have limited solubility, and therefore not likely to occur (2: 45). A second pathway is the possible release from the disposal area due to suspension and dispersion of the ash itself due to winds or other atmospheric phenomenon. Finally, the last path of escape of radionuclide is the emanation of  $^{222}\text{Rn}$  from the ash disposal area.

## **4.0 DATA QUALITY OBJECTIVES:**

### **4.1 STATE THE PROBLEM:**

WPAFB operates 2 heat plants that are fueled by coal which naturally contains low levels of the previously mentioned radionuclides. Recent studies indicate that radionuclide become enriched in coal ash, the powdery particulate by-product of coal combustion (1: 46). This concentration in coal ash combined with the large amount of ash produced over the past several decades may pose an environmental hazard resulting from ash disposal practices. These practices consist of placing the ash into an unlined landfill which does not provide protection against escaping natural radiation.

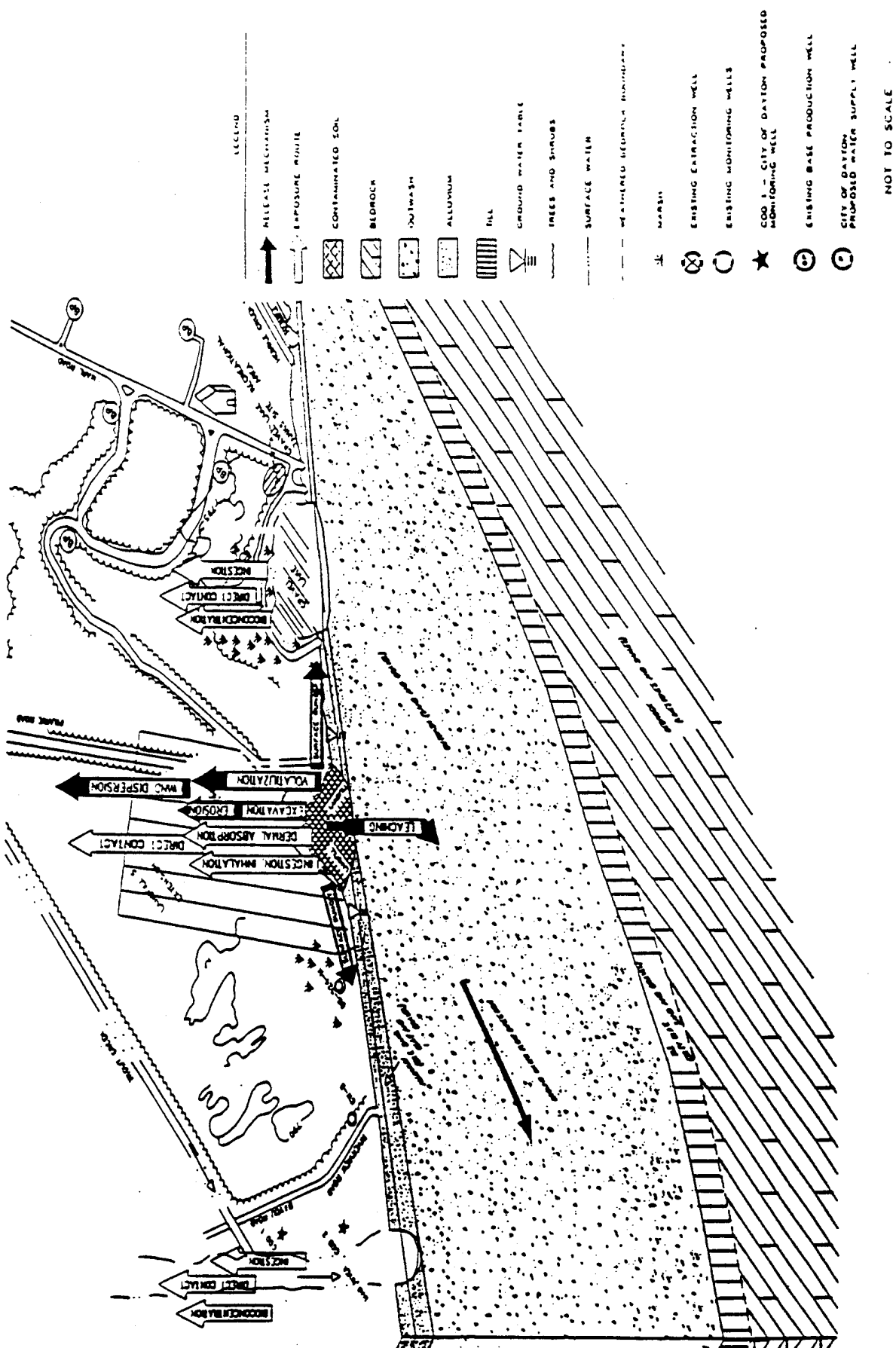


Figure 2-2 Conceptual Site Model- Southwest-Northeast Orientation.

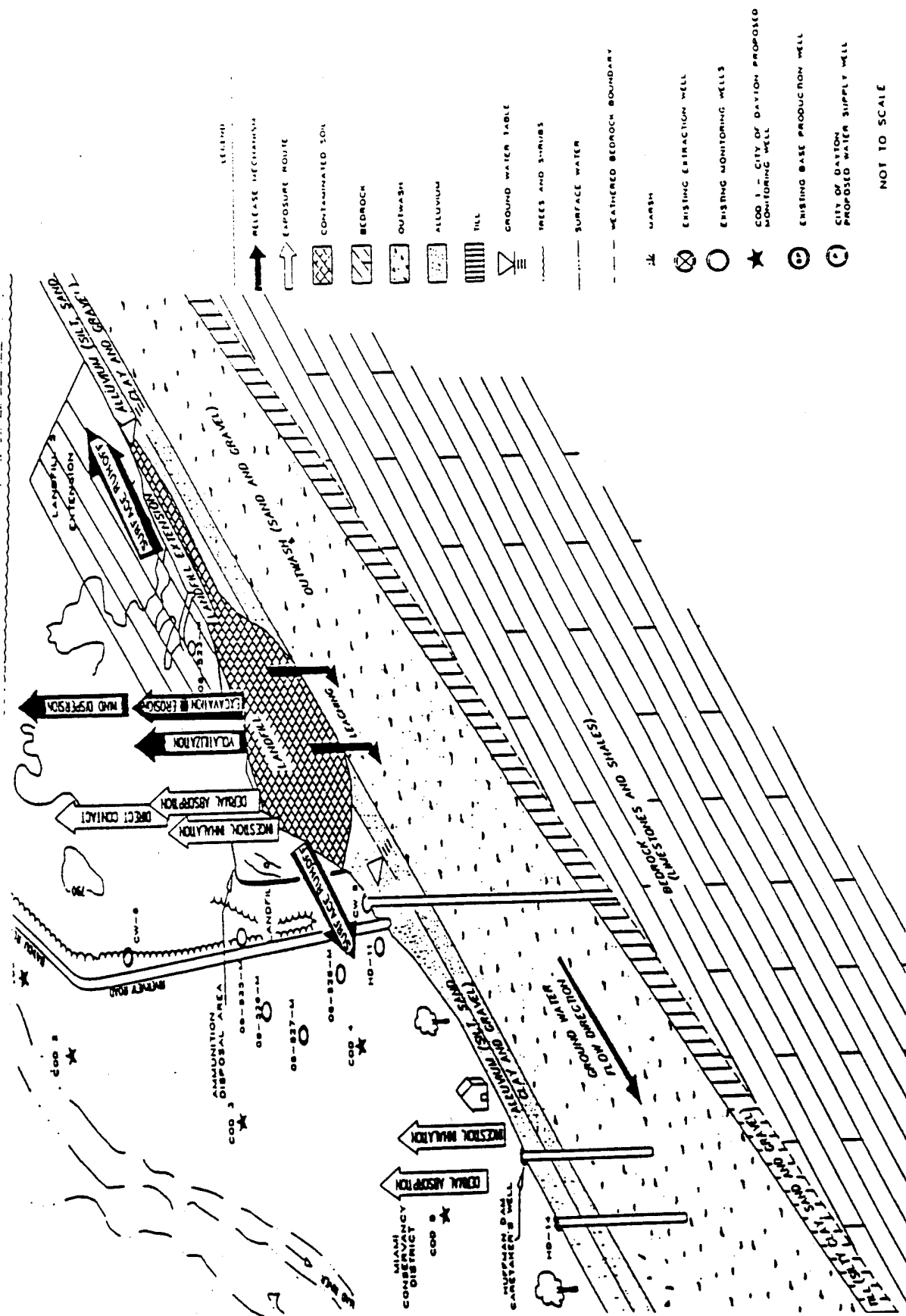


Figure 2-2 Conceptual Site Model Northwest-Southeast Orientation.

WPAFB has an area LF-5 that has been used as an ash disposal site for the past 40 years (3: 2-23). The purpose of this sampling effort is to determine the activity levels of various radionuclides in the ash disposal area. This information will be used to determine if the mean site radon "source potential" ( $^{226}\text{Ra}$  activity) is statistically significantly above background. If it is, then the amount of radon emanating from the site will be calculated.

#### **4.2 IDENTIFY THE DECISION:**

##### **A. The Decision:**

1. Determine if the mean activity level of  $^{226}\text{Ra}$  at LF-5 is statistically significantly greater than background levels.

##### **B. Actions That Could Result From the Decision:**

1. If activity levels at the ash disposal site are statistically significantly higher than background levels, recommend further assessment or a response action depending on the magnitude of the difference and the outcome of the radon emanation calculations.

#### **4.3 IDENTIFY INPUTS INTO THE DECISION:**

##### **A. Identify Informational Inputs:**

1. Mean activity levels of each contaminant of interest are required from the ash disposal area.
2. Mean activity levels of each contaminant of interest are required from background locations.
3. Spatial relationship between sample locations.
4. Area and volume of the ash landfill.

##### **B. Identify Sources for Each Informational Input:**

1. Mean activity levels can be obtained through analytical measurements of soil samples obtained from each of the respective areas.
2. Spatial relationship can be determined using geostatistical techniques.
3. Area and volume of the ash landfill can be determined from maps.

##### **C. Identify Potential Sampling Techniques and Analytical Methods:**

1. Grab samples using a shovel has been identified as a potential sampling technique.
2. Gamma spectroscopy is the proposed analytical technique.
3. Geostatistical analysis is the proposed method for determining spatial correlation and mean activity level of the site.

#### **4.4 DEFINE THE STUDY BOUNDARIES:**

##### **A. Spatial Boundaries:**

1. Define the Domain: The study will focus on the soil/ash located in the ash disposal area of WPAFB LF-5.

2. Specify the Characteristics of the Population of Interest: The mean activity levels of each contaminant of interest.

3. Define the Scale of Decision Making: Samples will be taken from the ash disposal area and from selected background locations on WPAFB. The mean activity levels of the contaminants of interest at the ash disposal area will be compared to the background mean activity levels to determine if they are statistically significantly different. Separate decisions will be made for each contaminant of interest.

##### **B. Temporal Boundaries:**

1. When to Collect Data: It is assumed that there are no systematic variations in the activity levels of the contaminants of interest over the sampling period. Therefore, samples may be taken at any time of the day.

2. Practical Considerations That May Interfere With the Study: WPAFB has awarded a contract to cap the landfill that contains the ash disposal area. The capping is scheduled to begin in April, 1995. All samples used for the study must be collected prior to the start of the capping project.

#### **4.5 DEVELOP A DECISION RULE:**

If the mean activity level of any of the contaminants of interest at the ash disposal site are statistically significantly greater than the mean concentration of the contaminants of interest at the background locations, then the site will be considered contaminated for that particular contaminant and further assessment or response will be determined, otherwise no further action will be taken.

#### **4.6 SPECIFY LIMITS ON DECISION ERRORS:**

A. Decision error Type I occurs when the decision maker decides the study site is contaminated, when in truth, the mean activity level is less than or equal to the background site. The primary consequence of this decision error is wasted resources. For this detection scenario, this decision error is considered a False Positive.

B. Decision error Type II occurs when the decision maker decides the study site is not contaminated, when in truth, the mean activity levels are greater than the background levels. If a study site that poses an unacceptable risk is not remediated, human health and/or environmental risk are increased. Future health and remediation costs may also result. For this detection scenario, this decision error is considered a False Negative and is more severe. The true state of nature for a Type I error is that the site is not contaminated. The true state of nature for a Type II error is that the site is contaminated.

C. Each contaminant of interest will be compared separately with the background levels. The Null Hypothesis ( $H_0$ ) for each comparison is that the mean activity level of the contaminant of interest at the site is less than or equal to the activity level at the background site. The Alternate Hypothesis ( $H_a$ ) is that the mean activity of the contaminant of interest at the site is greater than the mean activity at the background site.

D. We will use a two sample t test to determine if the source at the ash landfill was statistically significantly higher than background. A two sample t test was applied to the landfill and background mean  $^{226}\text{Ra}$  activities. The two sample t test was used because the sample size of the background sampling effort was small (less than 30) and the variance of the population was unknown. This test was also chosen because it offered a minimum beta ( $\beta$ ) value.  $\beta$  is the probability of type II error (not rejecting  $H_0$  when  $H_0$  is false).

In order to use the two sample t, two assumptions had to be made. First, both populations were assumed to be normal, so that  $X_1, X_2, \dots, X_m$  (regular study) was a random sample from a normal distribution and so was  $Y_1, Y_2, \dots, Y_n$  (background study) with the X's and Y's independent of one another. The second assumption made was that the value of the two population variances  $\sigma^2_1$  and  $\sigma^2_2$  were equal, so that their common value could be denoted by  $\sigma^2$  (which is unknown).

Since  $\sigma^2$  was unknown it had to be estimated. Because  $\sigma^2$  was assumed to be the variance of both the X and Y distribution, the following equation was used to estimate it.

$$S_p^2 = \frac{(m-1) \cdot S_1^2 + (n-1) \cdot S_2^2}{m+n-2}$$

Where  $S_p^2$  is the pooled estimator of the population variance,  $S_1^2$  and  $S_2^2$  are the variances of the regular study sample and background study sample respectively, and m and n are the sample sizes for the regular study and background study respectively. This estimate, commonly known as the pooled estimator depends on both the  $X_i$ s and the  $Y_i$ s. As might be expected, more weight was given to the sample that corresponded to the larger of the two sample sizes.

Once the estimator of the population variance was calculated, the following two sample t test was derived for testing.



Null hypothesis:

$$H_0: \mu_1 - \mu_2 = \Delta_0$$

Test Statistic:

$$t = \frac{\bar{X} - \bar{Y} - \Delta_0}{S_p \sqrt{\frac{1}{m} + \frac{1}{n}}}$$

Alternative hypothesis:

$$H_a: \mu_1 - \mu_2 > \Delta_0$$

Rejection Region:

$$t \geq t_{\alpha, m+n-2}$$

Where  $\mu_1$  and  $\mu_2$  are the regular study and background study populations respectively,  $\Delta_0$  is zero (if the means are equal),  $S_p$  is the pooled estimator of the population variance,  $\bar{X}$  and  $\bar{Y}$  are estimators of  $\mu_1$  and  $\mu_2$  respectively,  $\alpha$  is .05, and  $m$  and  $n$  are the regular study and background study sample sizes respectively.

The test was set up so that if the null hypothesis was accepted it would mean that  $\mu_1$  and  $\mu_2$  were equal and the landfilled coal ash had no effect on the  $^{226}\text{Ra}$  activity. The alternative, or researcher's hypothesis was set up so that if the null hypothesis was rejected in favor of the null it would indicate that the regular study  $^{226}\text{Ra}$  mean activity was statistically significantly greater than the background study  $^{226}\text{Ra}$  mean activity. In other words, the landfilled coal ash resulted in increased  $^{226}\text{Ra}$  activity.

## **5.0 FIELD APPROACH:**

### **5.1 AVAILABLE RESOURCES:**

Limited funds are available for this sampling effort. Therefore, use of a cone penetrometer or mechanized drilling apparatus is not financially feasible. Due to the objectives of this study, manual alternatives are acceptable. These alternatives include the use of a hand auger or shovel. Other equipment available for use in this study include, but is not limited to:

Plastic Gloves	Auger	Tape	Deionized Water
Steel-toed boots	Shovel	Marinelli Beakers	Computer Resources
Eye Protection	Hammer	Decontamination Equipment	Laboratory Resources

## 5.2 PHASE I (Pilot Study):

### A. Sample Collection:

Based on historical and geological information, two main assumptions are presumed and will be tested in the pilot study. First, based on the geological cross-sections in figures 1-5 and 1-6, the fly ash is homogeneously distributed throughout the site. Second, since the radionuclides have limited solubility, there is no variation in radioactivity levels as depth increases due to the leaching process. With these assumptions in mind, a systematic sampling approach with an aligned grid will be used. Detailed procedures can be found in appendix A, Filed Sampling Protocol. This method was selected to ensure complete coverage of the site and ensure unbiased selection of sampling points.

In order to encompass the ash disposal area, a 500' x 500' foot square sampling grid was constructed. A systematic aligned grid system was used to determine 36 initial sampling points 100' apart, one at each node of the grid. This method was selected to ensure complete coverage of the site and ensure unbiased selection of sampling points. (2: 89) Also, an additional 34 sampling points were located at 5, 10, and 20 foot intervals along a 200' transect extending north and a 200' transect extending east of grid location #22. (see Figure 5-1) The samples collected at these shorter intervals are required to provide the structure needed for geostatistical analysis.

Samples will also be taken from three background locations (see Figure 5-2) for comparison. The locations of the three background samples were chosen based on their representativeness of uncontaminated local soil conditions. The samples will be taken at a depth of 24 inches and handled and analyzed in the same manner as the ash disposal site samples.

Due to the limitations mentioned above, soil samples will be collected using a hand held shovel. Since the site is assumed to be homogenous (until otherwise proven) and due to the equipment limitations, the samples will be taken to a depth of 24 inches. The samples will be placed into a Marinelli beaker, labeled, and transported to the lab to be analyzed by gamma spectroscopy.

### B. Laboratory Analysis:

The analytical method used, gamma spectroscopy, is a non destructive technique for determining gamma emitting radionuclides in environmental samples. It is designed to detect gamma photons with energies ranging from approximately 10 to 2000 kiloelectronvolts (KeV). A sample will be placed in a lead shield on a high purity germanium detector and then counted. The data will be collected and transformed into a format that can be analyzed by Genie-PC gamma assessment software. The detector is calibrated for both energy and peak efficiency. A report will then be printed identifying the peaks utilized, the shape and height of the peaks, the activity of each radionuclide identified, and the corresponding counting error.

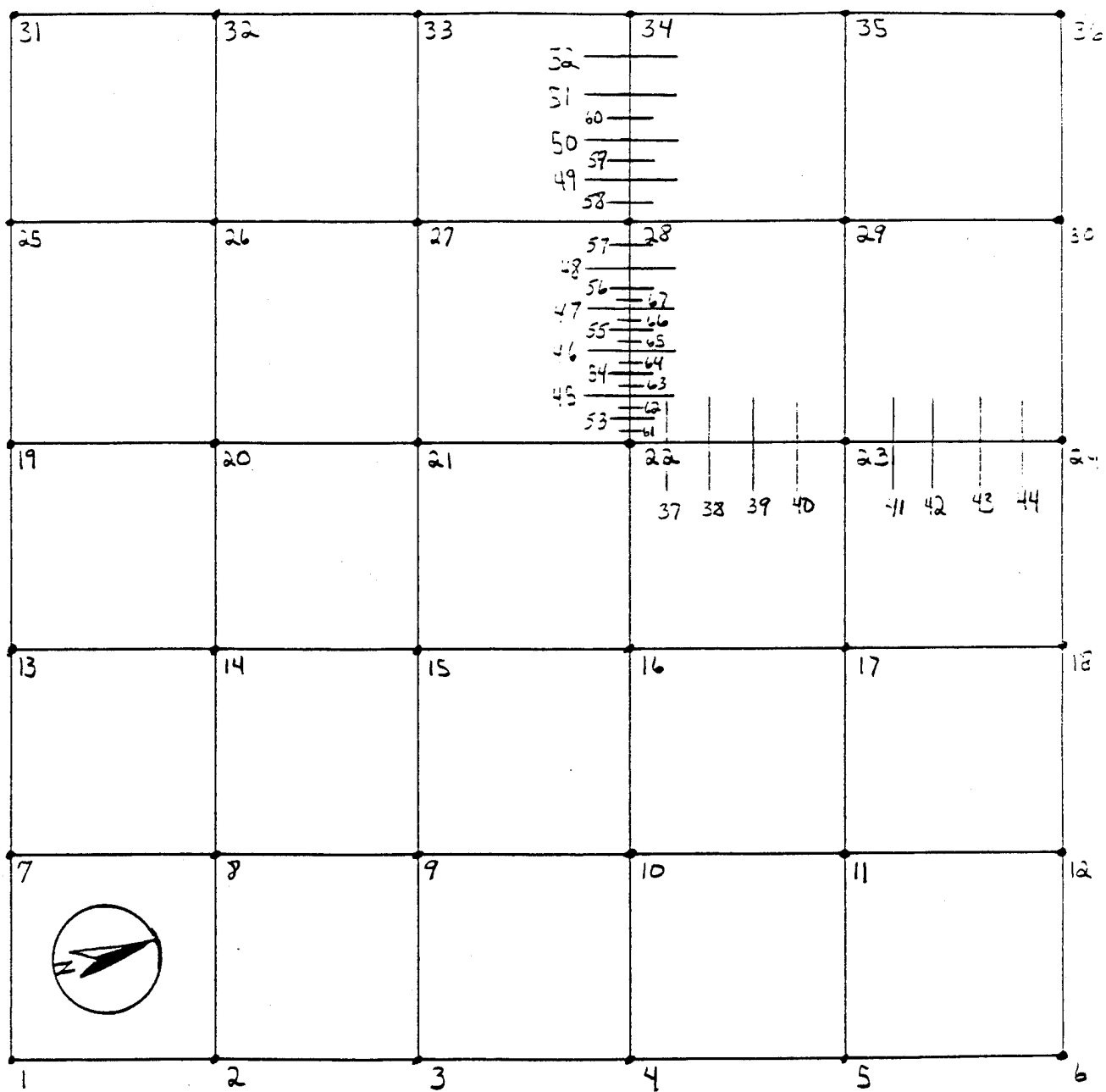


Figure 5-1 Sampling Grid.

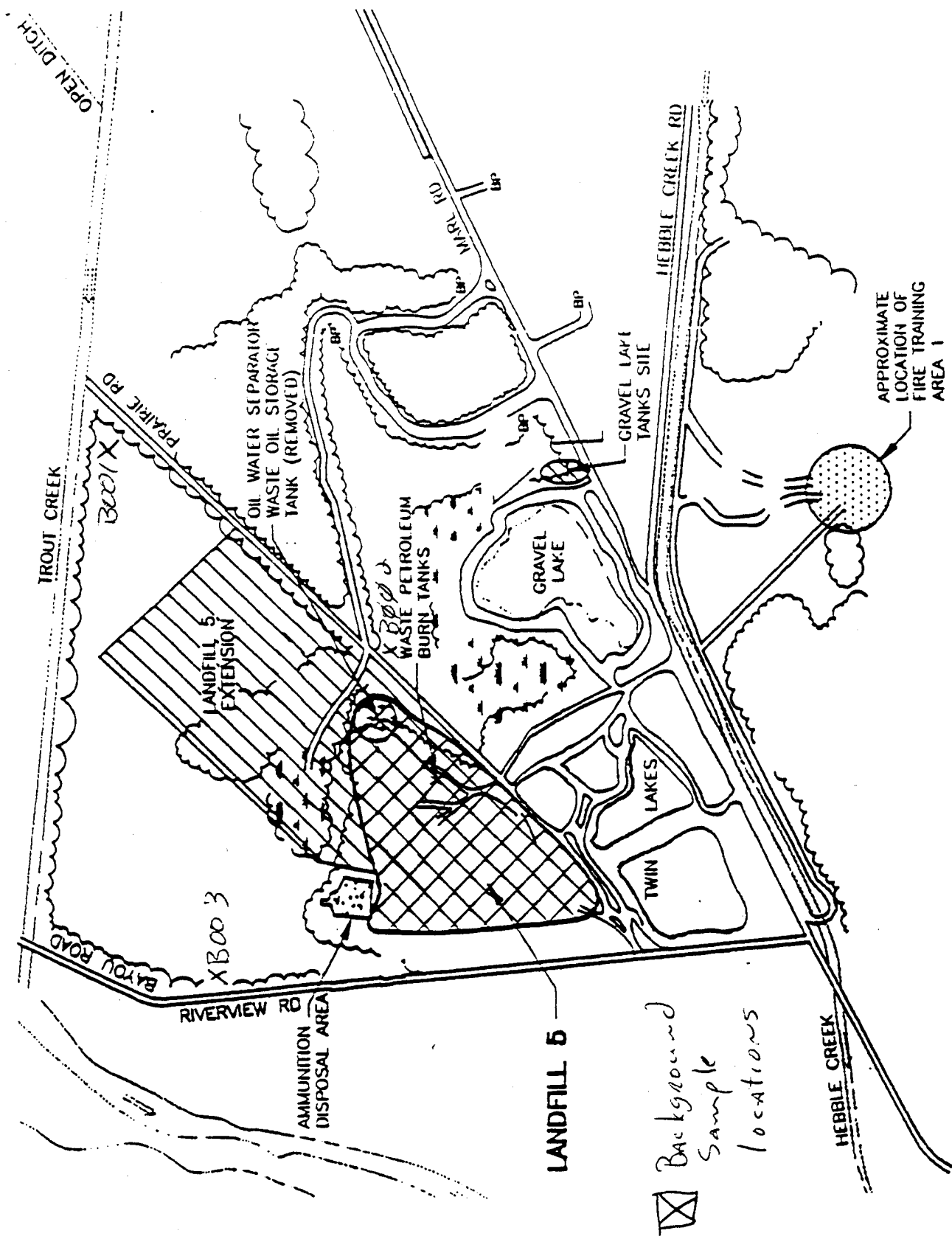


Figure 5-2 Background Sample Locations.

### C. Statistical Analysis:

A combination of ordinary univariate statistical and geostatistical techniques will be used to verify the assumptions made, determine spatial correlation at the site, and determine the inputs for the next phase of sampling (number of samples required, location, etc.). These techniques include, but are not limited to, frequency tables, histograms, probability plots, contour plots, variogram analysis, covariance plots, and correlation plots. If no spatial correlation exists, traditional statistical techniques will be used for the regular study instead of geostatistics.

### **5.3 PHASE II (Regular Study)**

The same procedures used in the pilot study will be followed for taking additional samples in the regular study. Also the same analysis techniques will be used to determine the levels of radionuclides in the samples. Once the samples are analyzed, the site mean activity levels of the nuclides will be determined using either geostatistical (if correlation exists) or traditional statistics (if no correlation exists).

### **6.0 QUALITY ASSURANCE/ QUALITY CONTROL (QA/QC):**

To ensure that the data collected in the field is representative and valid, a number of QA/QC checks will be performed. Details about these checks can be found in Attachment II, Quality Assurance Program Plan (QAPP).

### **7.0 WASTE HANDLING:**

Waste generated due to the sampling efforts will be containerized and characterized and, if necessary, disposed of in accordance with applicable base, local, state and federal regulations. Details regarding the handling of waste will be addressed in the Field Sampling Protocol.

### **8.0 HEALTH AND SAFETY:**

#### **8.1 SITE RESPONSIBILITY:**

The project manager (thesis student) has the ultimate responsibility for field work at the site. He shall coordinate on-site health and safety activities and shall provide technical supervision for the ongoing activities on the site.

## 8.2 CONTAMINATION:

The degree of hazard potential, from an on-site worker health and safety standpoint, varies depending on the task involved and on the area the activities are conducted in. For work being conducted at the ash disposal area, surface activities present minimal risks to personnel. Previous studies (WPAFB RI/FS) have indicated that the organic vapor content in this area is below detectable limits. However, there still exists a potential for the release of organic vapors through the soil. As a precautionary measure, the organic vapor content of the air will be sampled using a photoionization detector with readings taken at breathing zone height. If organic vapors are detected, a benzene calorimetric tube will be used to determine its airborne concentration. Depending on the concentration levels present, appropriate personal protective equipment will be required from sampling personnel. If organic vapors are not present, level D PPE will be worn by sampling personnel. Table 1 below lists volatile organic contaminant levels:

TABLE 1  
VOLATILE ORGANIC CONTAMINANT LEVELS

<u>Contaminant</u>	<u>Exposure Limit in Air</u>	<u>TLV/TWA</u>
Benzene	1 ppm	1 ppm
Toluene	100 ppm	100 ppm
Ethylbenzene	100 ppm	100 ppm

Another potential hazard comes in the form of combustible gases that escape from the subsurface of the landfill. To minimize the hazard, the concentration of combustible gas will be monitored using a combustible gas indicator. The following criteria in table 2 will be used to evaluate and take action concerning the flammable or explosive vapors:

TABLE 2  
COMBUSTIBLE GAS CRITERIA

<u>Lower Explosive Limit</u>	<u>Action</u>
-----	-----
10 to 20 percent	Use nonsparking tools
Greater than 20 percent	Evacuate site

The final hazard to workers results from the gamma radiation in the coal ash itself. In order to monitor for radiation exposure film badges will be worn during sampling

operations. Additionally, a pocket dosimeter will be worn. This device will be checked at the end of each day against the criteria below.

TABLE 3  
RADIATION DOSE CRITERIA

Exposure Limit	Action
Less than 5 mrem	Continue normal operations
Greater than 5 mrem	Notify Radiation Safety Officer

### 8.3 LEVELS OF PROTECTION:

Based on the known site hazardous characteristics and the type of work being performed, personnel at the site will be required to wear personal protective equipment. The equipment used to protect the body against contact with known or anticipated chemical hazards has been divided into four categories according to the degree of protection afforded:

Level A - Should be worn when the highest degree of respiratory, skin, and eye protection is needed.

Level B - Should be worn when the highest level of respiratory protection is needed, but a lesser level of skin protection is allowable.

Level C - Should be worn when the types of airborne substances are known, the concentration is measured, and the criteria for using air-purifying respirators are met.

Level D - Is primarily a work uniform. It can be worn in areas where only boots and gloves can be contaminated or where there are no inhaleable toxic substances.

Level D protection will be required for all workers at the site. If initial air monitoring shows levels of organic vapors the protection level will be up graded to the appropriate level by the project manager. Additionally, a pocket dosimeter and film badges will be worn during the sampling operations to detect radiation exposure levels.

#### **8.4 EMERGENCY RESPONSE:**

Medical emergency telephone numbers are listed below. In case of life threatening emergency transport injured personnel directly to the base emergency room.

##### **EMERGENCY NUMBERS**

Base Emergency Room	(513)-257-2968
Ambulance Service	911
WPAFB Fire Department	(513)-257-7033
WPAFB Police Department	(513)-257-6516
Environmental Management Office	(513)-257-5537
Ohio State Highway Patrol	(513)-890-1111



ATTACHMENT 1  
FIELD SAMPLING PROTOCOL

# SAMPLING PROTOCOL

## 1.0 GENERAL PROVISIONS

A. Health and Safety: Sampling Team leader has ultimate responsibility for field work at the site. The sampling team leader will coordinate on-site health and safety activities and provide technical supervision for ongoing activities on the site.

1. Contamination: The degree of hazard potential, from an on-site worker health and safety standpoint, varies depending on the task involved and on the area that the activities are conducted in. For this study, the activities will be limited to surface work (top 2 feet of soil). The major exposure routes are anticipated to be via skin contact with contaminated materials. The potential does exist for possible inhalation of volatile organic compounds (VOCs) which have been detected in the groundwater. However, this is highly unlikely since the activities of this study are confined to the top 2 feet of soil and the groundwater is at least 40 feet below the surface. The air will be screened for VOCs prior to the start of work and every two hours while work is in progress to ensure the no VOCs are present. If detected, the site will be evacuated until personnel can obtain proper personnel protective equipment (PPE). Table 1 below lists volatile organic contaminant levels:

TABLE 1  
VOLATILE ORGANIC CONTAMINANT LEVELS

<u>Contaminant</u>	<u>Exposure Limit in Air</u>	<u>TLV/TWA</u>
Benzene	1 ppm	1 ppm
Toluene	100 ppm	100 ppm
Ethylbenzene	100 ppm	100 ppm

Another potential hazard comes in the form of combustible gases that escape from the subsurface of the landfill. To minimize the hazard, the concentration of combustible gas will be monitored using a combustible gas indicator. The following criteria in table 2 will be used to evaluate and take action concerning the flammable or explosive vapors:

TABLE 2  
COMBUSTIBLE GAS CRITERIA

<u>Lower Explosive Limit</u>	<u>Action</u>
10 to 20 percent	Use nonsparking tools
Greater than 20 percent	Evacuate site

The final hazard to workers results from the enhanced natural radiation in the coal ash itself. In order to monitor for radiation exposure TLD badges will be worn during sampling operations. Additionally, A pocket dosimeter will be worn. This device will be checked at the end of each day against the criteria below.

TABLE 3  
RADIATION DOSE CRITERIA

Exposure Limit	Action
Less than 5mrem	Continue normal operations
Greater than 5mrem	Notify Radiation Safety Officer

2. Other Hazards: Tripping, slipping and fall hazards should be pointed out and corrected whenever possible.

3. Personal Protection: Based on the known site hazards and the type of work being performed, personnel at the site will be required to wear personal protective equipment. There are four levels of protection:

Level A: Should be worn when the highest degree of respiratory, skin, and eye protection is needed.

Level B: Should be worn when the highest level of respiratory protection is needed, but a lesser level of skin will suffice.

Level C: Should be worn when the types of airborne substances are known, the concentration is measured, and the criteria for using air purifying respirators are met.

Level D: Primarily a work uniform. it can be worn in areas where only boots and gloves can be contaminated or where there is no inhalable toxic substances.

Previous studies have indicated that there are no measurable levels of VOCs present at the surface, therefore for this study, level D protection will be required unless otherwise specified. Also as mentioned above, a pocket dosimeter and film badges will be worn during the sampling operations.

4. Safety Briefing: A safety briefing will be conducted before the start of each work day. It will be composed of the following items:

- a. Lifting safety (lift with your legs/not your back)
- b. Accident notification (Team leader will be notified immediately of all injuries on the site)
- c. Routes to the hospital and emergency numbers (911)
- d. Site specific hazards (contaminant, weather, miscellaneous)
- e. Evacuation

B. Equipment Inventory: The following equipment will need to be procured for this study. In addition, before proceeding to the site, sampling team leader will personally conduct an inspection of all equipment, which is composed of the following:

- 1. Hand auger kit (3 bits, two extensions, one handle, one shovel, one bar)
- 2. Measuring Tape (100')
- 3. Visqueen
- 4. 4 Buckets (3 filled with tap water)
- 5. Soap (non phosphate)
- 6. Sterile Marinelli beakers (one for every sample to be taken at a minimum)
- 7. Plastic Gloves
- 8. Wooden Stakes
- 9. Scrub brush
- 10. Black marker
- 11. Hammer
- 12. Filtered water (2 gallons)
- 13. Log Book
- 14. Rigid tape measure
- 15. Knife
- 16. String
- 17. Labels for beakers
- 18. Chain of Custody forms
- 19. Drager Tube

Ensure equipment is in good repair, and that all digging equipment is clean.

## **2.0 FIELD SAMPLING DESIGN**

### **2.1 Site Criteria:**

A. The site was chosen because it was the location of coal ash disposal for Wright Patterson Air Force Base (WPAFB) for the past 40 years. It is located at WPAFB landfill #5.

B. The geology of the site was discussed earlier in Data Quality Objectives section.

## 2.2 Sample Method:

A. The sample method for this study was chosen to be a systematic approach using a 500' by 500' square grid. This method was chosen because it ensures complete coverage of the site. It will also help determine the need for geostatistical analysis. The grid will be partitioned off into 25 equally spaced cells (each cell measuring 100' by 100'). One sample will be taken from each node at a depth of 24 inches, for a total of 36 samples.

B. Also, an additional 34 sampling points were located at 5, 10, and 20 foot intervals along a 200' transect extending north and a 200' transect extending east of grid location #22. The samples collected at these shorter intervals are required to provide the structure needed for geostatistical analysis.

## 2.3 Sampling Grid Layout:

A. Don personal protective equipment (PPE)

1. Rubber gloves
2. Steel toed boots
3. Eye protection

B. Perform screening of airborne VOCs and combustible gases using Drager Tube and Hnu meter respectively.

1. If screening indicates that the VOC levels are above prescribed limits, evacuate the area and contact the base bioenvironmental engineer for proper PPE.
2. If screening levels are below prescribed limits, proceed with grid layout.

C. Lay out perimeter of the rectangular grid as shown in Figure 1 using string, tape measure, and wooden stakes.

1. The perimeter of the main rectangle should be approximately 500' by 500'

D. Section off the individual square cells within the rectangular grid.

1. Each cell should be 100' by 100'.

E. Based on the randomly selected starting point, fix the location of the sampling sites at the nodes of the cells

1. Mark the sampling location in each cell with a stake.

Figure 1 Grid Layout.

## 2.4 Set Up Decontamination Area:

The decontamination area will be located adjacent to the area of interest (see Figure 3).

- A. Lay out and stake down a 15' by 6' visqueen sheet.
- B. Berm the edges by laying wooden stakes on their side around the periphery of the sheet. This will ensure that any spilled material is contained.
- C. Place all four buckets in a row, from left to right on the laid out visqueen: Scrub, Wash, Rinse, and Final Rinse.
- D. Pour water into the two buckets labeled Scrub and Rinse. Fill the buckets until they are 3/4 full.
- E. Pour the soap solution into the bucket labeled Wash. Fill the bucket until it is 3/4 full.
- F. Pour De-ionized water into the bucket labeled Final Rinse. Fill the bucket until it is 3/4 full.
- G. Measure the conductivity of the Final Rinse water with the conductivity measuring device, and mark the result in the log book.

## 2.5 Log Book:

Log the weather conditions, date and time, general site conditions, and members present for observation and sampling before the first sample is taken. Log the information in the appropriate section of the log book.

## 2.6 General Procedures For The 24" Deep Samples:

- A. Cut visqueen into 6' by 6' sheets--1 for every sample location.
- B. Proceed to the first cell and remove the marking stake, center visqueen on sampling location.
- C. Cut 6" by 6" hole (one shovel blade wide) in the visqueen centered on the sampling location.
- D. Record sample location, sample number, names of samplers, time, and general physical conditions of the sample location. Note soil characteristics(wet, dry), soil profile(clay layer, rocks), and any abnormalities in log book.
- E. Using the shovel, remove soil to a depth of 24 inches, placing the displaced soil on visqueen and mix to create a consolidated sample.

F. If immovable obstacles are encountered before the 24 inch depth is reached, sample site should be moved to the left on the x coordinate (towards grid origin) in six inch increments until sample depth is achievable. For each move, start a new pile of dirt and note in the log book.

G. Place consolidated sample into Marinelli beaker until full.

H. Tamp soil firmly in beaker; add more soil to create full beaker , re-tamp.

I. Close beaker tightly and ensure labels are filled out and in place as described in the sample identification section..

J. Decontaminate equipment according to procedures detailed below.

K. Move sample to holding area.

L. Repeat procedure for each additional sample.

### **3.0 SAMPLE IDENTIFICATION:**

A. The following sample identification will be used in the execution of this study: The sample number assigned to each sample will consist of eight characters. The first two characters indicate the year (i.e. 95). The next three characters indicate the Julian date (i.e. 024). The last three numbers indicate the sample type and number (ie.P001). The convention for identification of the various sampling phases are as follows:

Phase I (Pilot study):	P001 - Pn (n samples)
Phase II:	S001 - Sn (n samples)

B. After the soil has been placed in the beaker, log the sample identification number in the appropriate section of the log book and on the label attached to the beaker.

C. Place filled out label on the Marinelli beaker.

### **4.0 DECONTAMINATION PROCEDURES:**

In order to prevent cross contamination of samples, equipment used to collect the samples must be decontaminated after each sample is taken. The following procedures must be followed:



A. Shovel Decontamination:

1. Dip shovel into bucket marked scrub and scrub with brush .
2. Keep scrubbing until no visible soil remains. If no visible soil remains, go to step 3.
3. Dip shovel blade into soap solution and agitate.
4. Dip shovel into rinse water and agitate.
5. Do final inspection. Ensure no visible contamination exists.
5. Dip shovel into final rinse and agitate.
6. Air dry

B. Hand Auger Decontamination

1. Dip auger into bucket marked scrub and scrub with brush.
2. Keep scrubbing until no visible soil remains. If no visible soil remains, go to step 3.
3. Dip auger into soap solution and agitate
4. Dip auger into rinse water and agitate.
5. Do Final inspection. Ensure no visible contamination exists.
6. Dip auger into final rinse and agitate.
7. Air dry

C. Final Decontamination at end of Day

1. Remove bit from hand auger
2. Dip auger in bucket marked scrub and scrub with brush.
3. Dip auger into soap solution and agitate
4. Dip auger into rinse water and agitate.
5. Do Final inspection. Ensure no visible contamination exists.
6. Dip auger into final rinse and agitate.
7. Measure conductivity of final rinse and log results in appropriate section of the log book.

D. Boots and Glove Decontamination

1. Dip boots and gloves into bucket marked scrub and scrub with brush.
2. Keep scrubbing until no visible soil remains. If no visible soil remains, go to step 3.
3. Dip boots and gloves into soap solution and agitate
4. Dip boots and gloves into rinse water and agitate.
5. Do Final inspection. Ensure no visible contamination exists.
6. Dip boots and gloves into final rinse and agitate.
7. Air dry

**5.0 WASTE HANDLING:**

For this RCRA site, all waste (excess soil, plastic sheeting, gloves, and rinsates) should be placed in separate DOT-approved 55 gallon drum, and labeled IAW applicable regulations. For this study, the following guidelines will be followed:

A. Clean Up and restore site

1. Place excess soil in hole and tamp down
2. Place visqueen and sampling waste into disposal container
3. Take rubber gloves off
4. Place plastic gloves in rolled up visqueen and place into waste container.

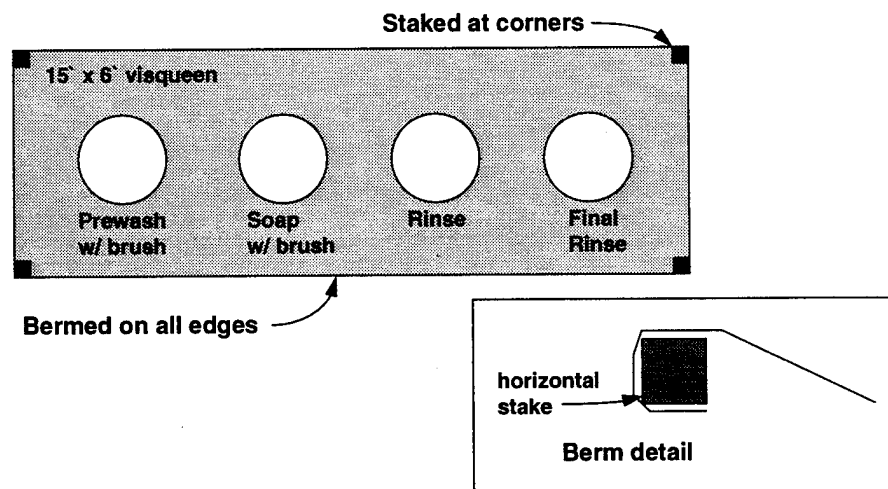


Figure 2. Decontamination layout

ATTACHMENT 2

QUALITY ASSURANCE PROJECT PLAN (QAPP)

## **QUALITY ASSURANCE PROJECT PLAN (QAPP)**

### **1.0 DESIGN:**

Prior to going to the field and accomplishing the sampling, Quality Assurance and Quality Control (QA/QC) will be accomplished in the following ways to ensure that the DQO level II data is obtained:

- A. A standardized labeling system will be used (see Figure 1). The labels will ensure that the collected samples will not become confused with any other samples in the laboratory.
- B. The Sampling Design will incorporate analysis of the rinsate used in the decontamination process. This test will provide feedback on the effectiveness of the decontamination procedures.
- C. Duplicate samples will be taken for the purpose of checking the precision of the laboratory analysis. One duplicate will be taken for every twenty field samples.

### **2.0 FIELD:**

Upon entering the field and accomplishing the sampling, QA/QC shall be addressed in the following ways:

- A. The forms created in the Design process will be checked to ensure correct data entry.
- B. Samples will be taken by the same individual each time, ensuring consistency in following the field sampling plan.
- C. The Sampling Log will be reviewed to ensure all of the required data was entered. This includes for each sample: site number, time, weather, and soil data (soil type and any unusual occurrences).

### **3.0 LABORATORY:**

QA/QC will be addressed in the following ways for the laboratory work:

- A. Ensure each sample is labeled and contains a uniform volume of soil, packed by hand.
- B. Sample Handling Procedures:
  - 1. Sample Acceptance: Samples brought to the laboratory are checked prior to analysis. Only samples that are correctly collected, stored, and documented will be analyzed. The Checklist which can also be found in the Lab Notebook is as follows:

- All samples must be in plastic Marinelli beakers.
- Marinelli beakers must not be leaking or broken.
- Marinelli beaker lids must be securely in place.
- Marinelli beakers must be clean and free from debris.
- Marinelli beakers must appear full of soil.
- Marinelli beakers must have a label.
- The label must have the field ID number clearly annotated on it

If any sample fails to meet the above criteria it will be rejected with a written statement, signed by the sample collection team leader and the sample analysis team leader.

2. Sample Storage - From the moment the samples reach the lab, they are to be secured and or supervised at all times. They will be stored in a designated secure area of the lab until analysis is complete. After analysis the samples will be stored in a long term secure area until the sample analysis team leader authorizes their destruction. Maintain samples in a secured and/or supervised area

C. Calibrate the Gamma Spectrometer (Analytical Device).

1. Analysis was performed to identify background interference.
2. The device was calibrated using a certified source to establish accuracy.
3. Daily energy and efficiency calibrations were accomplished to ensure temporal accuracy.

D. Limit Variance in data by minimizing the count times until variance is less than 15%.

E. Place samples one at a time in the detector, to limit contamination.

1. Unusual sources shall be kept away from the lab to limit contamination.

F. All data generated will be secured in the laboratory.

G. Duplicate and blank samples will be analyzed.

#### **4.0 RESULTS OF QA/QC CHECKS:**

A. Three rinse water samples (P011, P052, and P068) were analyzed using gamma spectroscopy. A high resolution/high efficiency germanium detector built by the Canberra Corp. was used for the analysis. More specifically, individual gamma peaks of each radionuclide of interest were looked for by placing the water sample directly onto the detector for a two hour count time. The gamma spectrum obtained was analyzed on a IBM 486 computer using the GENIE-PC Spectroscopy software package. Since each nuclide has its own characteristic energy, the individual peaks of the spectrum were

looked for by comparing them to energy calibration peak values obtained using a prepared standard spiked with known quantities of radionuclides.

Of the three rinse water samples analyzed, none of them showed any levels of the nuclides present in the soil. This indicates that no cross contamination occurred due to the decontamination process.

b. Two duplicate soil samples were also taken and analyzed using gamma spectroscopy. The following pairs of samples were taken from the same location: P031 and P031b, and P047 and P047b. Three sigma limits were established for each nuclide of interest of each sample. The nuclides for each pair of duplicate samples were compared to ensure that their means hooked each other, given the  $\pm 3\sigma$  limits. Each of the nuclides hooked and therefore the analytical process was in control.

### Bibliography

1. Jaworski Z. and D. Grzybowska. "Natural Radionuclides in Industrial and Rural Soils," The Science of the Total Environment, vol 7, no. 1, 45-52, (January 1977).
2. Ministry of Supply and Services Canada. Radioactivity in Coal, Ashes, and Selected Wastewater From Coal Fired Steam Electric Generating Stations. Ottawa, Ont.: Beauregard Press Limited, 1985.
3. Wright Patterson AFB. Remedial Investigation of Landfill #5, A Special Report, Dayton, OH, (December 1993).

**APPENDIX B**  
**STATISTICAL ANALYSIS FIGURES**



## HISTOGRAMS

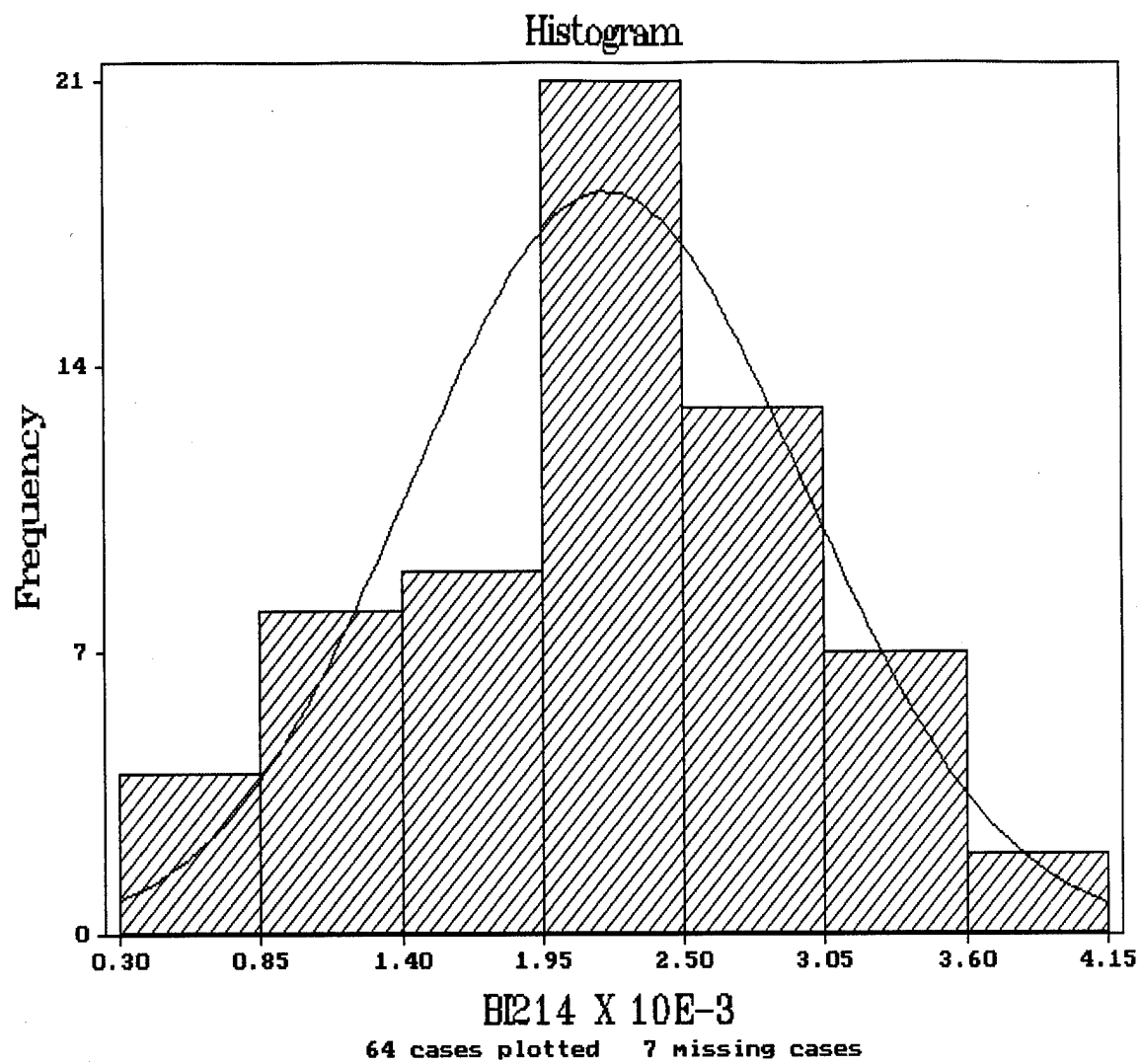


Figure B-1 Histogram of  $^{214}\text{Bi}$  Data.

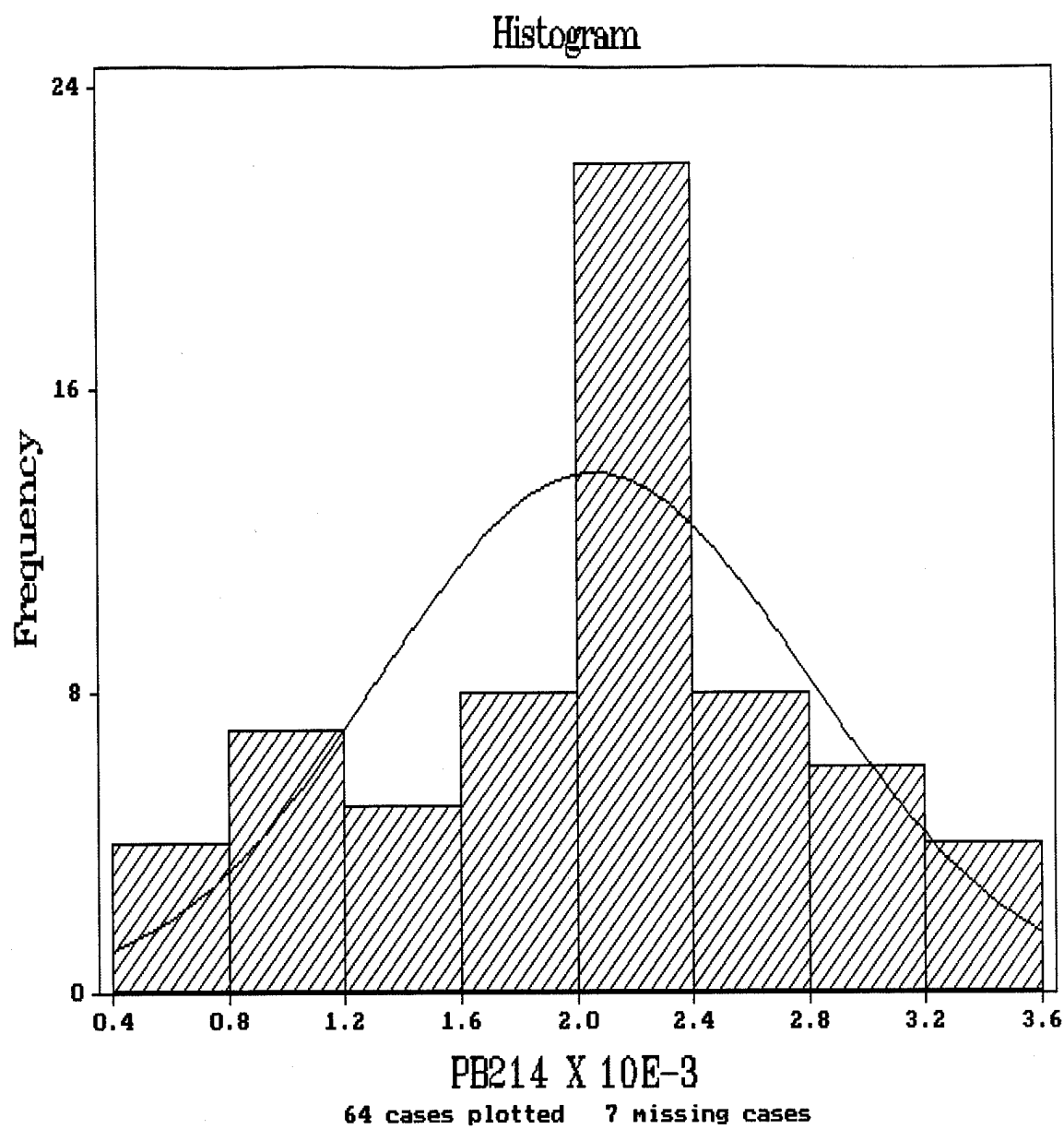


Figure B-2 Histogram of  $^{214}\text{Pb}$  Data.

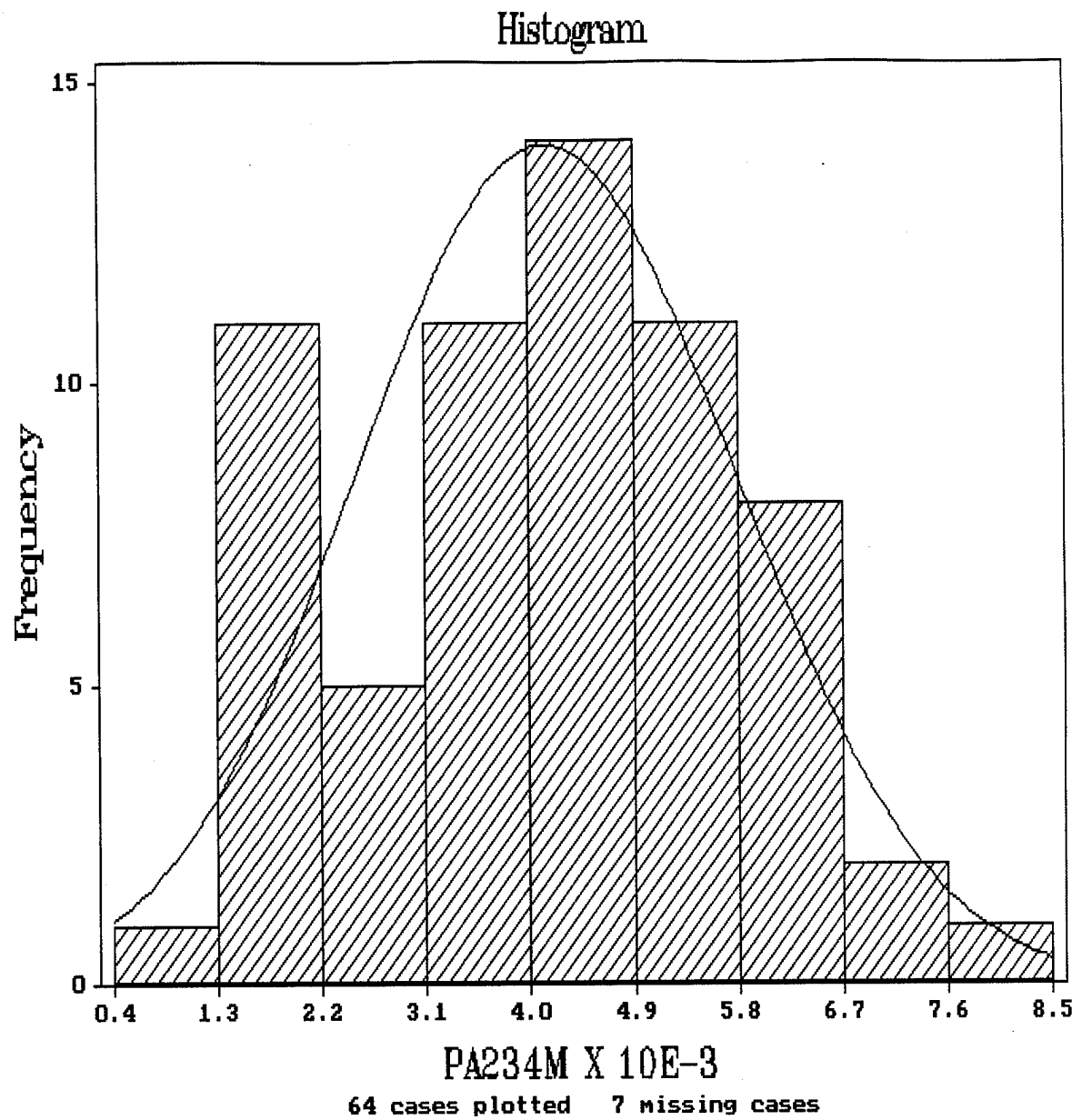


Figure B-3 Histogram of  $^{234m}\text{Pa}$  Data.

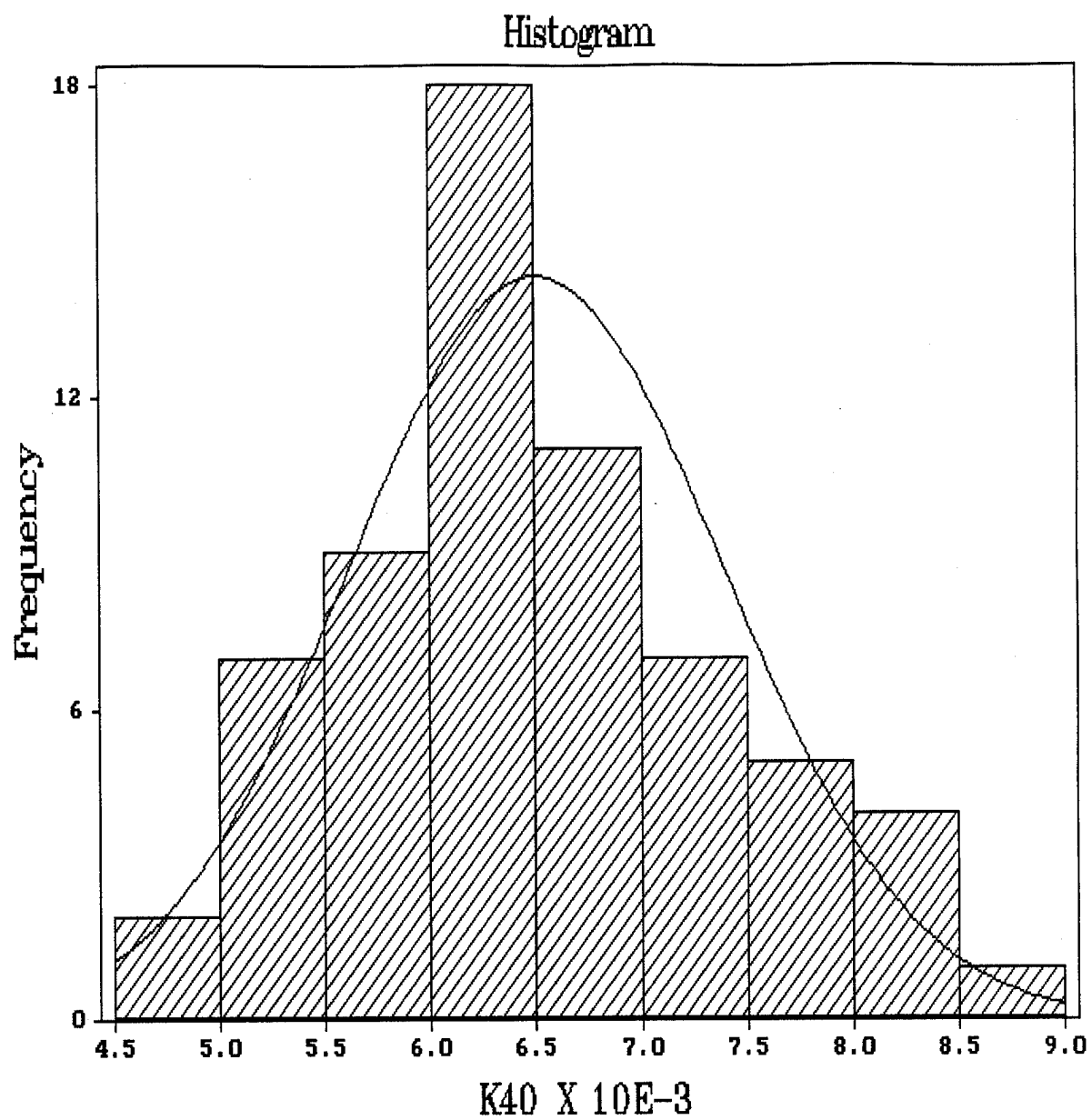


Figure B-4 Histogram of  $^{40}\text{K}$  Data.

WILK-SHAPIRO RANKIT PLOTS

Wilk-Shapiro / Rankit Plot of BI214

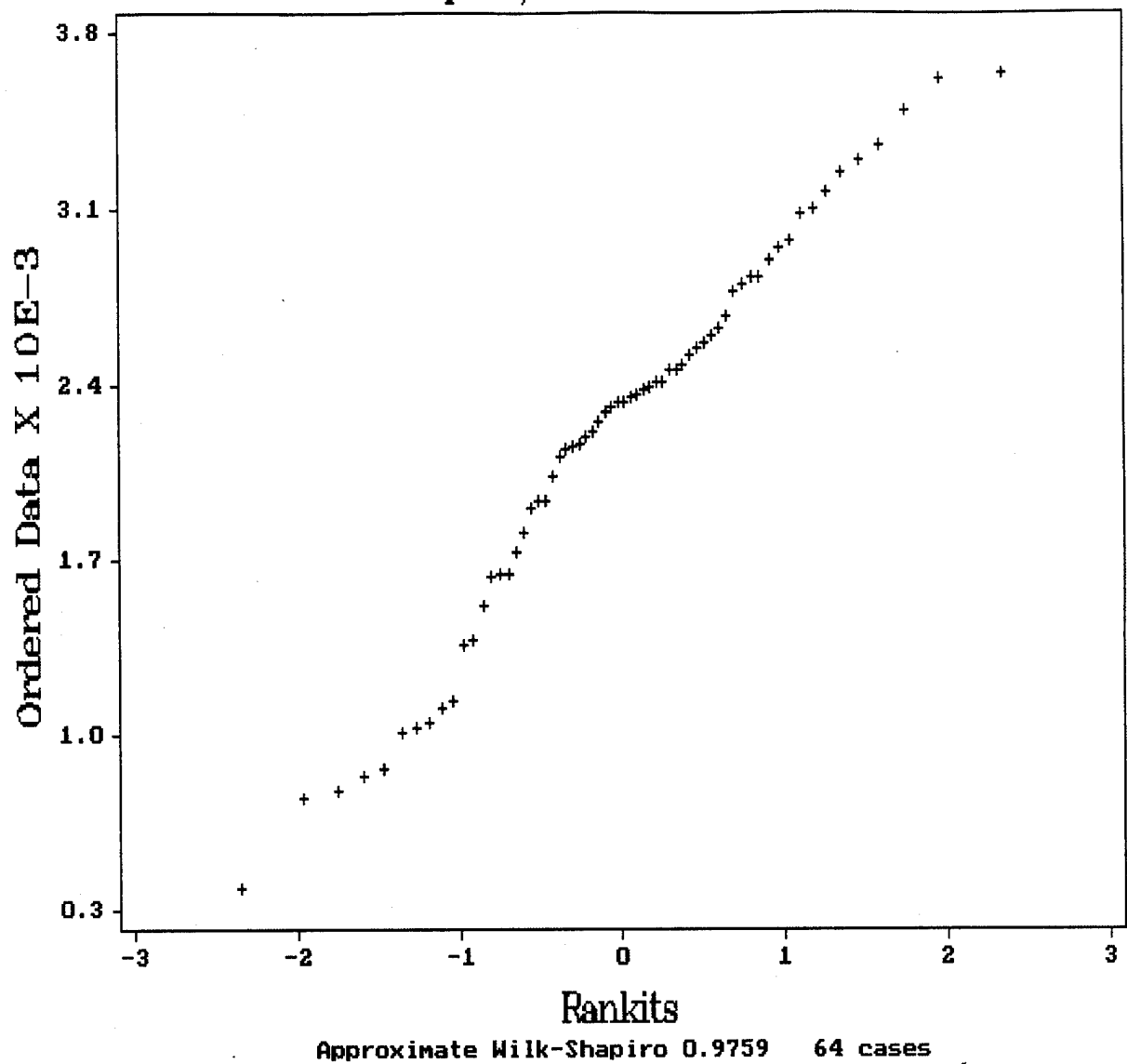


Figure B-5 Rankit Plot of the  $^{214}\text{Bi}$  Data.

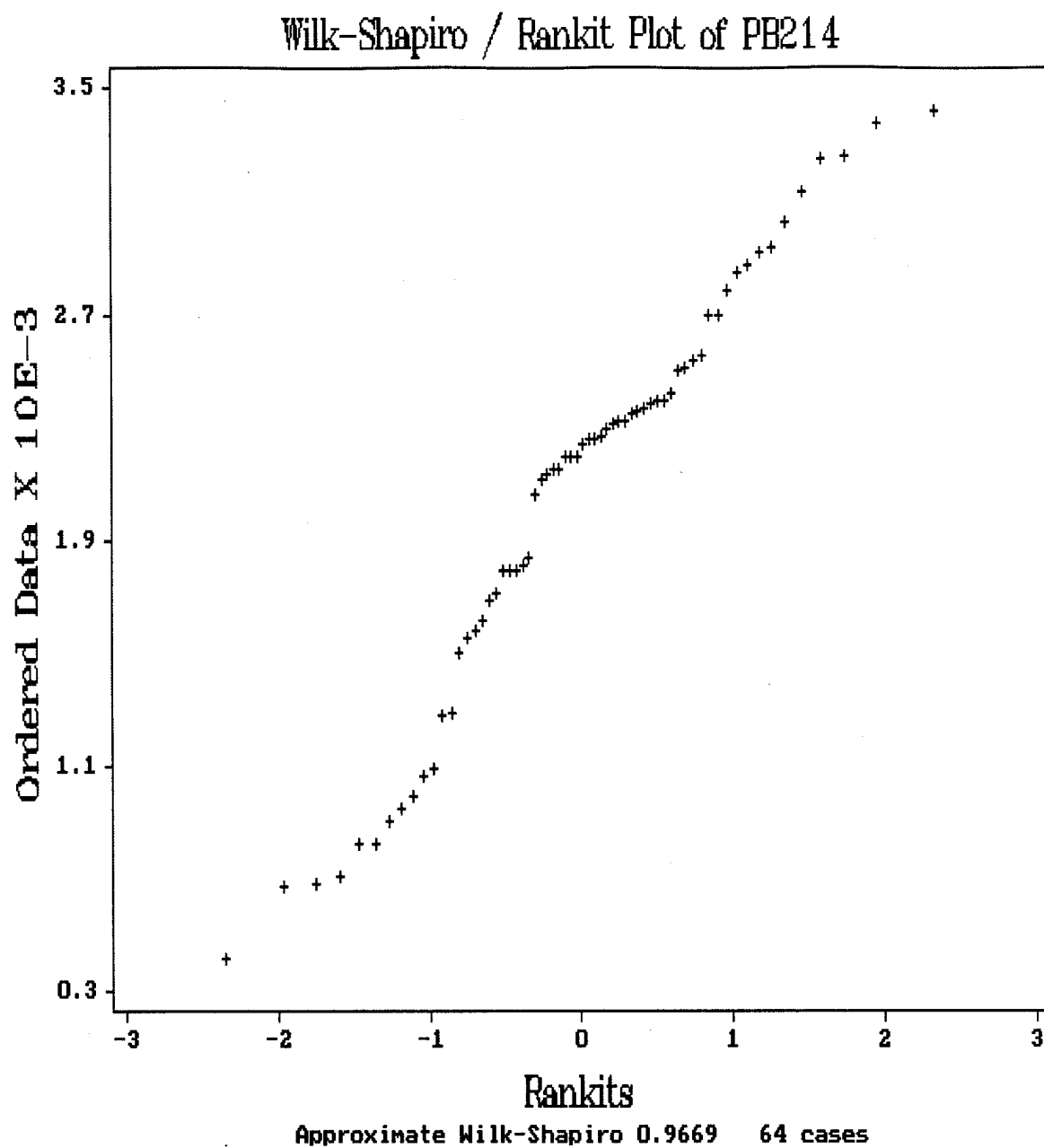
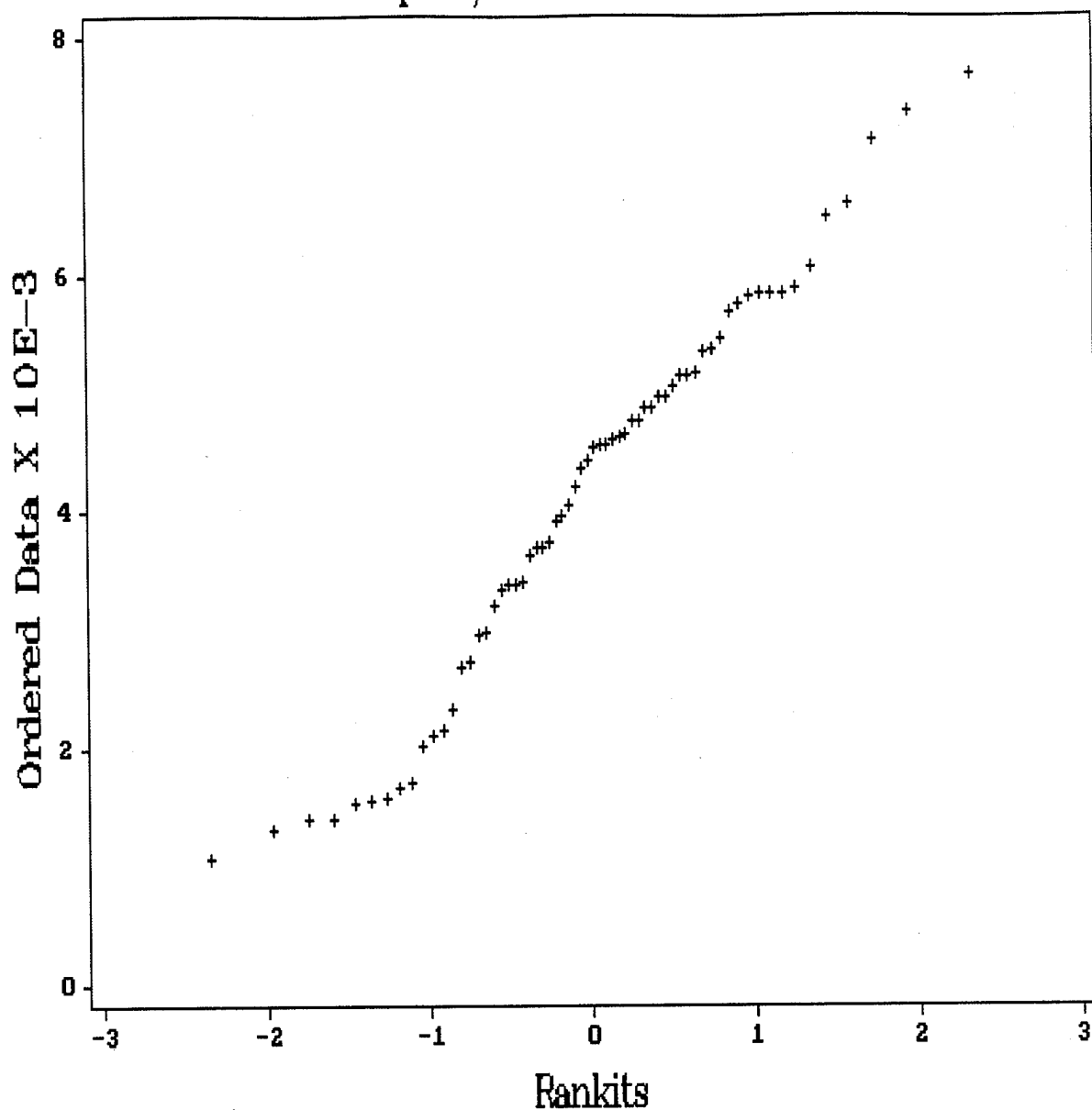


Figure B-6 Rankit Plot of the  $^{214}\text{Pb}$  Data.

# Wilk-Shapiro / Rankit Plot of PA234M



Approximate Wilk-Shapiro 0.9764 64 cases

Figure B-7 Rankit Plot of the  $^{234m}\text{Pa}$  Data.

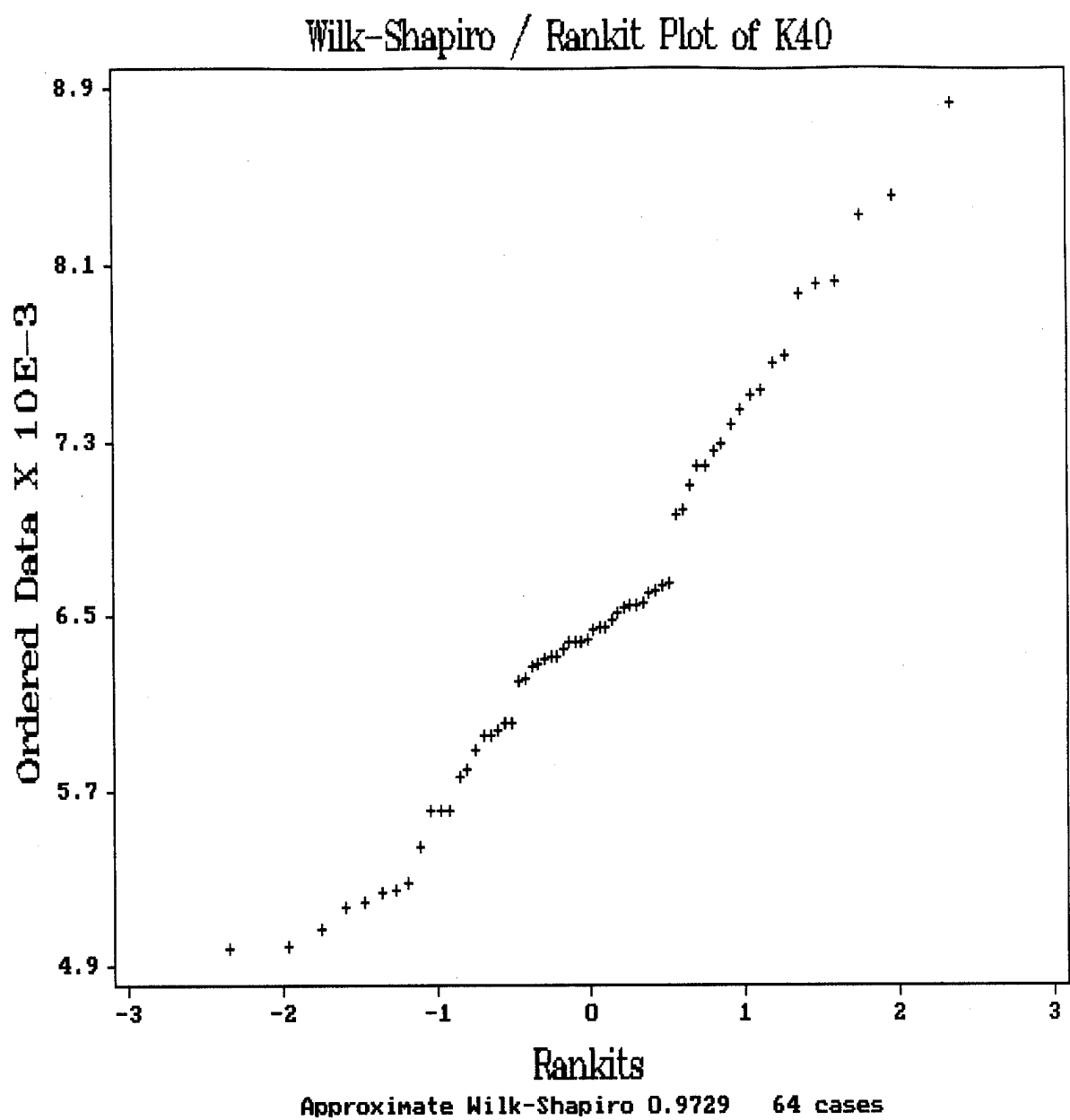
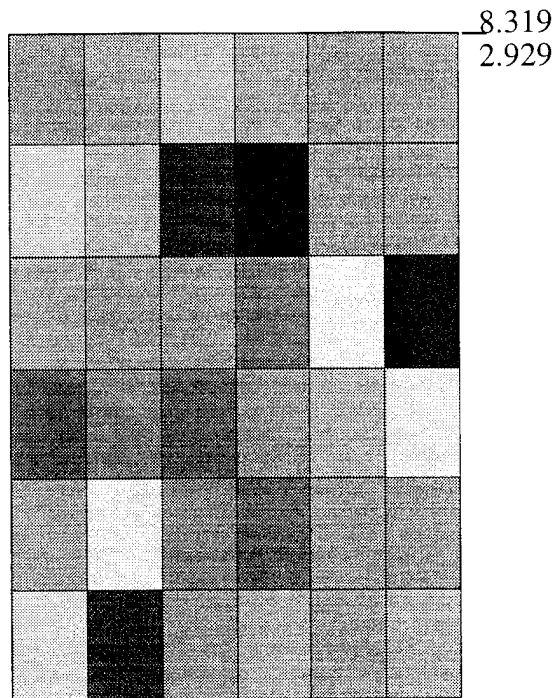


Figure B-8 Rankit Plot of the  $^{40}\text{K}$  Data.



### PLOTS OF INDIVIDUAL DATA POINTS



reg

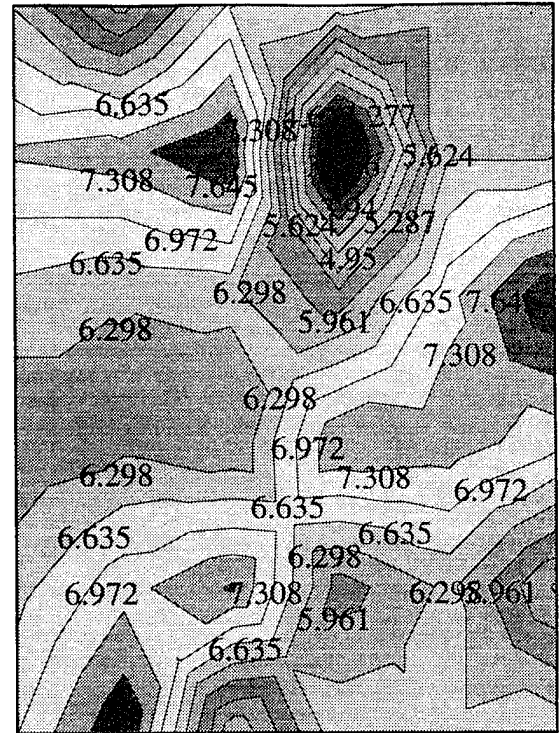
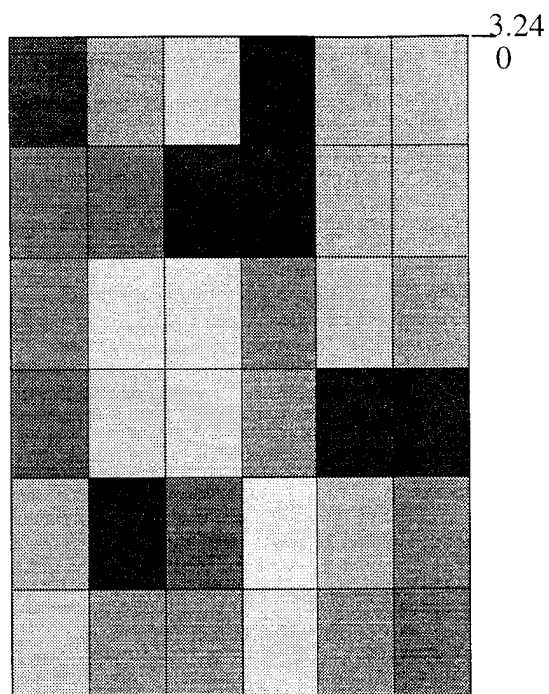
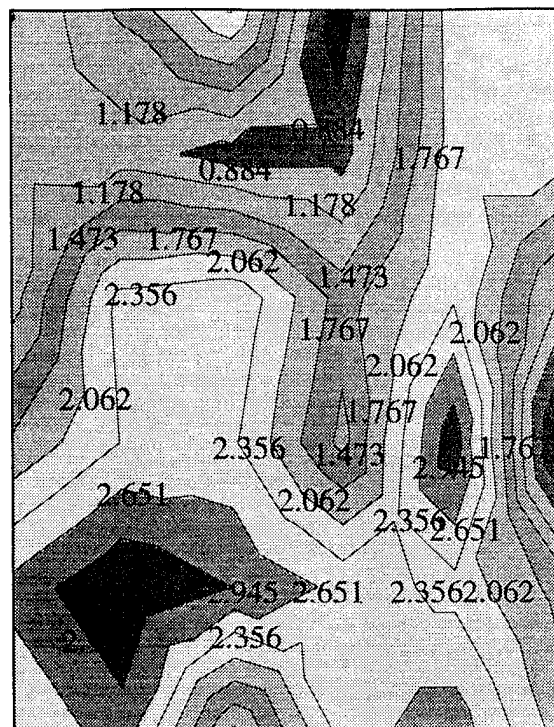
 $\text{wdse}_V$ 

Figure B-9 Plots of Individual Data Values for  $^{40}\text{K}$ .



reg



wdse

Figure B-10 Plots of Individual Data Values for  $^{214}\text{Bi}$ .

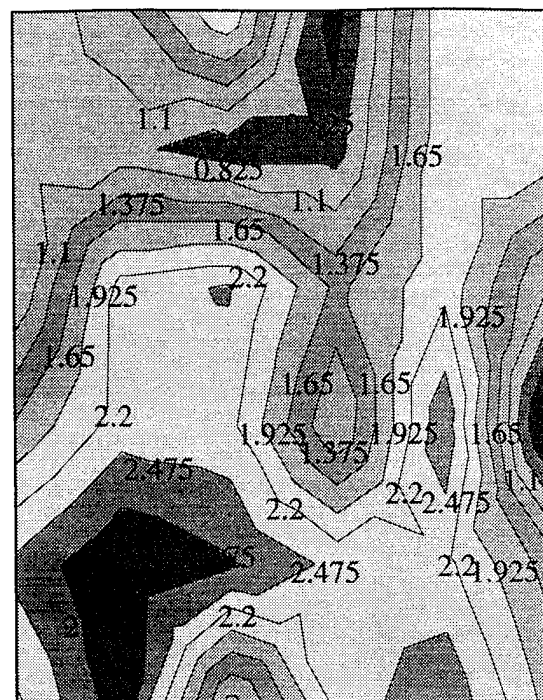
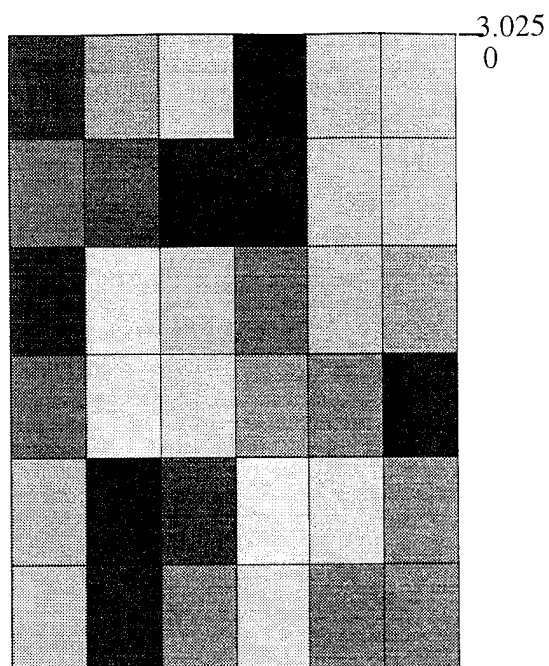
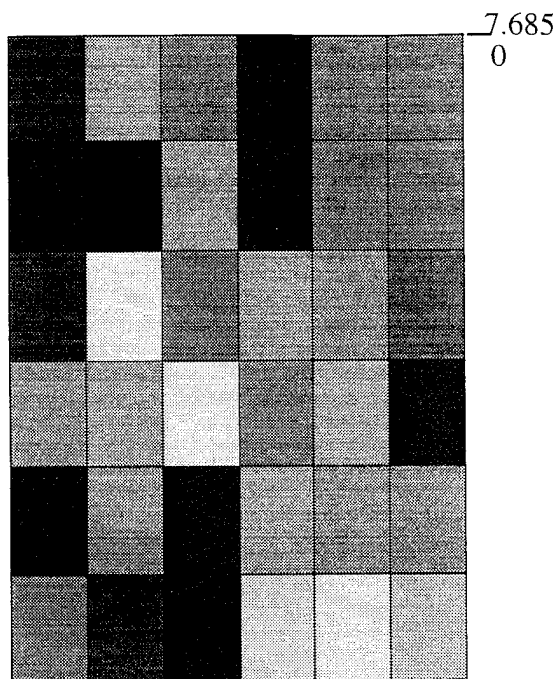
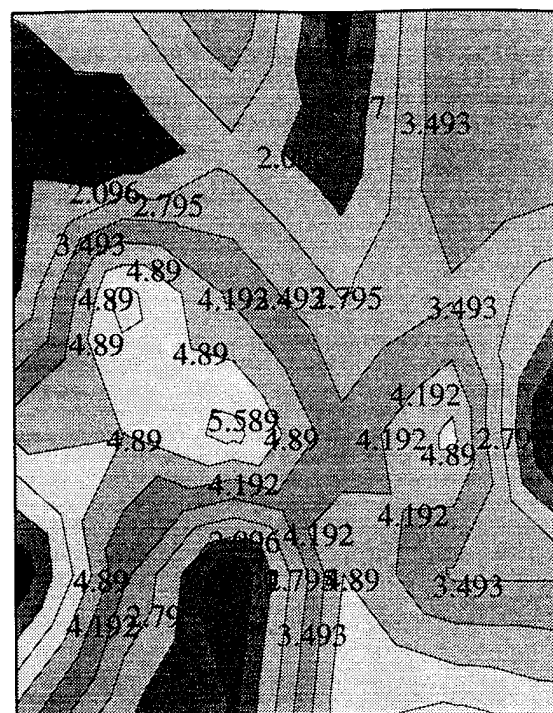


Figure B-11 Plots of Individual Data Values for  $^{214}\text{Pb}$ .



reg



wdse

Figure B-12 Plots of Individual Data Values for  $^{234m}\text{Pa}$ .

# PLOTS SHOWING EXTREME VALUES

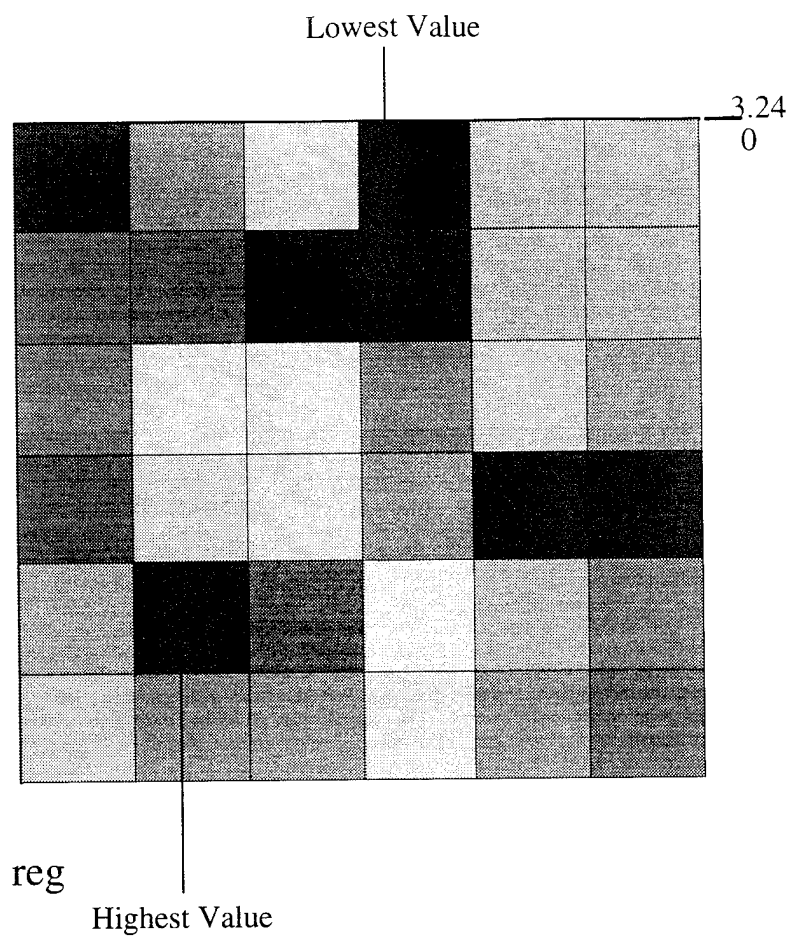


Figure B-13 Extreme Values for  $^{214}\text{Bi}$ .

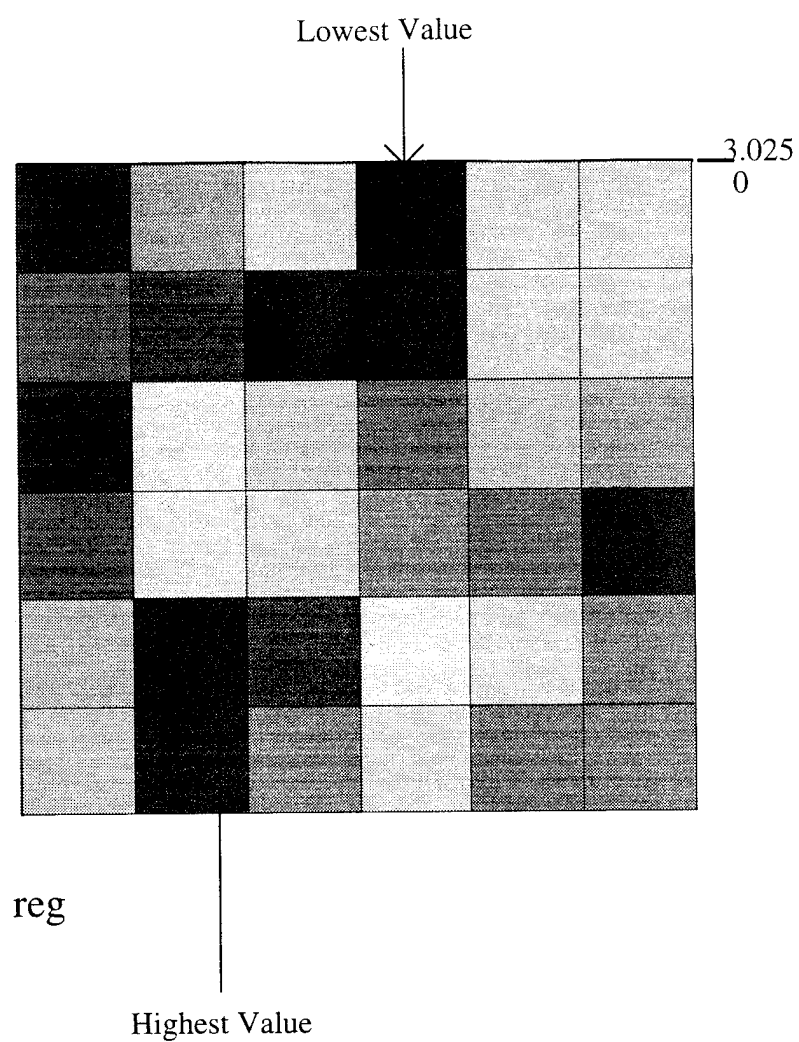


Figure B-14 Extreme Values for  $^{214}\text{Pb}$ .

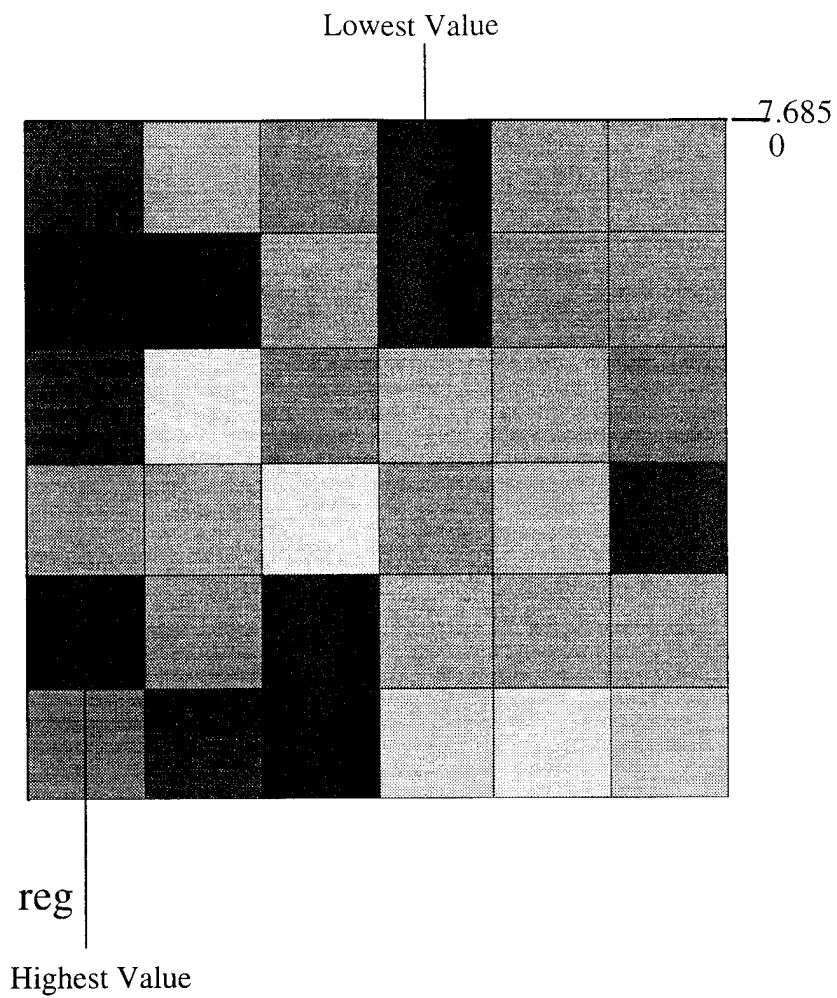
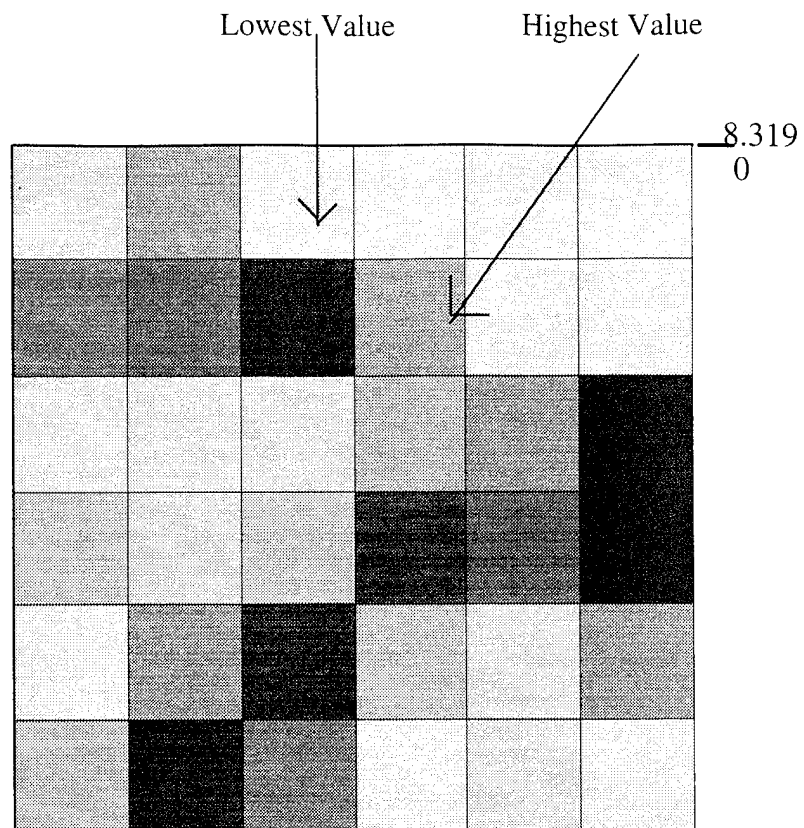


Figure B-15 Extreme Values for  $^{234m}\text{Pa}$ .



reg

Figure B-16 Extreme Values for  $^{40}\text{K}$ .



# PLOTS OF MOVING WINDOW MEANS

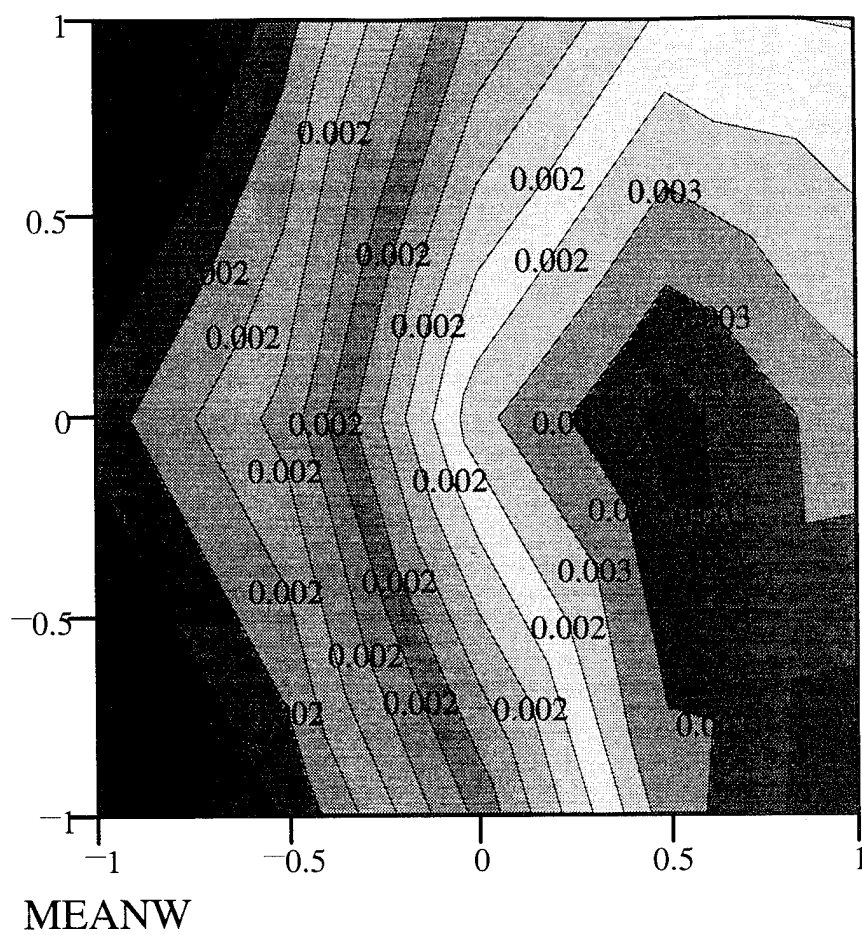


Figure B-17 Moving Windows of Means for  $^{214}\text{Bi}$ .

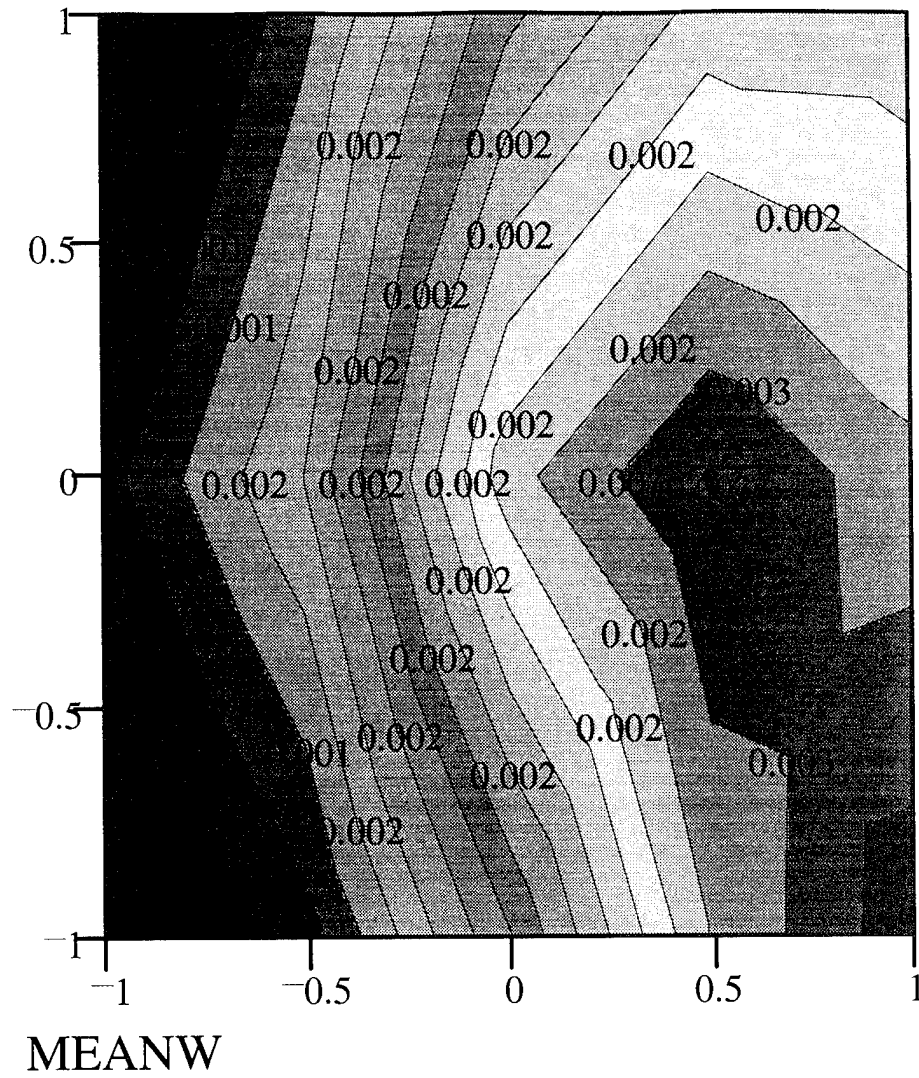
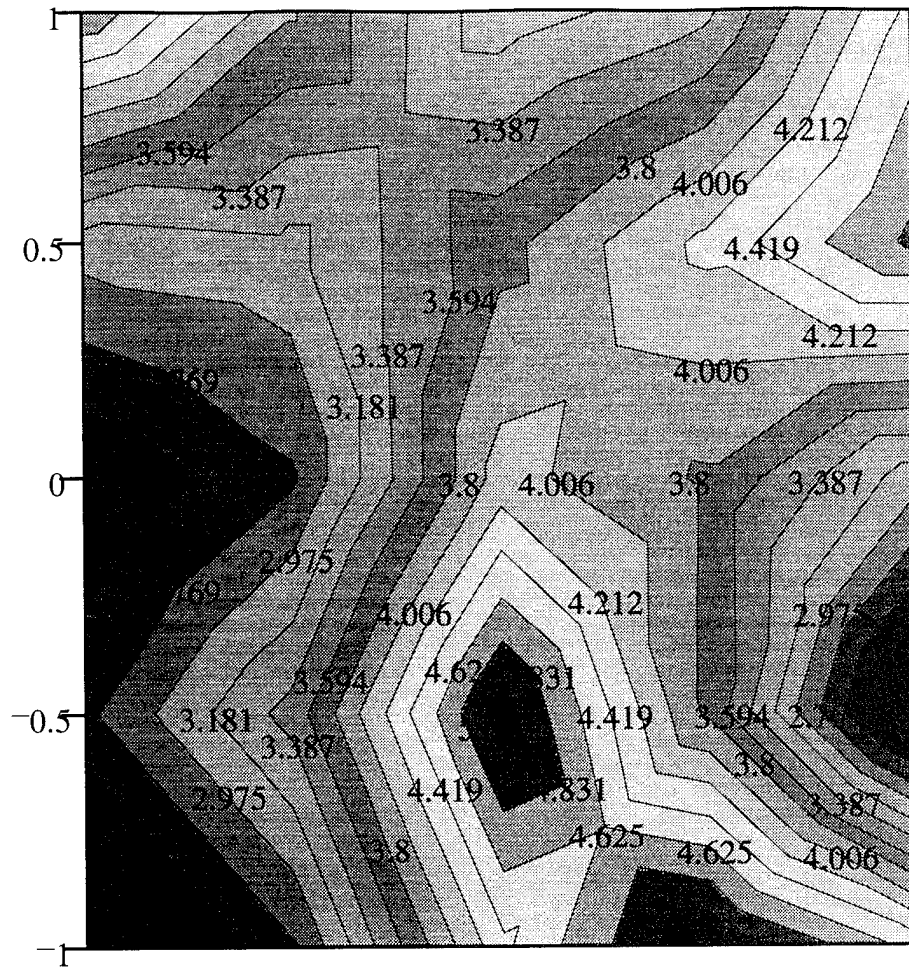


Figure B-18 Moving Windows of Means for  $^{214}\text{Pb}$ .



MEANW

Figure B-19 Moving Windows of Means for  $^{234\text{m}}\text{Pa}$ .

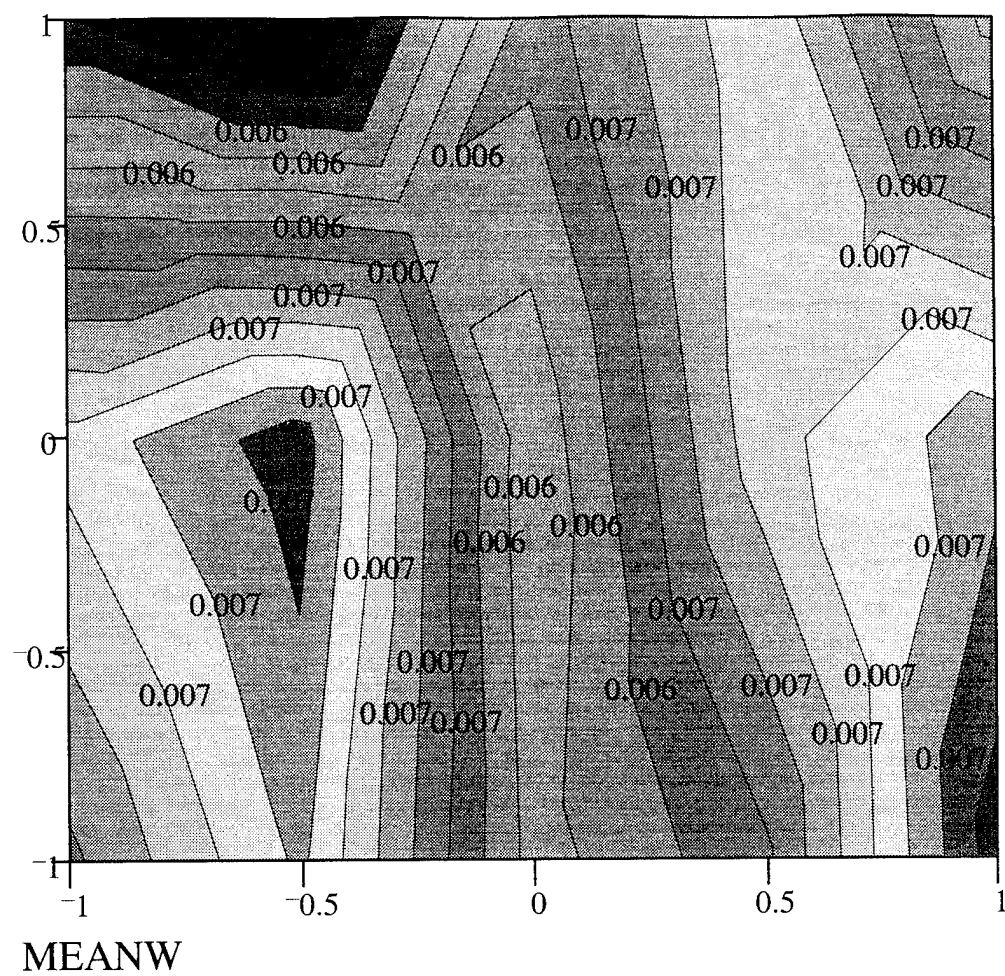


Figure B-20 Moving Windows of Means for  $^{40}\text{K}$ .

## VARIOGRAMS

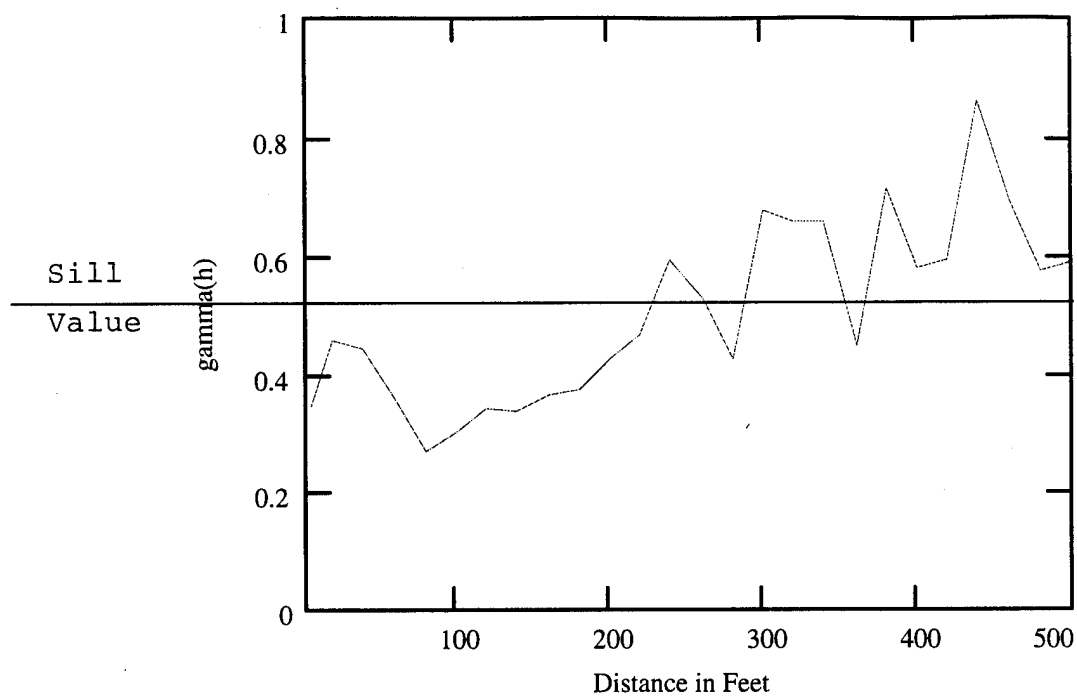


Figure B-21 Semivariogram for  $^{214}\text{Bi}$

Table B-1 Omnidirectional Vriogram Results for  $^{214}\text{Bi}$ .

No. of Pairs	Distance (ft)	$\gamma(h)$ Value	No. of Pairs	Distance (ft)	$\gamma(h)$ Value
20	5.0	.347	128	259.58	.525
186	17.83	.456	114	281.26	.425
146	37.56	.445	188	300.13	.674
130	57.72	.358	230	318.29	.659
126	78.06	.270	112	339.80	.657
310	100.52	.302	154	360.52	.450
230	119.12	.344	92	378.88	.714
244	139.98	.338	102	397.50	.580
146	158.93	.363	142	417.13	.593
150	179.76	.373	96	442.78	.861
298	201.38	.426	50	458.93	.690
286	220.72	.465	30	478.90	.574

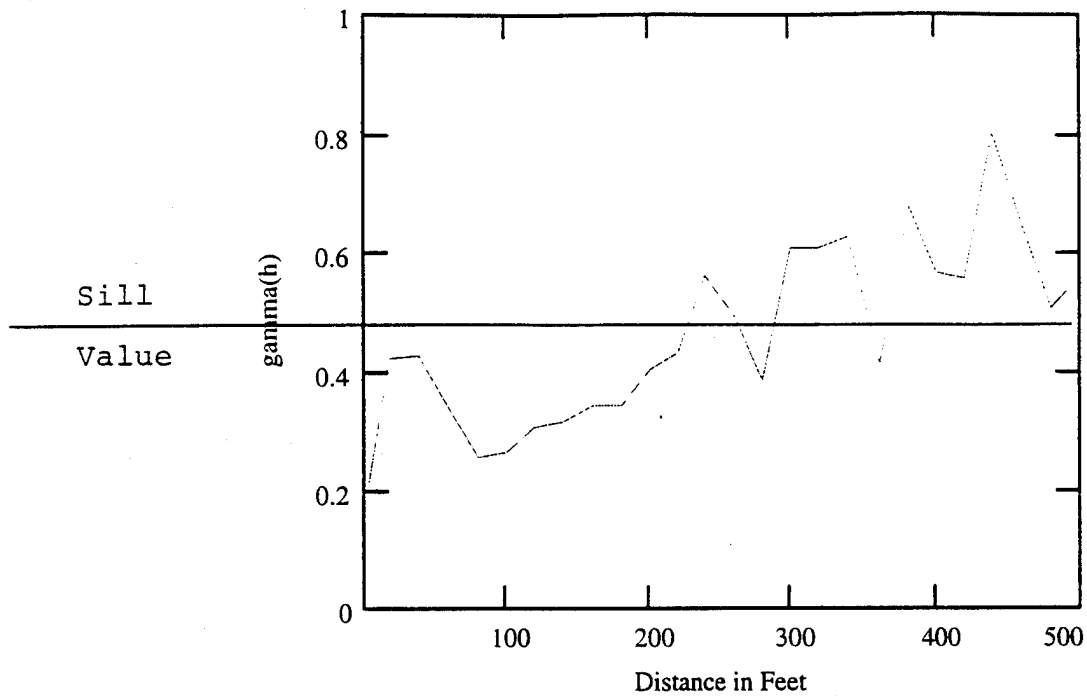


Figure B-21 Semivariogram for <sup>214</sup>Pb.

Table B-2 Omnidirectional Variogram Results for <sup>214</sup>PB.

No. of Pairs	Distance (ft)	$\gamma(h)$ Value	No. of Pairs	Distance (ft)	$\gamma(h)$ Value
20	5.0	.213	128	259.58	.489
186	17.83	.421	114	281.26	.385
146	37.56	.424	188	300.13	.608
130	57.72	.333	230	318.29	.606
126	78.06	.254	112	339.80	.624
310	100.52	.266	154	360.52	.411
230	119.12	.306	92	378.88	.674
244	139.98	.316	102	397.50	.565
146	158.93	.342	142	417.13	.554
150	179.76	.344	96	442.785	.801
298	201.38	.400	50	458.93	.639
286	220.72	.429	30	478.90	.503
132	238.64	.558	102	501.24	.557

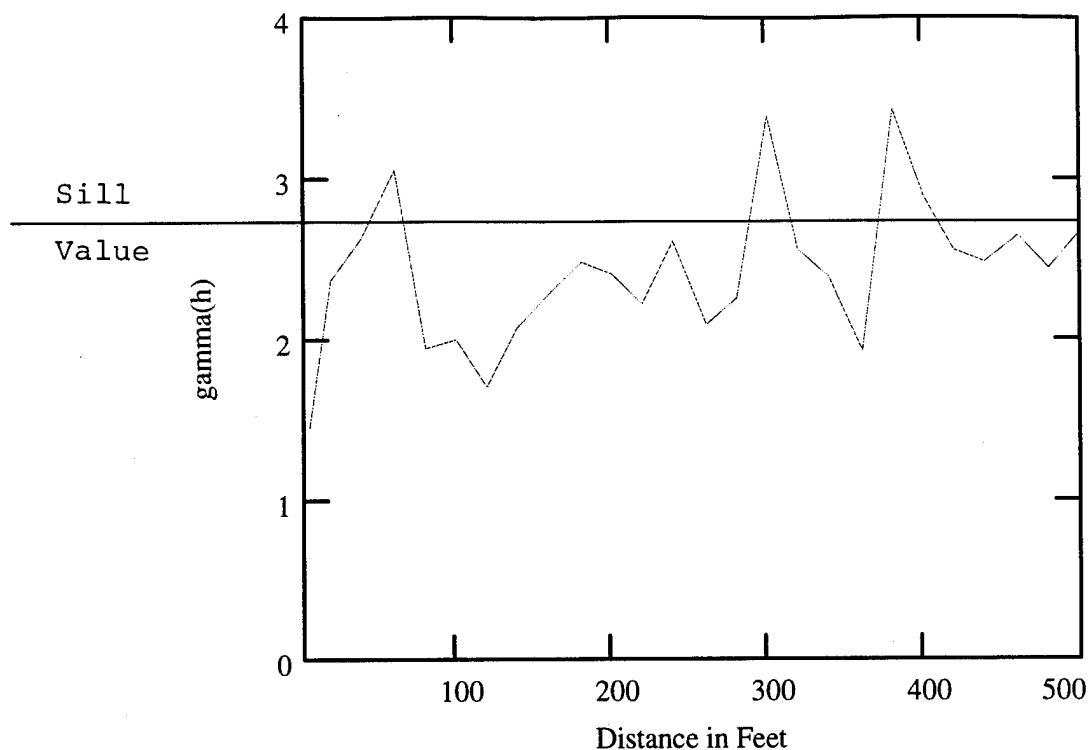


Figure B-23 Semivariogram for  $^{234m}\text{Pa}$

Table B-3 Omnidirectional variogram results for  $^{234m}\text{Pa}$ .

No. of Pairs	Distance (ft)	$\gamma(h)$ Value	No. of Pairs	Distance (ft)	$\gamma(h)$ Value
20	5.0	1.444	128	259.58	2.092
186	17.83	2.375	114	281.26	2.255
146	37.56	2.627	188	300.13	3.396
130	57.72	3.052	230	318.29	2.551
126	78.06	1.945	112	339.80	2.308
310	100.52	2.006	154	360.52	1.924
230	119.12	1.697	92	378.88	3.420
244	139.98	2.071	102	397.50	2.890
146	158.93	2.296	142	417.13	2.564
150	179.76	2.490	96	442.785	2.479
298	201.38	2.411	50	458.93	2.653
286	220.72	2.225	30	478.90	2.442
132	238.64	2.613	102	501.24	2.660

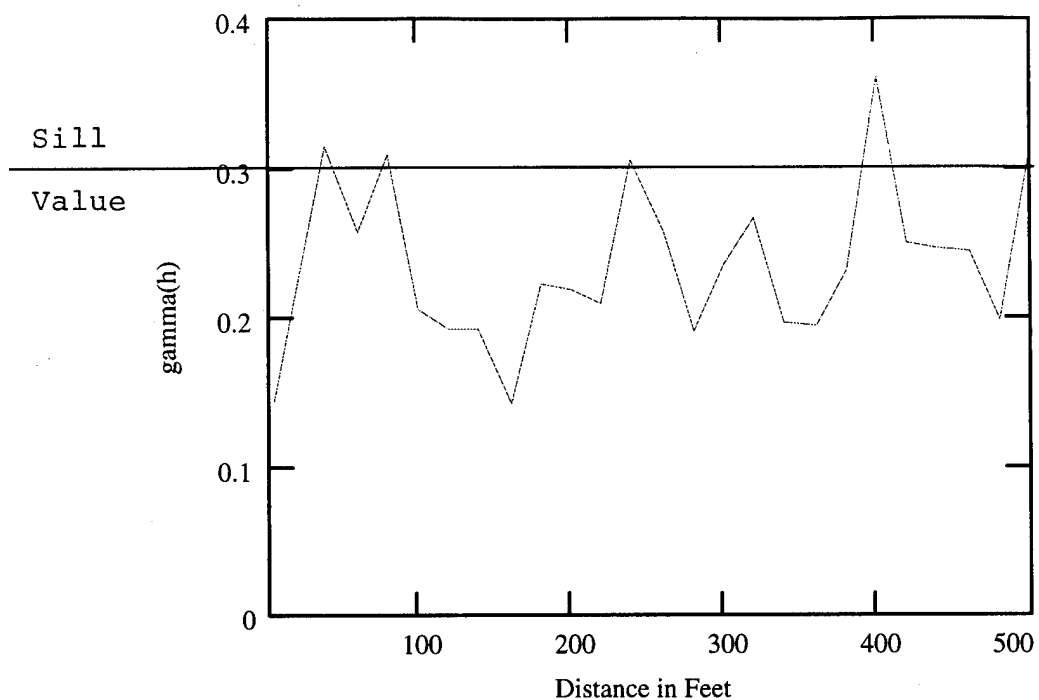


Figure B-24 Semivariogram for  $^{40}\text{K}$ .

Table B-4 Omnidirectional Variogram Results for  $^{40}\text{K}$ .

No. of Pairs	Distance (ft)	$\gamma(h)$ Value	No. of Pairs	Distance (ft)	$\gamma(h)$ Value
20	5.0	.144	128	259.58	.257
186	17.83	.215	114	281.26	.190
146	37.56	.315	188	300.13	.234
130	57.72	.257	230	318.29	.266
126	78.06	.309	112	339.80	.196
310	100.52	.205	154	360.52	.194
230	119.12	.191	92	378.88	.231
244	139.98	.192	102	397.50	.361
146	158.93	.142	142	417.13	.250
150	179.76	.222	96	442.78	.246
298	201.38	.219	50	458.93	.243
286	220.72	.209	30	478.90	.198
132	238.64	.306	102	501.24	.310



## Bibliography

1. Abel, K.H., Techniques for Chemical Analysis of Radionuclides in Fly ash: An Evaluation, Research Project Report #1620-8. Palo Alto, California. Power Research Institute, Inc. 1986.
2. Analytic Software. STATISTIX 4.0 User's Manual. St Paul, MN. 1992.
3. Beck, H.L., Carl Gogolak, Kevin Miller, Wayne Lowder. "Perturbations on the Natural Radiation Environment Due to the Utilization of Coal as an Energy Source," Natural Radiation Environment, vol. 2, Proceed. of Symposium at Houston, Texas, April 23-28, 1978, T.F. Gesell and W.M. Lowder (ed.) (April 1978).
4. Beck, H.L. and Kevin Miller, "Some Radiological Aspects of Coal Combustion," IEEE Transactions on Nuclear Science, NS-27, 689, (February 1980).
5. Byrnes, Mark E. Field Sampling Methods for Remedial Investigations. Boca Raton, Florida: CRC Press, Inc. 1994.
6. Boulding, J. Russell. Description and Sampling of Contaminated Soils. Boca Raton, Florida: CRC Press, Inc. 1994.
7. Canberra Nuclear Industries. Genie-PC. Meriden, CT: Canberra Industries, Inc. 1993.
8. Carlson, Claire and Domy Adriano. "Environmental Impacts of Coal Combustion Residues," Journal of Environmental Quality, vol 22, no 2, 227-248, (Apr-Jun 1993).
9. Devore, Jay L. Probability and Statistics for Engineering and the Sciences. Pacific Grove, California: Brooks/Cole Publishing Company, 1991.
10. DuPont, P. and J. Morrill. Residential Indoor Air Quality and Energy Efficiency. Washington, DC: The American Council for an Energy Efficient Economy. 1989.
11. Gilbert, Richard O. Statistical methods for Environmental Pollution Monitoring. New York, New York: Van Nostrand Reinhold. 1987.

Bibliography (con't)

12. Guimond, Richard J. and S. Windham. "Radiological Evaluation of Structures Constructed on Phosphate Related Land," Natural Radiation Environment III. Vol. 2, 1457-1475, (April 1978).
13. Isaaks, Edward H. and R. Mohan Srivastava. An Introduction to Applied Geostatistics. New York, NY: Oxford University Press, 1989.
14. Jaworski Z. and D. Grzybowska. "Natural Radionuclides in Industrial and Rural Soils," The Science of the Total Environment, vol 7, no. 1, 45-52, (January 1977).
15. Journel A. Fundamental Geostatistics in Five Lessons. Washington, DC: American Geophysical Union, 1989.
16. Karasek, James F. A Procedure for Determining the Resource Utilization Potential of Coal Ash. Masters Thesis. AFIT, WPAFB Ohio, 1981.
17. Kathren, Ronald L. Radioactivity in the Environment, Sources, Distribution, and Surveillance. New York, NY: Harwood Academic Publishers, 1984.
18. Knoll, Glenn F. Radiation Measurement and Detection. New York, NY: John Wiley and Sons, Inc., 1989.
19. Ministry of Supply and Services Canada. Radioactivity in Coal, Ashes, and Selected Wastewater From Coal Fired Steam Electric Generating Stations. Ottawa, Ont.: Beauregard Press Limited, 1985.
20. Moeller, Dade W., D. Underhill, and G. Gulezian. "Population Dose Equivalent From Naturally Occurring Radionuclides in Building Materials," Natural Radiation Environment III. Vol. 2, 1424-1433, (April 1978).
21. National Geographic Society. Energy: Facing Up to the Problem, Getting Down to Solutions. A Special Report, Washington, (February 1981).
22. National Research Council. Comparative Dosimetry of Radon in Mines and Homes. Washington, D.C.: National Academy Press, 1991.
23. Nazaroff, William and A. Nero. Radon and Its Decay Products. New York, NY: John Wiley & Sons, Inc., 1988.
24. Office of Emergency and Remedial Response. Data Quality Objectives Process for Superfund. Washington, D.C.: U.S. EPA, 1993.

Bibliography (con't)

25. Office of Radiation Programs. Radon Reference Manual. Washington, D.C.: U.S. EPA, 1987.
26. Tetra Tech, Inc. US Air Force Energy Plan 1979. Arlington, VA, 1979.
27. Wright Patterson AFB. Remedial Investigation of Landfill #5, A Special Report, Dayton, OH, (December 1993).

### Vita

Captain Richard S. Krysiak Jr was born on 2 September 1961 in Erie, Pennsylvania. After graduating from Technical Memorial High School in Erie, Pennsylvania in 1979, he entered the Air Force. He was selected for the Airman Education and Commissioning Program (AECPP) in 1984. Through this program he attended Oklahoma State University and earned his Bachelor of Science degree in Industrial Engineering and Management and his Commission.

He began his officer career as the Chief of Industrial Engineering at Carswell AFB, Texas. While there, he studied and improved operations within the Civil Engineering Operations shops and Administrative Branch. Next, he served as the Base Environmental Coordinator at Carswell. He developed the bases' \$65 million environmental base closure program which became Strategic Air Command's "model" environmental base closure plan. His next assignment was to Lajes Field, Portugal as the Base Environmental Coordinator. There he took a failing environmental program and brought it up to United States standards within two years. After his assignment at Lajes, Captain Krysiak entered the Engineering and Environmental Management program at the Air Force Institute of Technology in May 1994.

Premanent Address: 4205 Penrose Court  
Beavercreek, Ohio 45431

REPORT DOCUMENTATION PAGE			Form Approved OMB No. 0704-0188	
Public reporting burden for this collection of information is estimated to average 1 hour per response, including the time for reviewing instructions, searching existing data sources, gathering and maintaining the data needed, and completing and reviewing the collection of information. Send comments regarding this burden estimate or any other aspect of this collection of information, including suggestions for reducing this burden, to Washington Headquarters Services, Directorate for Information Operations and Reports, 1215 Jefferson Davis Highway, Suite 1204, Arlington, VA 22202-4302, and to the Office of Management and Budget, Paperwork Reduction Project (0704-0188), Washington, DC 20503.				
1. AGENCY USE ONLY (Leave blank)	2. REPORT DATE December 1995	3. REPORT TYPE AND DATES COVERED Masters Thesis		
4. TITLE AND SUBTITLE  Determining the Effects of Waste Coal Ash on Landfill Radon Levels		5. FUNDING NUMBERS		
6. AUTHOR(S)  Captain Richard S. Krysiak Jr.				
7. PERFORMING ORGANIZATION NAME(S) AND ADDRESS(ES)  Air Force Institute of Technology WPAFB, OH 45433-6583		8. PERFORMING ORGANIZATION REPORT NUMBER  AFIT/GEE/ENP/95D-04		
9. SPONSORING / MONITORING AGENCY NAME(S) AND ADDRESS(ES)		10. SPONSORING / MONITORING AGENCY REPORT NUMBER		
11. SUPPLEMENTARY NOTES  Approved for public release; distribution unlimited.				
12a. DISTRIBUTION / AVAILABILITY STATEMENT		12b. DISTRIBUTION CODE		
13. ABSTRACT (Maximum 200 words)  Coal contains trace amounts of the primary radionuclides $^{40}\text{K}$ , and elements of the $4n$ ( $^{232}\text{Th}$ ), $4n+2$ ( $^{238}\text{U}$ ), and $4n+3$ ( $^{235}\text{U}$ ) series including $^{220}\text{Rn}$ and $^{222}\text{Rn}$ . Combustion of coal by electric power and heat plants result in concentration of noncombustible mineral matter, including most of the radionuclides, in the coal ash. The increased radiation due to the concentration of radionuclides is known as technologically enhanced natural radiation.  The purpose of this research was to determine the effects of landfilled coal ash on one specific aspect of technologically enhanced natural radiation, radon levels. Soil samples were collected from the ash landfill at Wright Patterson AFB and from several background locations, analyzed using gamma spectroscopy, and the $^{226}\text{Ra}$ activities compared. A two-sample t test with a 95% confidence level indicated that the landfill mean was significantly higher than background. The landfill $^{226}\text{Ra}$ activity ( $4.78 \pm 1.58$ pCi/g) was 2.95 times higher than background ( $1.62 \pm 0.04$ pCi/g). Estimated outdoor and indoor radon emanation at the landfill was predicted to be enhanced by the same factor compared to background. Additionally, the indoor radon concentration calculated at a hypothetical structure built on the landfill (11.48 pCi/l) is above the Environmental Protection Agency's action level of 4.0 pCi/l.				
14. SUBJECT TERMS  Coal Ash, Radon, Landfill		15. NUMBER OF PAGES 155		
		16. PRICE CODE		
17. SECURITY CLASSIFICATION OF REPORT Unclassified	18. SECURITY CLASSIFICATION OF THIS PAGE Unclassified	19. SECURITY CLASSIFICATION OF ABSTRACT Unclassified	20. LIMITATION OF ABSTRACT  UL	